2016

Damageability improving of plastics for interiors

Davide Pezzetti-Tonion
University of Windsor

Damageability Improving of Plastics for Interiors

by

Davide Pezzetti-Tonion

A Thesis
Submitted to the Faculty of Graduate Studies
through the Department of Mechanical, Automotive, and Materials Engineering
in Partial Fulfillment of the Requirements for
the Degree of Master of Applied Science
at the University of Windsor

Windsor, Ontario, Canada
2016

Damageability Improving of Plastics for Interiors

by

Davide Pezzetti-Tonion

APPROVED BY:

A. R. Riahi
Department of Mechanical, Automotive, and Materials Engineering

---

A. Sobiesiak
Department of Mechanical, Automotive, and Materials Engineering

---

A. Edrisy, Advisor
Department of Mechanical, Automotive, and Materials Engineering

August 15, 2016

Declaration of Originality

I hereby certify that I am the sole author of this thesis and that no part of this thesis has been published or submitted for publication.

I certify that, to the best of my knowledge, my thesis does not infringe upon anyones copyright nor violate any proprietary rights and that any ideas, techniques, quotations, or any other material from the work of other people included in my thesis, published or otherwise, are fully acknowledged in accordance with the standard referencing practices. Furthermore, to the extent that I have included copyrighted material that surpasses the bounds of fair dealing within the meaning of the Canada Copyright Act, I certify that I have obtained a written permission from the copyright owner(s) to include such material(s) in my thesis and have included copies of such copyright clearances to my appendix.

I declare that this is a true copy of my thesis, including any final revisions, as approved by my thesis committee and the Graduate Studies office, and that this thesis has not been submitted for a higher degree to any other University or Institution.

Abstract

Nowadays, because of their light weight, superior impact performance, easy recyclability and low cost thermoplastic olefins (TPOs) have become the common choice for automotive interiors, but, due to their softness, these materials are weak to surface damage.

This study investigates the surface damage response of TPOs. The influences of TPO types, textures, scratch additives and colors on the investigated surface damage and its visibility have been analyzed.

The wear tests were performed in the rotational configuration, at room temperature and for three normal loads (5, 7.5 and 10 N). Textures characterized by large grains, deep depths and rough/round peaks have shown higher resistance to wear and to damage visibility. Among the considered geometrical features of the damage, the wear track depth have been found to be the most important for surface damage visibility of textured samples.

Dedication

To my parents

Acknowledgements

This project is the result of the double degree program between the University of Windsor and the Politecnico di Torino, in collaboration with FCA. I am proud, and I will always be, of have been part of this, and I am deeply grateful to all the people involved in this program, whose efforts have made this project real and possible. I would like to express my appreciations to the coordinators of the above-mentioned institutions: Dr. Andrzej Sobiesiak and Dr. Jennifer Johrendt, Dr. Giovanni Belingardi, Edoardo Rabino, Mohammed Malik and Ishika Towfic for their coordinating role in this experience.
I want to thank all the people involved in the performing and completion of my study, for their help, suggestions, comments, and, especially, for their time.

I would like to devote a special thank my academic advisor at the University of Windsor Dr. Afsaneh Edrisy, who has helped and sustained me during my whole work with patience and kindness. Without her presence, my study could not be realized.

My gratitude goes also to my academic advisor at the Politecnico di Torino, Dr. Davide Paolino. Despite the distance, he managed to sustain me, with suggestions and comments always meaningful and interesting.

I would like to express my gratitude for the assistance received during this whole year to my industrial advisors: Ewa Lebert and Douglas Peterson from the Chrysler Technical Center, and Maurizio Servetti and Vito Lambertini from the Centro Ricerche Fiat. Their knowledge and field-experience was fundamental for my work.

A very special thank goes to Ryan Fillion, Doug Boudreau and Marie Mills, for their technical help, and patience, in the performing of the tests and collection of the results.

An important mention goes to the Director of the International Student Center, Mike Houston, to the Administrator of the International & Exchange Student Services Michelle Fitzgerald, and to the Department Secretary and Graduate Secretary, Angela Haskell for their help in all the coordination issues, and for making my life in Canada easier and more pleasant.

I am deeply grateful to my family, for their encouragement and support in all these academic years. My first thought is for my parents, Valter and Gemma, who have sustained my choices, even though sometimes they did not share them, and who gave me values that have made me the man I am now. A big thank to my sister Sabrina, special person in my life and shoulder when my certainties shake. A huge thank to the rest of my family (grandmothers, cousins, aunts, uncles nanny and brother-in-law), who has been always by my side, no matter what, when or where.

A special thank goes to my girlfriend Federica, who has always sustained me, despite the ocean who divided us, and my choices that have put our relationship to the test.

I want to thank all the nice and funny International, Exchange and Canadian students that I met in Windsor during this year; they have contributed to make this experience unforgettable.

I am also truly thankful to my more-than-friends, who I left in Italy: Mirko, Andrea, Alessio, Simone, Marco, Mattia, Paolo, Denis, Jessica, Mariarosa, Claudia, Stefania, Valeria, and so on. I know that when I will be back, we will start again from where we left.

A special mention goes to that group of promising guys called *Politopi*: Mirko, Marcello, Andrea, Eduardo, Luca, Marco, Francesco and Davide. I am proud and lucky to have met

these guys, who, some from day one, some others later, have studied and struggled, but also laughed and celebrated with me in these academic years. This path would have been a lot more boring and harder without them. I would like to thank Nicola, with whom I shared great moments in the last months of this experience.

Finally, I express my gratitude to my fellows, who shared this year with me: Mirko, Marco, Davide, Marco, and Jerome. Some of us came in Windsor as strangers, now we leave with memories we will take with us for the rest of our lives.

"Make no little plans; they have no magic to stir men's blood and probably themselves will not be realized. Make big plans; aim high in hope and work, remembering that a noble, logical diagram once recorded will never die, but long after we are gone be a living thing, asserting itself with ever-growing insistency."

D. Burnham

Table of Contents

List of Tables

List of Figures

List of Appendices

List of Abbreviations

(S)COF	(Scratch) Coefficient of friction
Al	Alluminium
ANOVA	Analysis of variance
ASV	Automatic scratch visibility
CPN	Chrysler polymer number
DSLR	Digital single lens reflex
EPDM	Ethylene propylene diene rubber
EPM	Ethylene propylene rubber
FCA	Fiat Chrysler Automobiles
FLTM	Ford Lab Test Method
GL	Gray level
LDR	Letdown ratio
MF	Melamine resin
MGD	Modified gloss diffusion
PB	Polybutylene
PC	Polycarbonate
PE	Polyethylene
PMMA	Polymethyl methacrylate
PP	Polypropylene
PS	Polystirene
PTFE	Polytetrafluoroethylene
RGB	Red green blue color model

SAN	Styrene acrylonitrile resin
SEM	Scanning electron microscope
TPE	Thermoplastics elastomers
TPOs	Thermoplastics polyolefines
TPV	Thermoplastic vulcanizate
UHMWPE	Ultra high molecular weight polyethylene

List of Symbols

α	Recovery angle
β	Attack angle
ϵ	Strain at failure
γ	Surface energy
γ_{ab}	Interfacial energy
γ_d	Surface energy from dispersion forces
γ_p	Surface energy from polar forces
μ	Friction coefficient
μ_r	Friction coefficient due to deformation mechanism
μ_s	Traditional surface sliding friction coefficient
ρ	Reflected light intensity
ρ_{dd}	Diffractional scattering intensity
ρ_{sp}	Specular reflection intensity
ρ_{ud}	Multiple scattering intensity
ρ_s	Specific weight
σ	Ultimate tensile strength
σ_y	Yield stress
A	Area
A_p	Projected load bearing area
B	Brightness
b	Indenter related constant
b_f	Fatigue properties related constant

C	Contrast
c^2	Shape ratio
d	Indenter related constant
E	Elastic modulus
F_c	Critical load for onset of scratch visibility
F_f	Friction force
F_{fin}	Final normal load
F_o	Initial applied load
H	Hardness
h	Penetration depth
h_c	Contact depth
l	Scratch length
L	Normal load
L^*	Luminance CIELAB coordinate
M	Weight loss
M_o	Optical mass
n	Number of cycles
q	Scratch hardness correction factor
S	Ultimate tensile stress
S_a	light scattering average
S_d	Light scattering difference
T_g	Glass transition temperature
T_m	Melting temperature
V	Volume loss
W	Worn volume per unit slid distance
W_{ab}	Work of adhesion per unit of slid distance
X	Rheological factor

Chapter 1

Introduction

The use of polymeric materials, and especially of thermoplastic polyolefines (TPOs) in automotive interior applications is extensive, as highlighted in figure 1.1, and it is expanding. Light weight, possibility of recycling and low costs are the main reasons for the utilization of this material type. Light weight potentially increases the efficiency of vehicle, lowering the amount of energy requested for transportation, reducing the emission and improving the environmental sustainability. The latter is also fostered by the possibility of recycling. Low costs, also related to the capability to process this material as thermoplastics, lead to an economic advantage, because company can enter in the market with a more competitive price.

Automotive interiors have two main requirements: mechanical integrity and aesthetic appeal. Mechanical integrity means that the components have to maintain their shape and not to break during the vehicle utilization life. At the same time, the appearance of interiors is able to give to customers a certain perception of quality and luxury, hence it is part of the customer decision making process. For this reason, interiors must keep their appearance during the car usage, and this is no more just a warranty issue, but a long term customer satisfaction concern.

Due to the importance of aesthetic appearance, the susceptibility to surface damage and

Figure 1.1: Automotive interiors made of polymeric materials [60]

the visibility of that have become significant issues. Common types of surface damage are listed in table 1.1. Despite the development and existence of several types of test aimed at evaluating the surface damage resistance of polymeric materials, the behavior of these is far from be completely understood and analyzed. The main causes of the difficulty of these studies are the inherent complexity of the polymeric material response to surface damage and the features and characteristics of the wide range of possible deformation mechanisms. Indeed the sliding of an object, or in general of a counterface, on a polymeric surface induces a complex field stress, causing a deformation, according to a specific mechanism, to which is related a certain visibility. All of this depends strongly on material properties (young modulus, yield stress), on surface characteristics (texture, gloss, color) and external parameters (applied load, sliding speed, temperature). Moreover, actual tests are unable to capture some damage modes, e.g. scuff, which occur on the field, even though prescribed tests have been successful.

This thesis, developed in collaboration with the University of Windsor, Politecnico di Torino and FCA (Fiat Chrysler Automobiles), aims at studying the surface damage response of TPOs, evaluating the influences of several parameters like surface characteristics and material properties.

Table 1.1: Common surface damage types

Surface Damage	
Scratch	Damage characterized by the cutting action of sharp object on the surface of another object
Mar	Friction-induced damage in which the compression of the surface crests due to the sliding of a blunt object causes a damage
Abrasion	Wear-off by friction, similar to grinding
Scuff	Form of wear characterized by macroscopically observable changes in texture, with features related to the direction of motion

1.1 Thesis organization

The performed work is organized in this thesis in chapters listed below:

- *CHAPTER 2: Objectives and procedures.* It contains the description of the aims of the thesis, with the procedures followed in order to achieve them.

- *CHAPTER 3: Literature review.* In this chapter, information about the utilized materials are provided. A description of the most common tests utilized to asses the surface damage resistance of materials is included. Moreover, the basis of scratch visibility and wear of polymers, and the effect of several factors are given. Finally, possible solutions to evaluate the surface damage resistance are reported.

- *CHAPTER 4: Materials and experimental procedure.* This section is dedicated to the detailed description of the steps followed during the research. It includes specifications about the used material, the performed test, the preparation of samples and of the measurements collected.

- *CHAPTER 5: Results.* The data, resulting from the experimental work described in Chapter 4, are reported. The experimental results include worn volume and wear rate data, evolutions of the coefficient of friction (COF) during the test, measurements of the geometry of the damage and damage visibility information . Images obtained

through the microscope and *3D* representations of the damaged surfaces are also reported. The ANOVA analysis perfomed is included.

- *CHAPTER 6: Discussion.* The results shown in Chapter 5 are discussed and commented, with the aim of understanding the influence of normal load, surface texture, color and injection molding process characteristics on the surface damage behavior of the considered TPOs.
- *CHAPTER 7: Conclusions.* The finding of the research are outlined and summarized.
- *CHAPTER 8: Recommendations.* Some recommendations for future work are given.

Chapter 2

Objectives and procedures

Thermoplastics polyolefins (TPOs) are highly susceptible to surface damage. The sliding of a counterface would easily lead to a particular type of damage, which depends on a number of factors. Moreover, the damage would induce a certain visibility that involves a loss of perceived quality and aesthetic appeal.

The first objective of the thesis is an in-depth investigation of the surface damage response of thermoplastic polyolefins. First of all, a certain type of wear test has to be selected, and the test conditions, like applied normal load, sliding speed, temperature have to be adjusted. Information coming from the literature have been considered in order to set these parameters. Then, to understand the effect of different material and surface characteristics on the surface damage behavior of TPOs, a test plan has been developed.

By weighing the considered samples before and after testing, the loss of mass, hence the worn volume have been evaluated. From these, the wear rates have been calculated to quantify the wear induced by the process.

A high quality optical microscope has been utilized to observe and analyze the features of the induced surface damage. Subsequently, a surface profilometer has been used to get $3D$ representations of the damage, and to collect measurements significant from visibility point of view.

By means of a portable spectrophotometer, a direct measurement representative of the visibility of the surface damage has been obtained, and compared to the other results. Therefore, relationships between quantitative measurements of the damage and damage visibility could have been pointed out.

Finally, a statistical tool (ANOVA) has been used to compute the significance and the percentagse of contribution on the surface damage behavior of TPOs, of the considered factors.

Chapter 3

Literature review

In this section an overview of the materials analyzed in the thesis is provided. Then, the commonly utilized tests for the determining of the resistance of surface damage are described. The causes for surface damage visibility are explained and the bases of wear of polymers, and the influence of several factors on their tribological behavior are given. At the end, possible methods to analyze the surface damage response of polymers (scratch hardness and scratch maps) are reported.

3.1 ThermoPlastic Elastomers

Rubber-like materials are composed by long polymeric chains, with light cross-linking characterized by a high degree of flexibility and mobility, which are joined in a network structure. Very high deformability is the result of this high level of flexibility and mobility. When this type of materials are subjected to an external stress, the long chains can alter they configuration rapidly. Because of the network structure, the chains can coil and uncoil, but they are prevented to slip past each other. This leads to a highly extensible network structure; typical rubber can be stretched up to ten times the original length. Once the external forces are removed, the material returns to its original dimensions, essentially without residual strain. The responsible of the above explained behavior of this type of materials is the

network structure, which is obtained by linking together polymer chains. The linkage can be chemical or physical [53, 54]. While materials with chemical crosslinks cannot be re-processed once formed, physical crosslinks are not permanent, and they can disappear with a temperature increase. Physical crosslinks are defined as *heat fugitive*, and they can be obtained by:

- absorption of chains onto the surface of finely divided particulate fillers;
- formation of small crystallites;
- coalescence of ionic centers;
- coalescence of glassy blocks.

Material with physical thermoreversible network are technologically attractive because they can be processed as thermoplastic (i.e. by melt processing), and at the same time they exhibit the behavior of vulcanized rubbers. Materials of this type are called thermoplastic elastomers (TPEs). Most TPEs are phase-separated system. One phase is hard and solid at ambient temperature; this part gives to the TPE its strength. The other phase is an elastomer that provides flexibility and elasticity to the system. The two phases can be either chemical bonded by block or graft polymerization, either finely dispersed. Since the polymers constituting the two phases retain most of their characteristics, the service temperature range depends on their specific glass transition temperature T_g or crystalline melting temperature T_m. The maximum and minimum service temperatures are the points where the material undergoes transitions in its physical properties, ad example in the flexural modulus as shown in figure 3.1. At low temperatures, both phases are hard, thus the material is stiff and brittle. Above the soft phase T_g, the elastomeric phase softens and the material is elastic. Further temperature increase, above the T_m of the hard phase, leads to hard phase softening or melting; there the material is a viscous fluid. Therefore, it is possible to understand that the service temperature range lies in between the T_g of the elastomeric phase (lower service temperature) and the T_m of the hard phase (upper service temperature).

TPEs are designed to develop superior mechanical properties. To obtain these in a two-

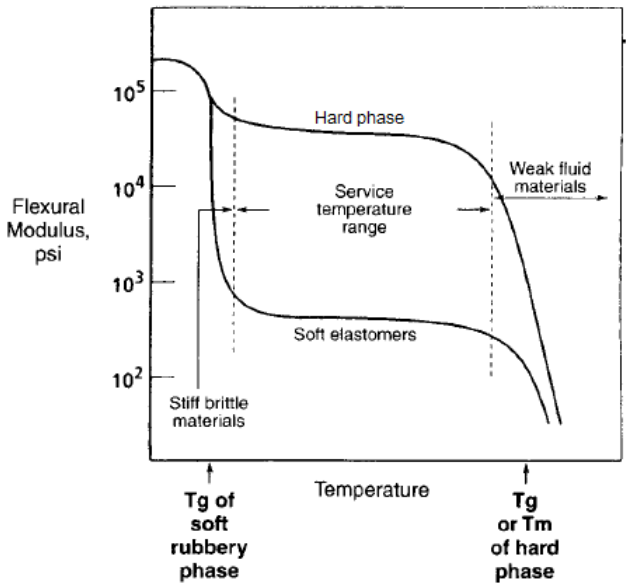

Figure 3.1: Stiffness of typical thermoplastic elastomers in dependence of temperature [53]

components polymeric system, the components should be neither so incompatible, nor so mutually soluble. Indeed, a slight degree of mixing is desirable, but the formation of a single-phase system must be prevented. The conditions that favor phase separation are: segments with highly different structure, segments with high molecular weight and low temperature. It is conceptually hard to understand why a system consisting of rubbery spheres embedded in a rigid thermoplastic should be capable of rubbery behavior. However, it is possible to consider that the complex morphology involves a hard phase reticulated structure that allows large deformations, with a rubbery phase, which facilitates the recovery from deformation [53, 54].

The main commercial types of thermoplastic elastomers are:

- Styrene-butadiene-styren triblocks;
- Polyester-based thermoplastic polyurethane elastomers;
- Polyether-based thermoplastic polyurethane elastomers
- Thermoplastic polyester elastomer;
- Thermoplastic polyamide elastomer;

Table 3.1: Properties of commercial thermoplastic elastomers

Type	*Soft phase* T_g (C)	*Hard phase* T_g *or* T_m (C)	*Oil resistance*	*Hardness range*	*Specific gravity*
S-B-S	-90	95 (T_g)	Poor	$60-90A$	0.94
S-I-S	-60	95 (T_g)	Poor	$30-40A$	0.92
S-EB-S	-60	95 (T_g)	Poor	$65-75A$	0.91
Polyester-urethane	-20 *to* -40	190 (T_m)	Good	$70A-70D$	$1.18-1.24$
Polyether-urethane	-60 *to* -80	190 (T_m)	Good	$40-90A$	1.1
Polyester	-40 *to* -65	190 (T_m)	Good	$35-75D$	$1.15-1.45$
Polyamide	-40 *to* -65	$120-275$ (T_m)	Good	$75A-65D$	$1.0-1.15$
PP/EPDM	-60	$140-165$ (T_m)	Poor	$60A-75D$	$0.9-1.1$

- Thermoplastic polyolefin rubbers.

Example of properties of the most common TPEs is shown in table 3.1. The major part of produced TPEs consists of block copolymers, which consist of two or more polymers attached at their ends in different configurations. The possible block copolymers architectures are shown in figure 3.2. The most common polymerization methods to prepare block copolymers are the following:

- Atomic polymerization is suitable for synthesis of tailored block copolymers, but it is demanding, since it requires high purity reagents and high-vacuum procedure to get rid of impurities;
- Cationic polymerization used for a limited range of monomers;
- Controlled/living radical polymerization is the most recent technique and its principle is to establish and equilibrium between a small fraction of growing free radicals and a large portion of dormant species;
- Polymerization Ziegler-Natta catalyst is used for the polymerization of Polyolefin based TPEs (TPOs);
- Polyaddition is used for thermoplastic polyurethanes.

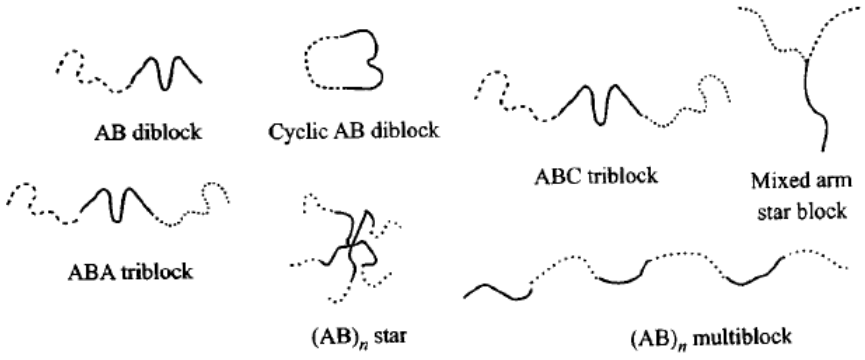

Figure 3.2: Block copolymer architectures [53]

3.1.1 Advantages and disadvantages

Advantages

TPEs advantages over conventional thermosets (vulcanized) rubber materials:

- Simple processing because the possibility of using methods for thermoplastics, which are more efficient and less expensive. Hence, the costs of the final part is lower;
- Shorter fabrication times, which leads to lower costs of finished part and higher productivity of the equipment;
- Possibility of scrap recycle, as with thermoplastics;
- Lower energy consumption;
- Better quality control and closer tolerances of ended parts;
- Lower quality control costs because of greater reproducibility and consistency of TPEs properties.

Disadvantages

TPEs disadvantages over conventional rubbers:

- High melting temperature and limited upper service temperature;
- Limited number of low hardness TPEs;
- Drying prior to processing (not always).

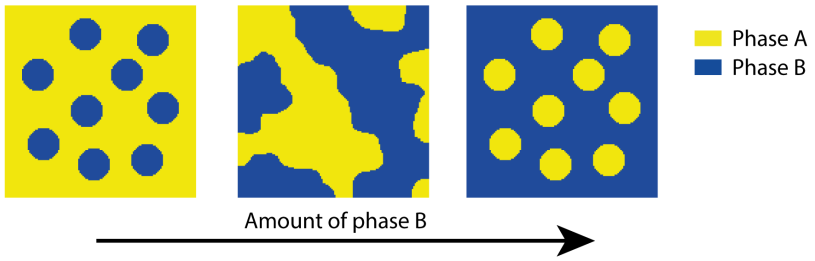

Figure 3.3: Morphology of hard polymer-elastomer blend [56]

3.2 Thermoplastic Polyolefins

Polyolefin thermoplastic elastomers are defined as materials combining semi-crystalline thermoplastic and amorphous elastomeric compounds [53, 54]. There exist several types:

- Blends (mechanical mixtures) named as TPOs;
- Dynamical vulcanized blends of copolymer and olefins named TPVs;
- Block copolymers;
- Stereoblock polymers;
- Graft copolymers.

The materials we are interested in are the TPOs, which differs from TPVs because the former are co-continuous phase systems (figure 3.3), while in the latter the elastomeric phase is crosslinked and discountinuous. Polyolefin blends TPEs (TPOs) are commonly based on ethylene propylene random copolymer (EPM), which represents the elastomeric phase, and isotactic polypropylene (iPP), which represents the hard phase. They are simple mechanical blends that can be prepared by mixing the two phases in high-shear compounding equipment, like internal or continuous mixer. The resulting structure is a three-dimensional, co-continuous structure shown in figure 3.3, where the continuous hard phase provides strength and the continuous soft phase provides flexibility. The polyolefin phase is always continuous, while the rubber phase may be continuous or discrete depending on the relative amount of rubber (continuous in the range $45 - 48\%$ of total volume), the rubber type, the mixing procedure and other ingredients presence. Because of its low cost and low den-

sity, polypropylene based thermoplastic elastomer blends are very interesting commercially. It shows resistance to oil, solvents and elevated temperatures because of the crystalline structure and relatively high melting point ($145 - 165\ ^{\circ}C$). The common choice for the elastomeric phase is EPDM or EPM (less expensive) because of their thermal stability, low cost, flexibility and structural similarity with polypropylene, which ensures good compatibility in blending. The common choice for the hard phase is isotactic polypropylene, both homopolymer and co-polymer with a small fraction of ethylene. In addition to the two main phases, other ingredients are included in the TPO formulation, for different reasons. These may be fillers, reinforcing agents, lubricants, antioxidants, colorants, plasticizers, flame-retardants, etc.

3.2.1 TPOs properties

Because of their formulation, TPOs show a wide range of mechanical properties, which cover the gap between soft rubber and engineering plastics. They can combine strength and toughness with properties and feel from soft conventional rubbers to stiff rigid products. The hardness of these products can range from 60 *Shore A* to 70 *Shore D*, while their flexural modulus can varies from 1000 to 25000 *psi* (6.9 to 1725 MPa). The specific values of properties like hardness, flexural modulus, tensile strength, impact strength and so on depend on the specific grade of TPO. It is worth to note that high content of soft phase induces high elongation at break and large recovery after break.

Service temperature

For a generic TPO, the service temperature range is in between -80° and $140\ ^{\circ}C$, for short-term exposure. As explained in the previous section it depends on the T_g of the soft phase and T_m of the hard phase, respectively. If long-term exposure is considered, the aging resistance of the material starts to be important, and the upper service temperature diminishes to $125\ ^{\circ}C$.

Chemical and electric properties

The chemical resistance to solvents to and fluids varies with the grades, but all TPOs are unaffected by water and aqueous solutions and resist acids and bases. However, hydrocarbon solvents tend to swell and soften TPO.
Because of their nature, TPOs are good electrical insulating materials; they have good dielectric strength and do not absorb moisture.

Adhesion

Only few adhesives are available for bonding with TPO components. Indeed, bonding to the TPO surfaces is difficult because they are chemically inert and they have low surface energy. Hot melt and anaerobic adhesives are able to give good results, but interlocks and interference fits are the most common and reliable methods.

Weathering

TPOs have a good weather and sunlight resistance; they maintain their original properties when exposed to these because of the absence of unsaturation in their backbone. However, discoloration can occurs, thus some special stabilizers are included to protect against that during outdoor exposure.

Paintability

Lot of parts made of TPOs have to be painted for aesthetic reasons (e.g. in automotive applications). As stated above, TPOs surfaces do not react with most paints. Hence, the surfaces have to be modified by creating polar groups on it. Some surface pretreatments are utilized to accomplish that (corona discharge, plasma treatment, flame treatment, chemical treatment, application of adhesion promoter primer, etc.).

3.2.2 TPO processing

One of the core advantages of this material type is that they can be processed on the standard equipment and with the standard techniques of thermoplastics. While the most

important processes for the manufacturing of products made of TPOs are injection molding and extrusion, other processing methods like vacuum forming, injection blow molding, extrusion blow molding, calendaring and thermoforming are available. TPOs do not require particular type of handling, and, since they are not hygroscopic, they do not necessitate drying prior processing.

Through injection molding several products can be manufactured; the reciprocating screw machine is preferred to the plunger injection molding machine because of the more uniform melt obtainable. Extrusion is used for production of profiles, tubing, hose, coat of wires and jacket of cables. Negative thermoforming has become important for the manufacturing of large automotive parts like automotive instrument panels. Slush cast molding, which is used manily for PVC, has bees adapted for powdered TPO materials for interior automotive parts.

3.2.3 Applications

Thermoplastic olefins are utilized for the manufacturing of a wide range of products in a variety of applications. The major market areas are: automotive, wire and cable, and mechanical goods [53, 54].

Automotive market is the largest for TPO applications. TPOs are used for exterior parts to replace metals, for components that can be easily damages by minor collisions, like bumpers, air dams, body side cladding, sight shield, stone deflectors, grills, valance panels, etc. Parts in the engine compartment can be made by TPOs, like heating air ducts, firewall pads and hood seals. Finally, interior applications include instrument panels, glove box doors, door panels, door insert, interior trim, air bag covers and dashboard. Figure 3.4 and 3.5 show some of the above mentioned TPOs automotive applications.

Wire and cable applications include flexible cords, appliance wires cable jackets, control cables, etc. The important features for these types of applications are excellent electrical resistance, ozone resistance and water resistance.

Figure 3.4: Automotive bumper [57]

Figure 3.5: Door panel of Jeep Renegade [58]

Mechanical goods market involves those applications where TPOs can substitute vulcanized rubber, like seals, electrical plug, wheels, pump impellers, etc. The main reason for the adoption of TPOs instead of conventional rubber in these applications is the possibility of scrap reutilization, so the recyclability.
Other TPOs applications include transmission belts, toys, sporting goods, luggage handles, shoe sole, sealants and hot-melt adhesives, etc. Applications of TPOs are shown in figure 3.6.

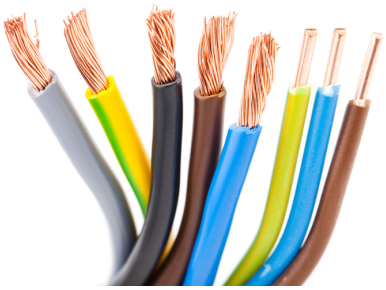

(a) Cable coating made of TPOs

(b) Components made of TPOs

Figure 3.6: Some applications of TPOs [53, 59]

3.3 Surface damage resistance tests

To face the problem of the surface damageability of polymeric components, researchers and companies have developed several types of test, aimed at evaluating the resistance to particular type of surface damage. The most common types of damage which have been addressed are scratch and mar. Nowadays, three test are the most widely utilized: Erichsen method, Ford Lab Test Method (FLTM) and the ASTM D7027 / ISO 19252 methodology.

3.3.1 Erichsen scratch and mar methodology

This method has taken his name from the machine utilized to perform the surface damage (Erichsen scrath hardness tester), and it is the most used scratch and mar resistance evaluation tool for molded-in-color automotive thermoplastics used for interior or exterior

in ornamentation or trim applications [42]. The machine utilized is shown in figure 3.7; it is basically a motor-driven device that can produce parallel cuts and cross-cuts at variable speeds, with the ability to produce the specified grid patterns at the specified loads. The device is equipped with interchangeable tips, for the testing of different surface damage. Indeed, the test is composed by two methods (A and B), for the evaluation of scratch resistance and mar resistance, respectively.

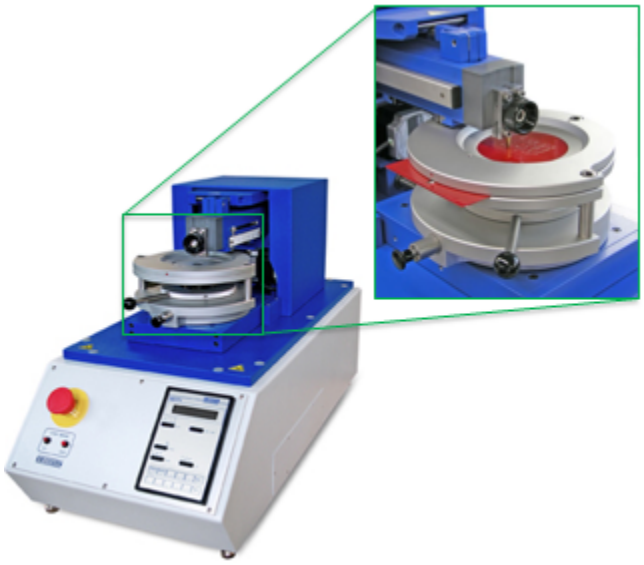

Figure 3.7: Erichsen scratch hardness tester [45]

Method A - Scratch testing

In the evaluation of the scratch resistance [42], the tip holder is endowed with a stainless highly polished steel ball of 1 ± 0.1 mm diameter. The normal load applied on the sample surface is constant and equal to 10 N, and the scratching speed is constant and equal to 1000 mm/min. Once the parameters are set and the sample positioned, 20 parallel scratches, at least 40 mm long and distant 2 mm each other are performed on the testing surface. Then the sample is rotated of 90°, and the same procedure is applied in the perpendicular direction. At the end of the test, on the surface there will be a grid similar to that showed in figure 3.9. It should be stressed out that the scratching is unidirectional. Once the grid is completed, a specthrophotometer is utilized to analyze the sample. A

spectrophotometer is an apparatus able to measure the intensity of light as a function of its wavelength. Here, it is utilized to measure the difference ΔL between the intensity of the light reflected from the damaged surface area and that reflected from the undamaged background, so it gives a measure of the luminance of the scratch. Figure 3.8 highlights the working principle of the specthrophotometer. This change in the luminance level is considered representative of scratch visibility.

Figure 3.8: Scheme of the specthrophotometer working principle [46]

The typical ΔL requirement for interior plastic molded-in-color trim is 0.9. This means that a material sample has passed the erichsen scratch test if the measured change in luminance is lower than or equal to 0.9.

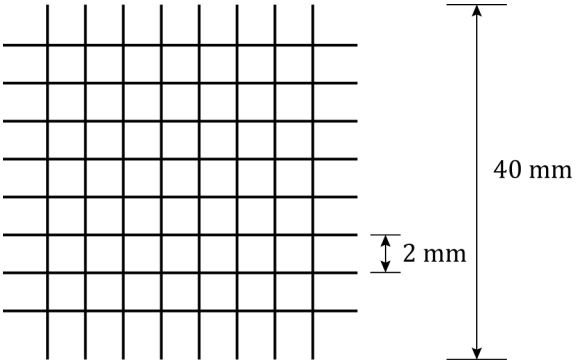

Figure 3.9: Scheme of the grid obtained on the sample surface

Method B - Mar testing

Mar is a surface damage different from scratch. It can be defined as a subtle non-recoverable plastic deformation, caused by compressive stress, which slightly scatters the light and alters the surface gloss [21]. To obtain this type of damage the indenter, the applied normal load and the scratching speed are different. The utilized indenter tip is a stainless highly polished steel disc tip of $7 \pm 0.2\ mm$ diameter, aligned to the travel direction across the specimen as shown in figure 3.10. The applied normal load is $7\ N$ and the scratching speed is $40\ mm/s$. A grid similar to that of method A is performed during the test, and at the end the sample surface is analyzed through a glossmeter. This is an apparatus able to measure the gloss of a surface (defined as the shine or luster on a surface). The glossmeter can be arranged with different inclination, so it is possible to collect information that depends on the position and slope of the sample, or, better, of the incident light beam (figure 3.11). However, usually the measurement geometry of the glossmeter is set to 60°. The difference between the gloss level ΔG measured on the damaged area and the one of the virgin background is the quantity considered representative of mar visibility [42].

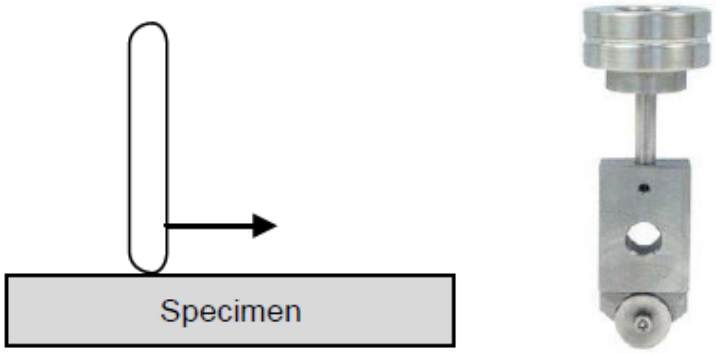

(a) Schematic of mar phenomenon

(b) Mar indenter

Figure 3.10: Mar indenter motion and geometry [42]

The typical ΔG requirement for interior plastic molded-in-color trim is 0.9. This means that a material sample has passed the Erichsen mar test if the measured change in gloss is lower than or equal to 0.8 at sample level, or 1 at component level.

The sample utilized in the Erichsen test method are flat plastic plaques, or regions cut

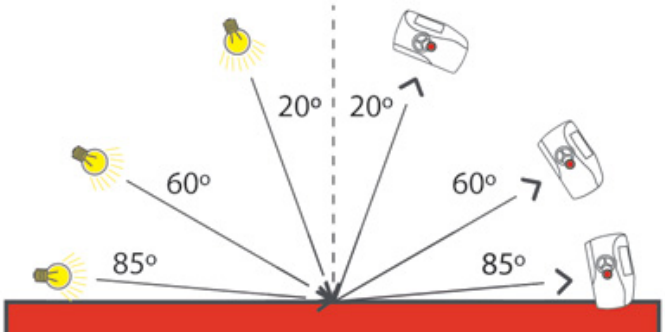

Figure 3.11: Schematic of glossmeter functioning [47]

from plastic parts which are sufficiently flat to provide for accurate assessment and adequate size so as to permit $\geq 40\ mm$ length scoring, both longitudinally and crosswise. Samples are pre-conditioned in a controlled atmosphere of $23 \pm 2°C$ and $50 \pm 5\%$ relative humidity for at least 24 hours prior to testing, and minimal surface handling has to be guaranteed to prevent interference or damage of the evaluation area. The test is performed at $23 \pm 2°C$. It is interesting to note that the ΔL value is an absolute difference value, which is not able to account for differences in virgin surface nature of materials under comparison. Hence, the normalization of the ΔL value against the luminance of the virgin surface has been proposed by *Liu et al.* [14]. This is in essence a measure of the contrast with respect to luminance. Comparing the results of the Erichsen test utilizing this normalization to those of the ASTM D7027 methodology (explained later), it was found that the value of the dimensionless ΔL relative to the visibility onset from ASV is within 1%, which is not so different from the prescribed ASV contrast criterion value of 3%. This is interesting, and it suggests that since the change of L needs to reach a certain value for visibility, this value is not unique, but it varies depending on the material due to differences in virgin surface nature. In another work, *Liu et al.* [41] have tested polymeric materials following the Erichsen procedure, but varying the applied normal load; they found that, the load at which the scratch becomes visible in the Erichsen test corresponds well with the onset of scratch visibility detected through ASV. Hence, due to the strong correlation that has been found between the onset of scratch visibility (ASTM/ISO) and the quality criteria of the Erichsen test, if the contrast criterion is considered (dimensionless ΔL), it has been

suggested that luminance contrast, rather than absolute difference, is a better measure for ranking materials regarding to scratch visibility.

3.3.2 FLTM Method

One of the scratch test methodologies utilized by automotive companies is the FLTM five-fingers method (Ford Lab Test Method BN 108-13) [5, 13, 39]. The simple machine used to simulate the customer usage is shown in figure 3.12. It consists of five beams, 250 mm long, attached to a movable platform. The end of each beam is endowed with a scratch pin, whose tip is a highly polished hardened steel ball of 1 ± 0.1 mm diameter. Dead weights are placed on each pin to exert a force; each pin is loaded differently, to obtain five different loads: 7 N, 6 N, 3 N, 2 N and 0.6 N. The beams are driven by compressed air, and through their motion, they generate scratches on the surface of the polymeric material under testing. The prescribed scratching speed is 100 mm/s. Generally, tests are performed at room temperature. Once the scratches are obtained on the surface, images of that are

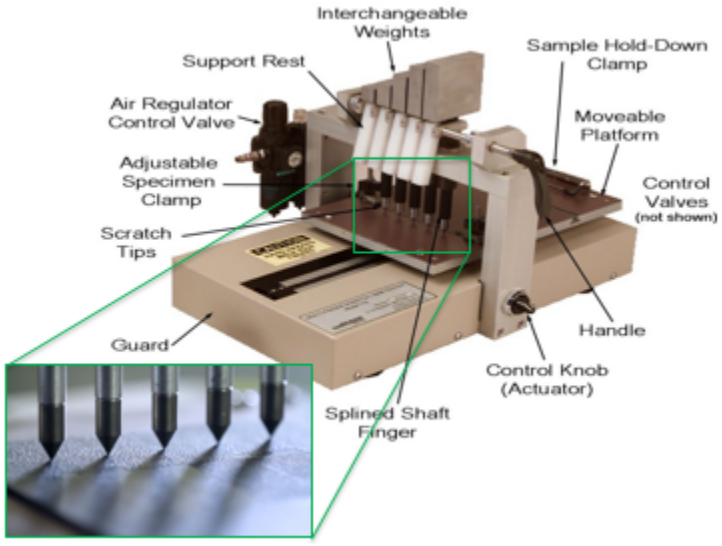

Figure 3.12: FLTM testing machine [48]

collected through a reflected light polarizing microscope and an image analyzer with an Image Analysis Software is utilized. This evaluates the total grayscale value of the object, which is the sum of the gray level values of all the pixels forming the object. Indeed, at each pixels a gray level value GL is assigned, ranging from 0 (= black) and 255 (= white).

Then, the optical mass of the object M can be computed:

$$M = \sum_i GL_i \tag{3.3.1}$$

Where the sum is extended to all the pixels composing the object. The brightness B of the object can be evaluated:

$$B = \frac{M}{A} \tag{3.3.2}$$

Where A is the area of the object. Finally, the percentage change in the brightness between the scratched area and the background, and it can be expressed as:

$$\Delta B = \frac{B_{scratch} - B_{background}}{B_{background}} \times 100 \tag{3.3.3}$$

where ΔB is a measure of the scratch visibility, thus of the scratch resistance of the material.

3.3.3 ASTM D7027 / ISO 19252

This is a recent scratch test methodology, developed at Texas A&M University [43]. In this procedure a single pass scratch under progressive load is performed. The schematic of test apparatus is shown in figure 3.13. It consists of a sample stage, clamping devices, a spring load system and a horizontal motion servo system. The spring-load mechanism is a stylus scratcher in which a 1 mm diameter spherical tip is used to scratch the surface of the specimen. The driven mechanism is able to exert a normal load from 0 to 75 N. The motion servo system consists of a high-precision motor controlled via microprocessor that actuates the scratch stylus motion. The horizontal speed can be range between 0 to 400 mm/s. The machine can be endowed with devices to monitor the normal load, friction force, instantaneous scratch depth and horizontal position. The most widely used test configuration involves progressive normal load from 1 to 30 N, and the test speed is 100 mm/s; the scratching distance is 100 mm. Once the scratch is completed, the damaged area is analyzed by different means. Generally, both optical microscope and SEM (Scanning Electron Microscope) analysis are utilized to evaluate and understand the features of the damaged area, the dominant deformation mode and the evolution/transition between them. Furthermore, images of the scratch are gathered through a photo PC scanner. The scanning is performed in a direction perpendicular to the scratching direction, because this is the

worst case for what regards scratch visibility [16, 41]. An automatic scratch visibility (ASV) software is utilized to analyze the images collected. This analysis tool detects the point of scratch visibility onset. Hence, due to the linear relationship between the progressive normal load and distance from the beginning of the scratch, the critical load for scratch visibility onset F_c can be evaluated:

$$F_c = F_0 + \frac{x}{l}(F_{fin} - F_0) \tag{3.3.4}$$

Where F_0 is the applied load at the beginning of the scratch test, F_{fin} is the final normal load, x is the distance from the beginning of the scratch of the point of scratch visibility onset and l in the scratch total length. The criterion, which is used in the definition of

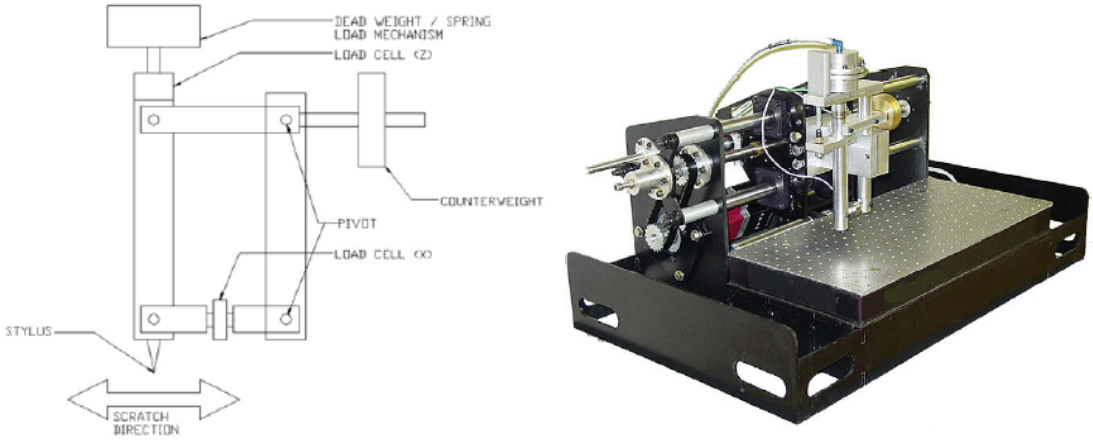

(a) Schematic of scratch machine [43] **(b)** example of scratch machine [22]

Figure 3.13: ASTM scratch machine

the point where scratch visibility has started, is composed by three parts [16]. The first one can be called contrast criterion. This is based on the fact that human eye detects an observed objects because of both the intensity of the reflected light from the object and of its contrast against the background. Hence, what is considered important here is the difference in the brightness level between the damaged portion of the material surface and its virgin surrounding. The contrast C can be expressed as:

$$C = \frac{|B_0 - B_b|}{B_0 + B_b} \times 100 \tag{3.3.5}$$

Where B_0 and B_b are the brightness level of the object considered (the scratched area in this case) and the background brightness values, respectively. From researches performed on the recognition process of human eyes, an object becomes visible when its contrast is larger than the sensitivity criterion, which is $2-3\%$ for the sharpest human eyes. Hence, according to the first part of the scratch visibility criterion applied by the ASV software, the onset of scratch visibility occurs in the point where the contrast of the scratch against its background exceeds 3%. Color can affect the contrast criterion. Indeed, different sample colors can obscure or enhance the human visual sensitivity of polymer surface, even though the considered material is the same. Ad example, it is known that green samples have presented a lower critical load, i.e. earlier scratch visibility onset, than red samples. This is related to physiological aspect of human eyes, in particular to the color sensitivity of retina cells. These are more sensitive to green light, less to red and least to blue. To account for the influence of color, thus to avoid biased results, the perceived brightness levels of the sample surfaces are weighted with regards to red, green and blue (RGB) color space:

$$Brightness = R \times 0.299 + G \times 0.587 + B \times 0.114 \tag{3.3.6}$$

In addition to the contrast of the damage, the visibility of a scratch depends also on its size. The reason of that is related to the visual acuity of human eyes. Visual acuity is defined as the capability to resolve a spatial pattern separated by a visual angle that is $1/60^\circ$ for normal human eyes. Considering a typical inspection distance of 30 cm from the surface and the eye, the smallest feature size distinguishable by human eye is about 90 μm. This means that any objects smaller than this should not be considered as visible, even though the contrast is above the prescribed 3%. The last factor that must be considered is continuity. Because of stick-slip motion, so periodical changes from static to dynamic movement of the scratcher tip, some discontinuity can be introduced. Similarly, the possible presence of dust or defects on, or close, the surface can cause discontinuities. Scratch visibility caused by these local discontinuities cannot be considered as onset of scratch visibility, thus the continuity criterion has been introduced to discard these discrete visible damages from the scratch resistance evaluation. This continuity criterion has been chose to be 90% in a distance of 2 mm (twice the diameter of the scratch tip) of the consecutive scratch path length. Therefore, according to the above explanation, the onset of scratch visibility can be

defined as the first point where all the described criteria (contrast, size and continuity) are concurrently satisfied.

One of the main advantages of the ASTM D7027/ ISO 19252 is due to the utilization of a progressive load. Indeed, as the load increases, the damage obtained on the surface changes [22, 34], as it is possible to note in figure 3.14. It starts as a very mild and hardly visible damage which includes recoverable elastic deformation, viscoelastic deformation and "mar". Mar is a smooth, subtle non-recoverable plastic deformation, caused by compressive stress, which slightly scatters the light and alters the surface gloss. In the first range of loads, strong polymers may not present detectable damage, while weaker polymers show small scale deformation. As the normal load increases, a fish-scale pattern occurs and develops as the scratching process continues. This is a typical surface damage for PP based materials, like TPOs, dominated by plastic drawing of material beneath the tip and it consists of a periodic concave damage pointing toward the scratching direction. The periodicity of this damage is caused by the stick-slip motion. According to this phenomenon, initially the scratcher tip adheres to the surface of the polymer, no relative motion occurs between the two, and the stress on the surface induces deformation in the material under the indenter. The tangential stress increases until it exceeds the critical stress, the slip starts, and material piles up ahead of the indenter. Once the stress has become lower than the critical one, the stick process happens again. Hence, the periodicity results from the accumulation and release of the tangential force. For weak and more brittle polymers (like PS), the surface damage that occurs is similar, but it is called pseudo fish-scale, because the parabolic feature is no more present. Moreover, this deformation pattern is accompanied by cracks and voids nucleation. In the last region of the scratch, the very high load causes the scratcher tip to penetrate deeper into the material leading to significant material removal; this region is called material removal zone.

It is interesting to note that stronger polymer do not present any fish-scale or pseudo fish-scale damage, in the considered load range [22]. Indeed, the damage is still subtle until high load is approached; then parabolic cracks form. Those have a periodic nature, and they are convex pointing to the direction opposite to the scratching one. Once they have formed, they can propagate in brittle fashion and become denser as the load increase or they

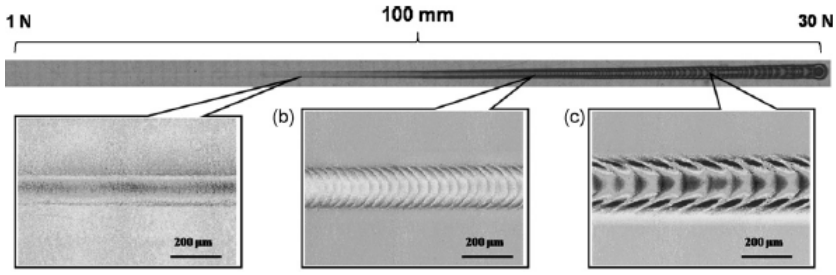

Figure 3.14: Evolution of surface damage on TPO tested according to ASTM D7027 methodology: (a) smooth ironing, (b) periodic fish-scale and (c) severe damage involving material removal. [16]

can open without a large extension, depending on the brittle or ductile nature of the strong polymeric material. From the analysis of the tests results, it was found that the onset of scratch visibility, hence the critical normal load, verifies close to the beginning of periodic fish-scale pattern caused by stick-slip motion. Therefore, the scratch becomes visible when the deformation of the polymer surface passes from elastic regime, to plastic regime [34].

3.4 Scratch hardness

In the past, it has been tried to relate the scratch behavior of polymeric materials to the indentation hardness. Several hardness tests methods were considered, but at the end it was found that these were inadequate to explain the differences in the scratch response of different polymers, so they cannot be considered representative of material scratch resistance [13, 18, 39]. This is mainly due to two factors. The first one is the difference in the utilized indenter, while the second, more important, is the difference in the nature of the two tests/phenomena. Indeed, indentation test is a quasi-static test, while scratch test is a dynamic process, influenced by the dynamic friction coefficient during the sliding process. Because of that difference, a new parameter called scratch hardness has been defined, and it has become one of the most common method to assess the scratch behavior of polymers. Similarly to the indentation hardness, scratch hardness is defined as the ratio between the applied normal load L and the projected load bearing area A_p:

$$H_s = \frac{L}{A_p} \tag{3.4.1}$$

The complexity of this parameter lies in the determination of the projected load bearing area A_p, highlighted in figure 3.15. Indeed, while in the indentation hardness test the indenter was fully supported by the surface area, in scratch tests, the indenter is only partially supported. During scratching, the front leading part of the indenter tip is fully supported by the polymeric material, but the rear half is only partially supported by part of the material that has been recovered. The amount of the recovered material depends on the nature of the material, and, in particular, on its viscoelastic properties. A perfectly plastic material involves no material recovery while a perfectly elastic material would recover totally the previously deformed material.

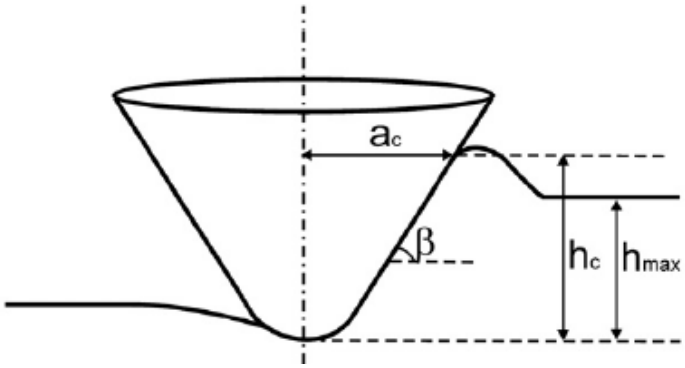

(a) Schematic representation of deformation during scratching

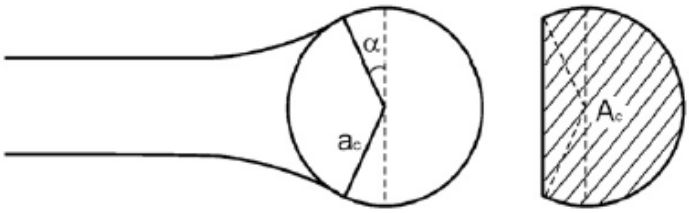

(b) Schematic representation of recovery angle and contact area during scratch test

Figure 3.15: Schematic of scrath geometry [18]

Polymers, which present a more or less pronounced viscoelastic behavior, are able to recover partially the imposed deformation, causing a partial support of the rear part of the indenter. Due to that phenomenon, the determination of the extent of the load bearing area is not simple. Indeed, the estimation of the contact area from the residual profile is not correct because of the significant healing presented by polymers.

In the literature, it is possible to find several methods, developed with the purpose to solve this issue. *Briscoe* [11] has proposed the introduction in the scratch hardness formula of a parameter q, which takes into account the recovery capability of the considered polymer:

$$H_s = q\frac{L}{A_p} \tag{3.4.2}$$

Hence, this parameter varies according to the type of material tested and how the material supports the indenter ($q \simeq 2$ for rigid plastic materials and $q > 1$ for viscoelastic plastic materials). Due to the impossibility of measuring the parameter q with sufficient accuracy, this method has revealed unsatisfactory. *Gauthier and Schirrer* [18] have built a system capable of measuring the instantaneous contact area during the test by means of an optical microscope endowed to a microscratch tester, but this technique is limited to only transparent materials, quality not possessed by scratcher available on the market.

Therefore, many attempts have been made to predict the true contact area in different ways, by considering indenter geometry, pile-up formation and recovery taking place at the rear side of the indenter.

Pelletier et al. [44] have suggested a model to predict the recovery occurring behind the indenter and the pile-up formation ahead of it. This model is based on a parameter , defined as the ratio between the strain imposed by the indenter and the maximum strain a material can accommodate without yielding. This has been called *rheological factor* and it has been found to be function of the ratio between the elastic modulus and the yield stress and of the indenter geometry:

$$X = \frac{E}{\sigma_y} tan\beta \tag{3.4.3}$$

Where E is the Young modulus, σ_y is the yield stress and β is the attack angle (figure 3.15). Another parameter has been introduced to characterize the pile-up formation. This is the ratio between the contact depth h_c and the penetration depth h, and it is called *shape ratio* c^2:

$$c^2 = \frac{h_c}{h} = 0.25339 lnx + 0.5017, X < 80 \tag{3.4.4}$$

$$c^2 = \frac{h_c}{h} = 0.0684 lnx + 1.2984, X \geq 80 \tag{3.4.5}$$

According to this model, the shape ratio can be considered as function of the rheological factor only. Finally, the load bearing area is influenced by the recovery angle α, which can

be related to the rheological factor too:

$$\alpha = \frac{1}{b + dX} \tag{3.4.6}$$

Where b and d are constant values related to the indenter geometry. Hence, starting from the rheological factor X, through these equations, the contact depth h_c and the recovery angle α are estimated; then, with geometric considerations the contact radius and the contact area are calculated. Finally, these values are utilized to evaluate the scratch hardness. According to this model, material with similar rheological factor X would have similar contact depth and recovery angle, hence similar load bearing area and material recovery. Similarly, material with not so different X would have similar pile-up of material. However, this has been experimentally disproven [18]. An example of that disagreement for a set of polymers can be seen in figures 3.16, 3.17 and 3.18. This means that the rheological factor alone is not able to describe the complexity of the scratch phenomenon accurately. Therefore, the ratio between the elastic modulus and the yield stress is not the unique important parameter, but other factors, such as the flow properties of the material, strain hardening and the viscoelastic characteristics may have considerable influence on the scratch behavior.

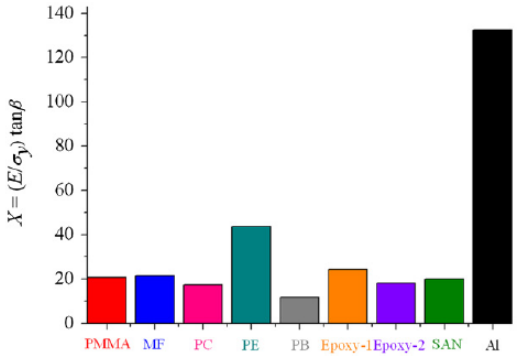

Figure 3.16: Rheological factor of materials calculated for a strain rate of $10^{-2}s^{-1}$ [18]

Despite the possibility to evaluate the scratch hardness, more or less accurately, using one of the above mentioned methods, its correlation with the scratch visibility is still to be analyzed. In the past, the projected load bearing area was usually expressed in function of the scratch residual width. It has been demonstrated that the scratch width is not always a

measure sensitive to the material nature, and the material scratch hardness evaluated in this way has shown to have very poor correlation with scratch visibility [10, 32]. On the other hand, if the scratch hardness is evaluated expressing the load bearing area as a function of the scratch depth, a good correlation between scratch hardness and scratch visibility exists. Therefore, the lower the scratch depth, the lower the scratch visibility [39]. However, it is worth to stress out that scratch visibility is complex parameter, which is not ascribable to a single parameter, like the groove depth only. Indeed, it depends on the amount of light scattering, which depends on the size and type of the damage features, and on the contrast with the undamaged background [16].

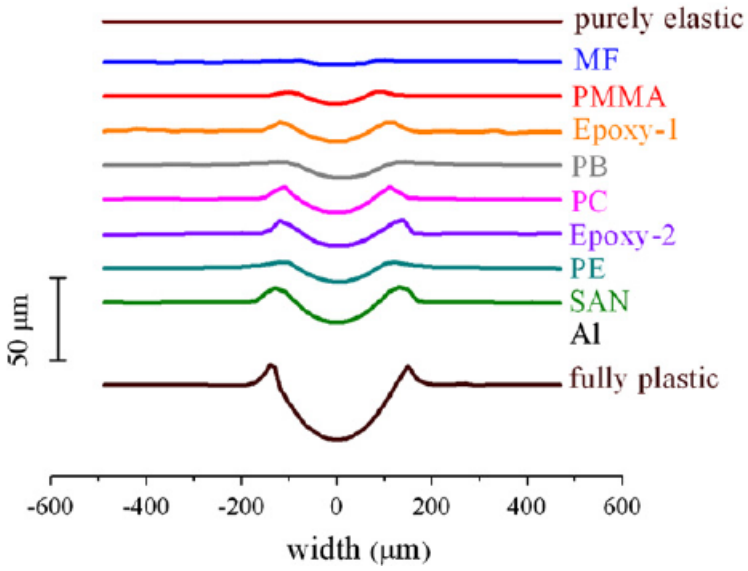

Figure 3.17: Profiles of the transverse sections of the scratch tracks. The profile of the fully plastic material was obtained by taking X = 1000. [18]

A possible improvement in the estimation of the scratch hardness is to evaluate that during a progressive load test [32]. Usually, the scratch hardness has been evaluated in constant load scratch tests. Instead, if this is evaluated in a progressive load scratch test, it is possible to estimate the scratch hardness for a range of load, and not for only one. The value obtained is not free from errors, but it is a significant improvement respect the conventional method. To do so, a graphic method is usually adopted. Through an image analysis tool, the geometry of the scratch track is analyzed and the projected load

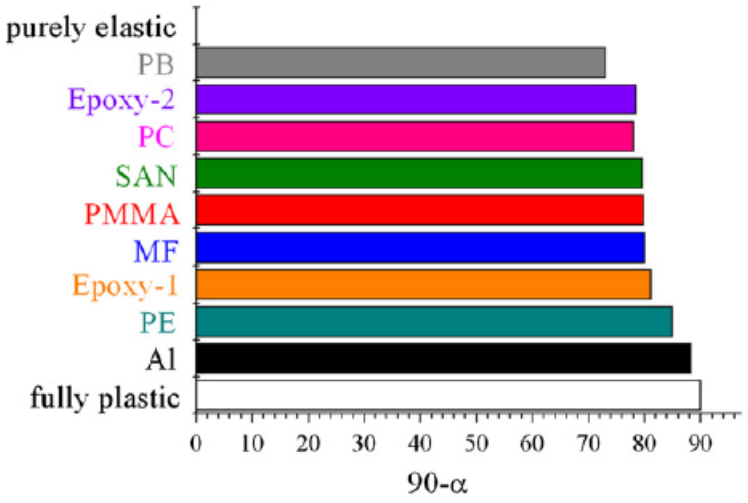

Figure 3.18: The angle representing the area not in contact with the indenter [18]

bearing area evaluated. Then, the applied normal load is plotted against the load bearing area; the scratch hardness is the slope of the obtained curve. The obtained curves for a set of polymers is shown in figure 3.19. It is possible to note that the curves are almost straight lines, and this means that the scratch hardness is constant whatever the applied load. The robustness of this graphical method seems to hold, even though the possible effects of stick-slip motion and skin-core morphology. The former results in local variation of scratch width, due to periodic accumulation of stress and plastic deformation ahead of the tip, and consequent release of strain energy. The latter highlights the presence of different morphologies depending on the penetration depth: amorphous near the surface, transition zone, and a deeper crystalline zone. These zones show different hardness, and depending on the depth of penetration of the tip, the scratch hardness may change. However, the effects of these two phenomena are found to be negligible.

Scratch hardness of TPOs is influenced by the content of rubber, by the content of filler, by the geometry of the indenter, by the test temperature and scratch velocity [18, 19]. In the analysis of the effects of these factors, it is worth to remember that the scratch hardness of polymers depends on the elastic modulus and yield strength, mainly.

Rubber is included in the polymeric material to improve the impact strength and to obtain a “soft touch” for the component. However, scratch hardness diminishes as the rubber content increases, and its decrease is related to the reduction in the yield stress and elastic

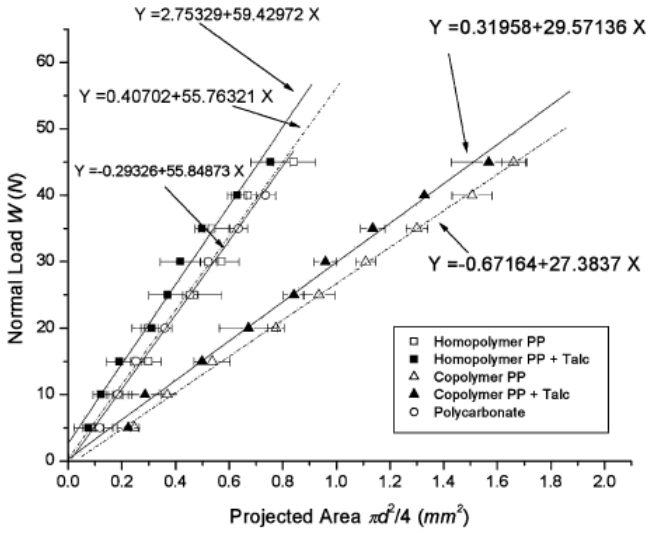

Figure 3.19: Graphical method of obtaining scratch hardness for different materials [32]

modulus (figure 3.20).

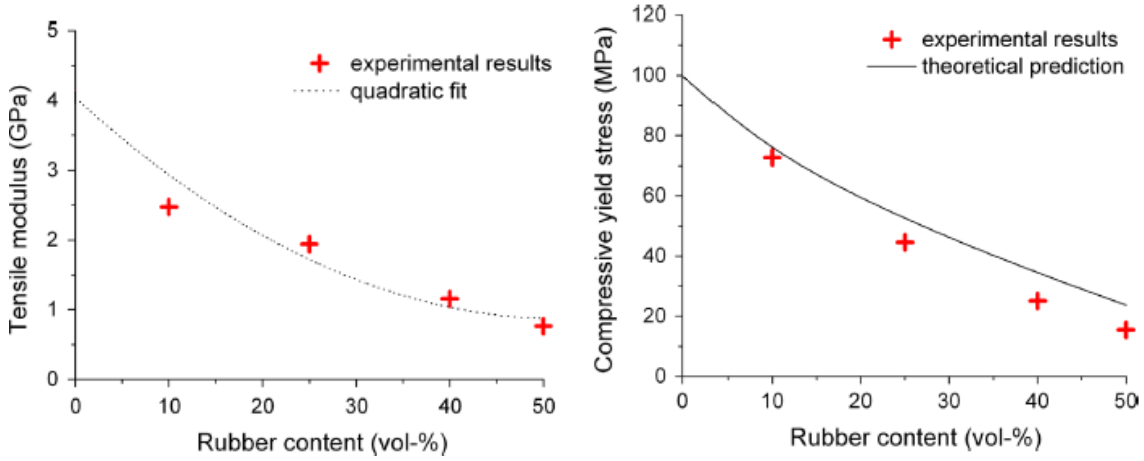

(a) Elastic modulus **(b)** Yield stress

Figure 3.20: Effect of rubber content on the modulus and yield stress of SAN. This trend can be generalized to other polymers [19]

The incorporation of fillers in a polymeric matrix usually results in a scratch hardness enhancement. This increase in scratch hardness seems to be related to two main causes. Firstly, fillers can improve the bulk mechanical properties (mainly the elastic modulus as shown in figure 3.21, while the yield stress is almost unaffected), but the main cause of

scratch hardness increase is the mechanical interaction between the indenter and the filler particles. Indeed, filler particles oppose higher resistance to the indenter penetration and motion, limiting the deformed area.

Generally, the scratch hardness of polymers presents a decreasing trend with the cone

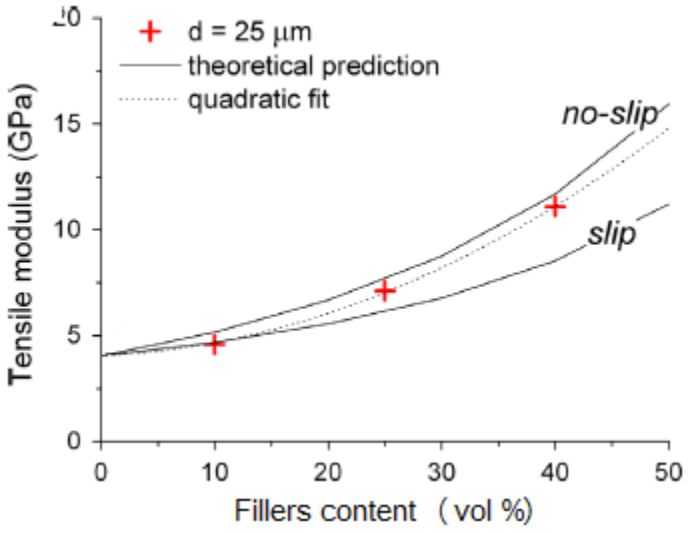

Figure 3.21: Effect of fillers content on the modulus of SAN. This trend can be generalized to other polymers [19]

angle, it decreases at higher bulk temperature because of bulk softening heating, and it increases at high scratching speed, despite the interfacial heating [1, 11]. Indeed, frictional heat has less time to dissipate at high speed, thus it does not dissipate in the bulk of the polymer. Moreover, high speed causes strain rate induced hardening; thus, the material provides greater resistance to deformation, so larger scratch hardness.

3.5 Scratch deformation maps

Wear deformation maps were first built for metals, with the purpose of identifying the dominant wear deformation mechanism among all the possible mechanisms and analyzing the way these wear modes interact each other, varying some important parameters. *Briscoe et al.* [1, 11] have taken this principle, and they have applied that to the scratching of polymers. Scratch deformation maps have been constructed, and they have become one of

the method to assess the scratch behavior of polymers. These scratch deformation maps are able to show the influence of the applied normal load, of the sliding velocity, of the indenter geometry and of the temperature on the surface deformation mechanisms of polymers.
Polymers are characterized by a large number of surface deformation mechanisms, even though the ranges of variation of the test parameters are narrow. Indeed, under different contact conditions the scratching phenomenon for polymers is generally accompanied by a number of surface deformation mechanisms, which are dictated by the relative energies of the potential dissipation processes at the contact area. Practically, the proportions of the different deformation mechanisms vary naturally, seeking for the minimization of the dissipated energy requested for the material displacement process. This means that under certain conditions, the dominant scratch deformation mode is the one, which requires the least amount of energy dissipation.
An example of scratch deformation maps is showed in figure 3.22. It is possible to note that the observed mechanisms depend on the applied load and strain and on the structure of the polymer. At low loads and low strains, the specimen can undergo a deformation characterized by a ductile flow of material around the indenter tip; this is called viscoelastic ploughing and no evidence of failure could appear. At more severe conditions, the nature of the polymer plays an important role. Amorphous materials (more brittle) present cracks on groove edges inside it; semi-crystalline materials are featured by regular formation of cracks inside the groove, due to the periodic squeezing and reaching of the elastic limit of the material in front of the indenter. Under severe conditions, non-amorphous materials show completely brittle deformation accompanied by the formation of chip (machining), while semi-crystalline materials could undergo cutting, which constitutes of deep grooving and cracks due to surface tearing. Possible ironing could occur at mild conditions; this is a smoothing of the surface with no detectable failure, generally caused by blunt indenters.

Therefore, typical scratch deformation modes are the following:

- Ductile ploughing. This is a plastic deformation or accommodation of the indenter motion without fractures. Its regime is usually at low load and sharp indenter, and at intermediate cone angles ($60° - 90°$) and higher load. If at intermediate cone angles the load is lower, an elasto-plastic deformation accompanies ductile ploughing.

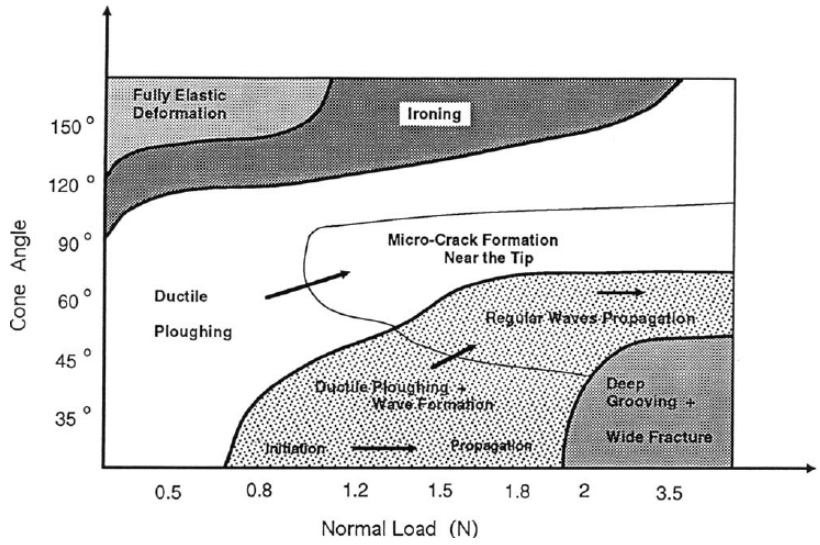

Figure 3.22: Scratch deformation map for PE. The picture shows results from scratch tests performed at room temperature for a range of cone angles and normal loads and at a scratching velocity of 2.6 mm/s [11]

- Edge cracks. They are brittle cracks which run perpendicularly to the scratch groove. Usually, these occur with sharp cone angle and high load.
- Brittle machining and chip formation. They happen at very high load and sharp cone.
- Deep grooving. At the highest load and sharpest cone angle.
- Ironing. With blunt indenter ($> 90°$), the deformation passes from ductile ploughing to this phenomenon, which consists mainly of elastic deformation of contact asperities and some plastic deformation. If the applied load is very low, entirely elastic process, so full material recovery, occurs.

Obviously, different polymers will show different proportions of the deformation mechanism due to their nature [1]. Ad example, the brittle PMMA shows a wide range of brittle fracture and machining with high strain and load, while the more crystalline UHMWPE presents a very wide area of viscoelastic deformation, and brittle damage modes do not occur until very severe conditions are approached. This difference between the two materials is due to the higher viscoelastic nature of UHMPE. Scratch deformation maps were

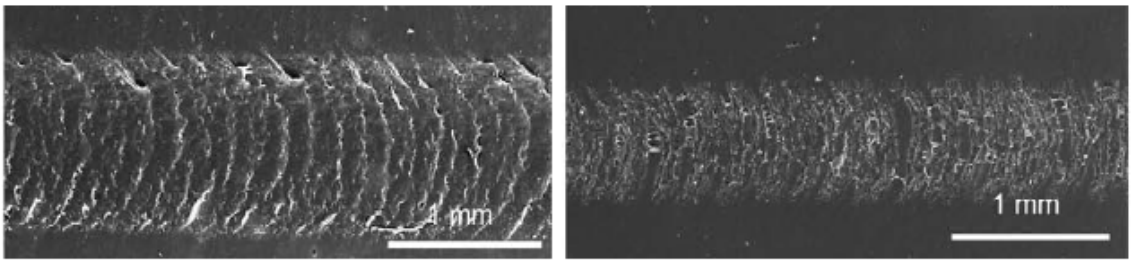

(a) 1 mm/s **(b)** 100 mm/s

Figure 3.23: Surface damage of TPO at different testing rate: (a) 1 mm/s and (b) 100 mm/s [22]

obtained testing the different material through a lever-type machine, using a specific indenter geometry and constant normal load and speed. Then the deformation mechanisms is investigated and positioned on the map. The procedure is then repeated varying the indenter and/or the load; at the end a scratch deformation map for a specific material at a certain speed is obtained. To evaluate the influence of speed and of temperature, maps at different speed and temperature have been constructed.

Initially, a speed increase leads to a more brittle scratch response [11]. Indeed, the typical fish-scale pattern can disappear leaving place to pseudo fish-scale pattern, cracks and/or craze. Figure 3.23 shows the damaged surface of a TPO, highlighting the differences due to the different adopted test speed. This can be explained considering that a strain rate increase, due to the increase of speed, leads to a more brittle response. As a consequence, on the deformation map, the regions of machining, microcutting and brittle fracture have become larger. On the deformation map, the ductile ploughing region becomes wider, as shown in figure 3.24, where the scratching velocity is lower than the one utilized for the map of figure 3.22. However, further increase of the scratching velocity leads to an opposite behavior: reduction of the brittle deformation region and promotion of ductile deformation modes. This can be understood considering the larger energy dissipation induced by the higher scratching speed. The dissipation of this energy on the surface and into the polymer leads to local heating, which rises the temperature in the contact area. High temperature enhances the viscoelastic properties of the material, suppressing the brittle deformation modes.

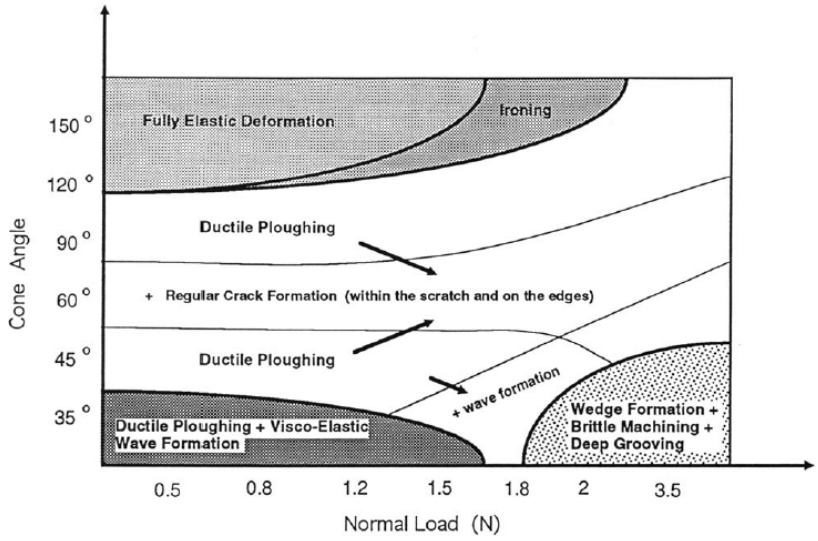

Figure 3.24: Scratch deformation map for PE. The picture shows results from scratch tests performed at room temperature for a range of cone angles and normal loads and at a scratching velocity 0.0026 mm/s [11]

From what it has been stated above, it is possible to deduce the effect of the temperature. Indeed, if the test is performed not at ambient temperature, but in a warmer environment, the brittle failure area is suppressed and the region of ductile ploughing is enlarged [11].

3.6 Scratch visibility

The resistance to surface damage of polymeric materials utilized for car interiors is important for two reasons: mechanical integrity, and aesthetic appeal. The important parameter for the latter purpose is scratch visibility. It is worth to stress out that the main goal of the improvements of surface damage resistance is to avoid and/or diminish the damage at all, but, when this is not possible, it is important to find ways to hide the actual damage. Scratch visibility is a complex parameter, because it is an optical characteristic related to a mechanical damage, and the establishment of modifications to reduce that are all but simple. This phenomenon is due to complex surface deformation and damage of polymers surfaces, which interact with the light, triggering the human eye perception of the scratch. In the literature, there are several attempts to explain the nature and the causes of scratch

visibility.

Scratching of thermoplastics can induce a whiter appearance, causing the so-called stress whitening. Indeed, transparent or translucent polymeric materials exhibit enhanced opacity and a whiter color leading to an increase in optical brightness. This is related to the passage from elastic deformation to plastic deformation, which involves the formation of microzones, because of crazing, cracking, debonding, the nucleation of microvoids and cavities, and the formation of stretched fibrils [6, 12, 13]. All these features are almost $\sim 1\ \mu m$ big, so they are able to interact with light because their size is similar to the wavelength of light (0.6 μm); thus, they are responsible of light scattering, which causes the damaged area to appear lighter.

It was found that the stress whitening entity also depends on the number of phases in the base resin [6]: the more the phases in the polymeric material, the whiter the appearance of the surface. This because microzones and voids nucleation is fostered by the debonding of additives (fillers, slip agents or rubber) from the polymeric matrix. If the bonding forces between the particles and the matrix are weak, e.g. if the particles are big, the breaking of the bonds is easy and the whitening level of the scratched area is high because of light scattering. Hence, one way to reduce surface whitening and to improve the scratch resistance is to enhance the adhesion forces between the additives and the polymer matrix, ad example by the use of coupling agents.

In addition to additive-matrix debonding, fillers (especially talc) can contribute to the increase of stress whitening because of delamination or exposure of their particles on the surface. The forces, and the consequent deformation, involved in the scratching phenomenon, cause this. Wollastonite seems to behave better than talc [13]; even though wollastonite-filled materials show similar fracture features, plastic deformation (which leads to stress whitening) is smaller and the debonding between wollastonite and the resin is hidden by the plastic deformation in the resin phase. Therefore, fillers, and in particular talc, play a dual role in scratch resistance: they improve the mechanical properties of material, leading to a smaller damage, but at the same time, the scratch visibility increases significantly due to the massive formation of voids and exposed talc particles on the scratched surface.

Stress whitening is highly influenced by polymer crystallinity [10]. Indeed, crystallinity is

important because of its bond with elastic modulus and yield stress. The reduced scratch damage and reduced white appearance relative to an increase of the crystallinity degree are attributed to the high modulus and yield stress of this materials.

Kody and Martin [12] have suggested that the scattered light, which is responsible of the scratch visibility and dictates the reflected light intensities, is caused by both fluctuations in the refractive index, due to voids formation, and birefringence changes, due to molecular orientation during plastic deformation. In their work, they have measured the reflected light intensity off the polymer scratched surface together with the light source intensity, by means of a light meter. This measurement has been compared to the average reflected optical light scattering intensity indicated by an image analysis software. It has been possible to estimate relative contributions of the two phenomena (voids formation and birefringence from orientation) by performing the measurement at different sample orientation: the sample has been rotated around the z-axis, and the two limit measurements (B = brightest = maximum intensity, and D = darkest = minimum intensity) have been considered. The scheme of this procedure is shown in figure 3.25. Then, two parameters were defined. The light scattering average S_a (between B and D) gives the mean light scattered of two positions, so due to refractive index fluctuation due to voids, and the light scattering difference S_d, which represents the reflected intensities changes as the sample is rotated, so caused by birefringence changes due to molecular chain orientation.

$$S_a = \frac{B + D}{2} \tag{3.6.1}$$

$$S_d = B - D \tag{3.6.2}$$

Both S_a and S_d have increased with the talc content, thus both microvoids and orientation have increased with it.

Rangarajan et al. [15] have proposed an optical imaging system that captures the relevant optical parameters (light intensity, spatial and angular distribution of light) necessary for the evaluation of the optical contrast, exploiting angle resolved light scattering measurements and geometric optics. The basic principles on which this procedure relies are:

1. people are more sensitive to sharp contrast rather than changes in the absolute intensity level;

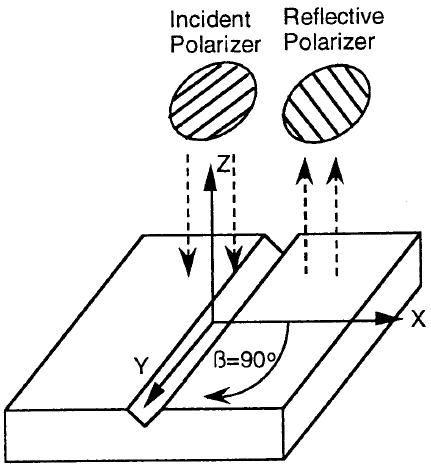

Figure 3.25: Schematic of light-scattering measuring apparatus. The samples are rotated under the crossed polarized lenses around the Z-axis. Sample position, β, is the angle between the polarization direction of the incident lens and the strain or scratch direction [12]

2. contrast is the stimulus which triggers the eye perception of the scratch;

3. the perceived visual quality is a combination of the measured optical contrast and human sensitivity to that.

Through the measurements of light scattering intensities of the damaged area and virgin background, in two different configurations, named specular and off-specular geometry, four optical parameters were determined. Those characterize the scratched area and its background and they are fundamental for the evaluation of optical contrast between the scratch and its surroundings that triggers the human eye perception of the damage. These are:

- the specular-background intensity, which is the intensity of the reflected light in the specular direction of the virgin surface;
- the specular-optical width, which is the width of the intensity drop at the scratch;
- the off-specular background scattering intensity, which represents the diffuse scattering from the undamaged area, and it is a combination of scattering from pigments and from surface roughness. Surface roughness causes a loss of specular intensity as well as an increase in the off-specular intensity;

- the off-specular scratch intensity, which is the scattering caused by the scratched area. It contains information about the portion of the scratched area that induces scattering.

The calculation of contrast from these it is not simple, because of the complex relationship between visual perception and damage. An example of the light intensity measurement is shown in figure 3.26.

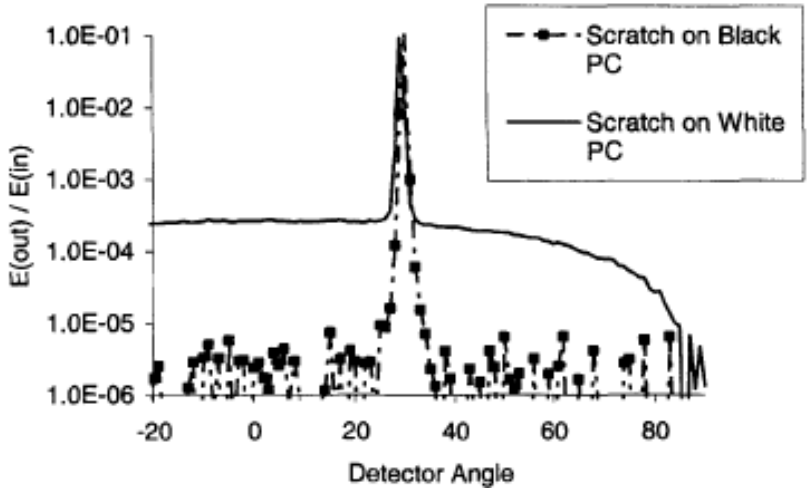

Figure 3.26: Angle-resolved scattering from scratches on black and white PC samples. Both samples exhibit similar specular intensity but the white sample shows much greater scattering at off-specular angles. Intensity is plotted on a logarithmic axis. [15]

Jiang et al. [16] have analyzed scratch visibility considering the way surface and light interact. Indeed, the light reflected by the surface ρ consists of specular reflection ρ_{sp}, diffractional scattering ρ_{dd} and multiple/subsurface scattering ρ_{ud}:

$$\rho = \rho_{sp} + \rho_{dd} + \rho_{ud} \tag{3.6.3}$$

While the first one is contained in the specular reflection cone, the second one has a directional distribution, as shown in figure 3.27. The last component is uniformly distributed and can be considered the background light reflection. It has been found that for smooth surfaces, whose roughness is lower than light wavelength, the specular reflection is the main component of the reflected light. On the other hand, if the surface roughness is similar or larger than the light wavelength, the specular reflection diminishes and the directional diffuse reflected field becomes dominant. By the utilization of a progressive load scratch

test (ASTM D7027), it has been established that at the beginning of the test, so at low load, only smooth ironing exists [16] and the scratch groove surface profile is changed, without variation in the surface roughness. Thus, the alteration of surface light scattering, which may trigger scratch visibility, is caused by the specular reflection from the raised groove profile along the scratch path (pile-up on the side). As the test proceeds, so the applied normal load increases, surface damage mechanisms such as periodic ductile drawing (i.e., fish-scale) and/or microcracking significantly vary the roughness of the scratch. The change in roughness causes the diffraction scattering component to dominate the total intensity of the reflected light reducing the specular component. Therefore, scratch visibility in these scratch conditions is due to diffraction scattering [16]. The influence on scratch visibility,

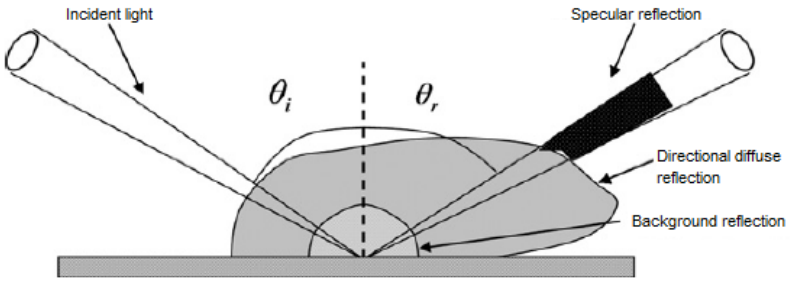

Figure 3.27: Components of surface light reflection [16]

so on the critical load for visibility onset, of the different directions of laser scanning with which the ASV software acquires images has also been studied. The lowest critical load occurs for the perpendicular orientation of the sample; the highest occurs for parallel scanning. This is the result of how the incident light interacts with the scratch groove, which is represented in figure 3.28. In perpendicular orientation, the light encounters the groove shoulder causing over-lightening and shadowing; thus, specular reflection from the change of the scratch groove profile can induce sufficient contrast for scratch visibility. On the other hand, in parallel scanning orientation, the incident light illuminates uniformly the groove area, with little shadowing. Then, it is the change of surface roughness the dominant factor for scratch visibility. In figure 3.29 it is shown an example of what stated above: for a certain TPO, there exist two different critical loads for onset of scratch visibility depending on the direction of the laser scanning.

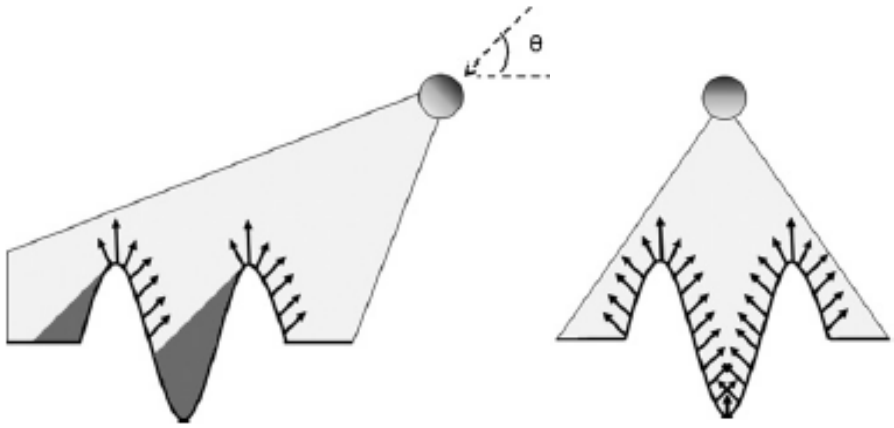

(a) Perpendicular orientation **(b)** Parallel orientation

Figure 3.28: Illumination of scratch path by incident light [16]

Thanks to the development of the ASTM D7027 / ISO 19252 scratch test, it has been possible to collect more information about the scratch visibility nature and on the influent parameters. Generally, a TPO tested according this procedure shows three regions [21, 22, 34]. The first region is called mar and it is characterized by a smooth, compressive-type damage that slightly scatters the light and alters the surface gloss. As the load increases, the scratcher tip starts pulling the material beneath in a ductile manner; the scratch groove is characterized by a parabolic fish-scale pattern. Further load increase leads to severe damage, where the tip penetrates deeper in the surface starting to displace the material around it; this is the last region. The onset of scratch visibility, considered as the point where the scratch damage can be seen by human eye, has been found to verify close to the beginning of periodic fish-scale pattern caused by stick-slip motion. Through SEM analysis of the scratch cross section, a yield zone was detected, which was not present before. Hence, it is possible to state that the scratch visibility is related to this yield area, which implies a transition from elastic to plastic deformation. Even though plastic deformation triggers the human sensibility to the scratch presence, brittle deformation mechanisms are even worse because the larger light scattering related to them; hence, ductile deformation mechanisms are better than brittle ones from a scratch visibility point of view.

The scratching speed can influence the scratch visibility, causing a reduction of the measured

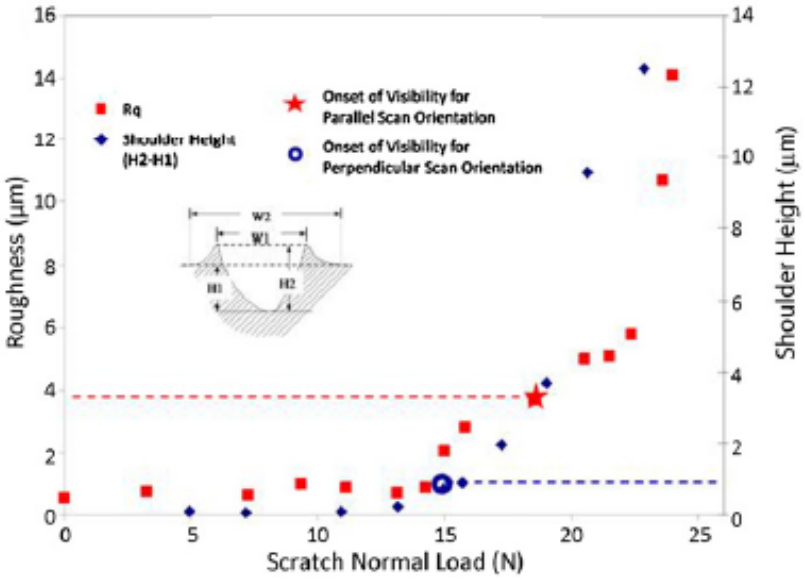

Figure 3.29: RMS surface roughness and shoulder height as a function of scratch normal load [16]

critical load, thus a worsening of the material scratch visibility resistance. Moreover, it has been discovered that an initial high surface roughness, like a wide and gross texture, is beneficial. Indeed, high roughness backgrounds are able scatter more visible light, hiding the scratch and delaying the onset of scratch visibility.

More recently, *Hamdi and Sue* [2] have proposed a new parameter for the quantification of scratch and mar visibility. Utilizing, again, the progressive load scratch test ASTM D 7027, they have plotted the contrast between the damaged area and the undamaged background against the applied normal load. The slope variation of these curves has been considered as representative of the surface damage visibility; this means that samples with lower rate of contrast change have higher surface damage visibility resistance. Good agreement between this quantity, and the results from both human survey on scratch visibility of the tested samples and of the ASV software prescribed by the ASTM D7027 scratch test has been found. Therefore, the rate of contrast change can be considered as a measure of scratch and mar visibility.

3.7 Friction

Friction is the resistance force opposite to motion direction, which develops at the interface of two elements in relative motion. It can be expressed as the product of the normal load L and the coefficient of friction μ:

$$F_f = \mu L \tag{3.7.1}$$

This coefficient has two natures: stationary or dynamic. The stationary coefficient corresponds to the force necessary to start the motion, while the dynamic one is relative to the tangential force needed to maintain the motion. The dynamic coefficient of friction is lower than the stationary one. In polymer sliding and/or scratching, this is thought to arise from energy dissipation phenomena in two different regions close to the sliding surface [26, 27, 50]. These regions are called interfacial and deformation region, and they are displayed in figure 3.30.

The adhesion component of friction comes from energy dissipation processes occurring in a small region very close to the interface. The modes of energy dissipation resemble plastic shear or fracture, which can happen both at the interfacial layer and at the original surface. The second contribution to friction comes from plastic flow and viscoelastic losses energy dissipation modes occurring in a much larger volume of material near to the contact. This component of friction is called deformation or ploughing/grooving component. Since these usually do not interact each other, it is possible to study them separately.

The adhesion term is the result of physical adhesion forces that form between the two surfaces in contact. Those are atomic/molecular interactions, which can occur because of the low distance between the two rubbing elements [27]. These interactions are due to several types of intermolecular bonding forces:

- Dispersion forces. These result from momentary dipole generating from electron movements. Two to three orders of magnitude less strong than covalent bonds;
- Dipole interactions. These are due to permanent dipole present in the materials because of poles formation due to electronegativity. Their magnitude is two orders of magnitude lower than the one of covalent bonds. Moreover, a permanent dipole can induce a dipole in the adjacent molecule, even if this is not polar initially. This

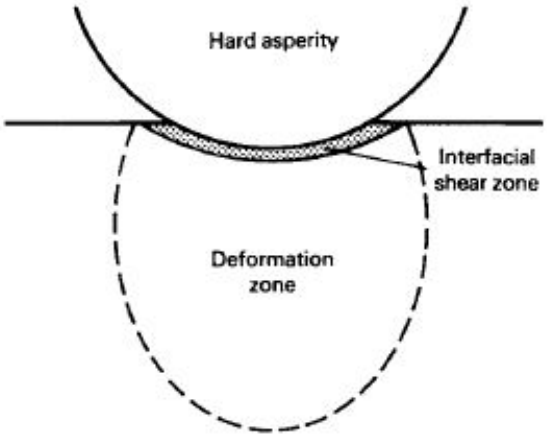

Figure 3.30: Schematic of the two friction dissipation zones occuring at the contact between the polymer surface and a hard asperity [50]

increases the strength of the permanent dipole itself, and the adhesive forces due to the induced dipoles are called induction forces;

- Hydrogen bonds. Hydrogen atom acts as a bridge between adjacent chains. This is the strongest among the intermolecular bonds;
- Ionic interactions. Between ions with different charges; they occur only in a particular group of polymer.

Intermolecular forces determine the surface energy. This can be split into two components depending on the type of intermolecular forces they result from:

$$\gamma = \gamma_d + \gamma_p \tag{3.7.2}$$

Where γ_d results from dispersion forces, while γ_p from polar forces. When two bodies are in contact, the Dupr's equation holds:

$$\gamma_a + \gamma_b = \gamma_{ab} + W_{ab} \tag{3.7.3}$$

Where the l.h.s. term is the sum of the surface energy of the two materials, while γ_{ab} is the interfacial energy of the contacting surfaces and W_{ab} is the work of adhesion per unit of surface area. To separate the two bodies, a work equal to W_{ab} has to be supplied. The work

adhesion can be calculated from the surface energies of the two surfaces and the interfacial energy, which can be determined from wetting angle measurements. Therefore, the surface energies are important in the sliding process. Indeed, during sliding, adhesive bonds are repeatedly formed and broken, thus a energy loss is involved in that process; this loss can be described through the surface energies of the involved materials. The adhesion work provides a measure of the effect of adhesive contacts.

The deformation term results from the deformation which material undergoes as soon as the contact starts. Indeed, during sliding, the asperities of the harder surface penetrate in the softer surface, and they displace material ahead of each asperity, generating pile-up of material with a bow wave appearance. Material is continuously displaced in the motion direction, and the surface layers are subjected to continuous alternating stress. The displaced material interacts with the sliding counterface, opposing resistance to the motion. Two cases are most common: simple plastic flow or cutting and elastic or viscoelastic grooving. In the second case, some of the energy that is fed in the polymer ahead of the contact is restored in the rear of the contact. The energy loss is related to the energy input and the properties of the material. It was found strong relationship between the deformation component of friction and the bulk properties, and different deformation mechanisms involve different resistance to motion [26, 27].

Jiang et al. [34] analyzed the influence of load and surface roughness on the friction. They have defined a parameter called scratch coefficient of friction SCOF, which is the ratio between the tangential force and the normal load, which can be express as:

$$SCOF = \mu_s + \mu_r \tag{3.7.4}$$

Where μ_s is the traditional surface sliding coefficient and μ_r represents additional scratch resistance force due to various deformation mechanism (like crazing, ploughing, cracking, etc.). Through this parameter, the transition in the deformation regime of the polymeric materials, from elastic to plastic regime, and between different deformation mechanisms during the ASTM D7027 scratch test can be addressed. Their results are shown in figure 3.31. It is possible to note that a certain level of roughness leads to the reduction of the SCOF, and, at a certain level of roughness, the higher the load the higher the friction coefficient. Moreover, the sensitivity of the friction coefficient to the applied load is higher

if the surface roughness is high (higher roughness lead to higher increase of the friction coefficient with load increment). Finally, it has been observed that the dependence of the friction coefficient on the roughness diminishes as the load increases; it seem that above a certain load level, all the surfaces present the same friction coefficient. These behaviors can be explained considering the contact between the polymeric surface and the smooth indenter (figure 3.32). Since two surfaces are in contact only at the asperity tips, the rougher the surface, the less will be the number of asperity contacts with the smooth counterface; thus the lower will be the tangential force required to move the indenter, so the smaller will be the friction coefficient. On the opposite, a smoother surface has more contact points with the counterface, so higher friction. When a high load is applied, localized compressive deformation occurs, which increases the actual surface of contact, so friction. It is obvious that the rougher the initial surface, the higher the effect of applied load increase, so the larger the increment in the friction coefficient. Therefore, the reduced SCOF together with the capability of scattering more visible light, hiding the surface damage, give to the polymer surface with high roughness improved scratch visibility resistance.

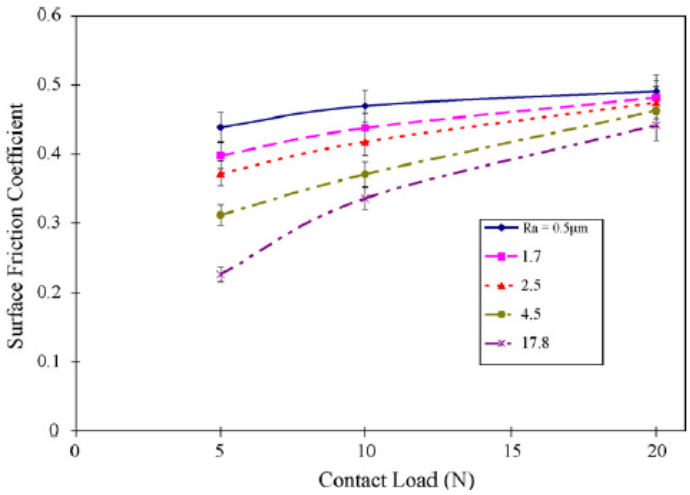

Figure 3.31: Effects of roughness and contact load on surface friction coefficient [34]

Considering the plot of SCOF against the applied load in figure 3.33, the influence of the latter on the scratch behavior has been retrieved. At low load level, friction mainly occurs on the surface, and the traditional component of friction dominates in the SCOF

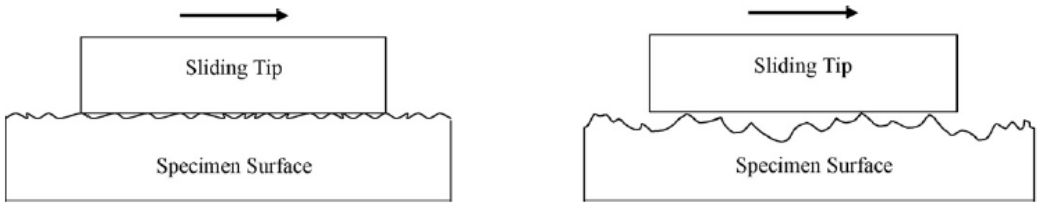

(a) Low surface roughness **(b)** High surface roughness

Figure 3.32: Illustration of roughness effect on the contact area of a smooth sliding tip surface against a surface [34]

equation. As the load increases, SCOF increases for two reasons: the traditional friction component increases because of larger contact area, and the other component of friction, related to the deformation mechanism, increases because of the inherent material resistance. This higher SCOF allows for the formation of fish-scale pattern. Further load increment would lead eventually to deeper penetration of the indenter into the polymer. There, the SCOF component related to material ploughing resistance is the major contribution, and the effect of the surface roughness and traditional friction component ceases. Because of that, all the tested plaques converge to the same SCOF value.

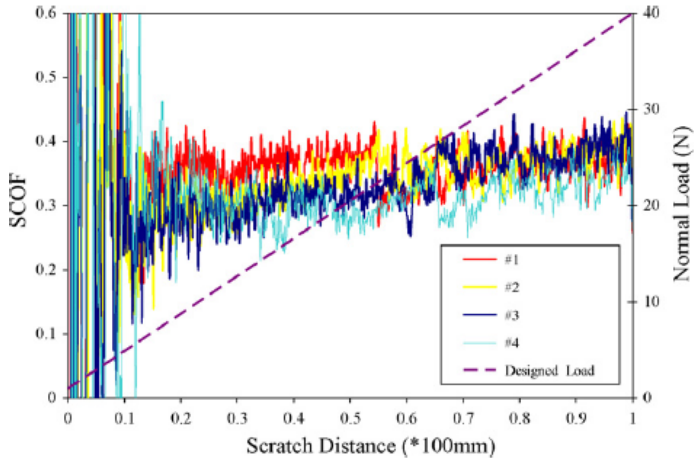

Figure 3.33: Scratch coefficient of friction (SCOF) vs. applied normal load for model TPO system with variation in surface roughness [34]

Wong et al. [32] have combined plot of the friction force vs. scratch distance with the images obtained through SEM analysis. They have discovered that large peaks of the

friction force occur at distances corresponding to transitions in the damage modes, so relationships between the friction force and the surface damage appear to exist. Moreover, the evolution of the friction coefficient, so its varying rate of increase has been proven to be related to the different damage modes occurring in scratching. To confirm further this thesis, a material that does not show any change in the damage mode has been analyzed, and it was found that the friction force and coefficient show a nearly constant slope over the entire scratch process.

Friction can be influenced also by scratching speed, temperature and environmental conditions.

The sliding or scratching of two contacting surfaces always involves some thermal effects. It is known that friction is a dissipative phenomenon where energy is converted into heat and the thermal state is a critical factor for the performances of a friction unit. The heat generation can come from the deformation of the contacting asperities during sliding or also by the origination and following breakdown of the adhesion bonds. Polymers are very sensitive to frictional heating, also because their viscoelastic characteristic, and variation in temperature affects both the shear strength of junctions and young modulus, but generally not at the same extent. Hence, the observed increase of temperature may increase or decrease the friction, depending on the particular polymer considered [25, 49].

For what concerns the scratch velocity, it is assumed that the friction is not influenced by that as far as the temperature contact varies insignificantly [49]. Anyway, the separation between temperature and speed is not possible, thus the interface behavior changes with sliding velocity. *Myshkin et al.* [49] stated that in the range $0.01 - 1.0\ cm/s$, the friction is unaffected by the sliding speed, while outside this interval, it exists a relationship between the temperature and the sliding velocity, which can be connected to the viscoelastic behavior of polymers. At low speed, the viscous resistance increases with speed, while at high speed, the elastic behavior dominates and the friction depends on the sliding velocity only slightly, or it diminishes with it. Moreover, at high velocity, the contact time is short, reducing additionally the friction force. At intermediate velocity, all the above-mentioned factors are in competition, thus a maximum of the friction force appears at a speed, which depends on the polymer properties. The friction vs. sliding speed behavior depends a lot

on the testing temperature: if this is close to the glass transition temperature, the influence of the speed on friction is intensified, while at lower temperature, there is limited influence only.
Environment can influence the friction of polymers, but usually the effects are much small than those for metals and this is also one of the reasons why lubricants can not be used effectively in the reduction of friction of polymers [25].

3.8 Wear

Wear can be defined as the progressive loss of material from the surface of a body due to relative motion and rubbing with a counterface. It involves three steps [33]:

1. Deformation of the surface asperities to support the load applied by the other body involved in the sliding process;
2. Detachment of some material from the surface;
3. Removal of the previously detached material from the contacting region.

No wear occurs until the last passage has been completed. This means that detachment of material from the surface is not enough to cause wear, but other processes, leading to the expulsion of the loose material in debris form from the contacting area, must occur. Indeed, it is possible that the detached material do not exit from this region, but it could undergo other type of processes, which may impede the material to be expelled. Wear is a process of great complexity, and the most important parameter is the wear rate. In its expression, the time factor is generally substituted by the sliding distance to make easier the comparison between different tests; thus, wear rate is defined as the volume of worn material, divided by the sliding distance.
Wear processes classification has gathered high attention during the past, but it is not well established even in present days. The problem in the classification relies on wear nature itself: wear is a system property, so it depends either on the properties of the considered materials, either on the sliding conditions [29]. In the past, four main schemes of classification were proposed (table 3.2), but all of these have failed in making clear

Table 3.2: Types of wear classification

Imposed conditions	Phenomena	Debris production route	Mode of asperity contact
Rough/smooth surface, corrosive enviroments, abrasive particles	Mild/severe, oxidation, transfer, seizure	Delamination, cutting, tearing, fatigue, cavitation, spalling, pitting, adhesion	Interfacial/bulk deformation, elastic/plastic displacement

distinction between the processes of particle detaching from a surface and the following ones leading to wear debris formation. Indeed, as stated above, particles detached from the surface rarely create immediately debris, but they are usually trapped in the contact zone and subjected to different processes. Processes responsible of debris formation may or may not be the same as those involved in particle detachment. Because of that, the above-mentioned classifications are unsatisfactory. The most widely accepted wear classification is the one distinguishing between five main wear mechanisms: abrasion, adhesion, fatigue, corrosion and erosion. However, it should be kept in mind that particles detachment and wear debris formation result from combinations of the above-mentioned wear mechanisms, which could operate either simultaneously or successively.

Abrasive wear involves the cutting or ploughing action of a hard asperity of one surface on the other, or of a hard particle included in one of the two surfaces. A simple model exists for metals, in which the removed volume of material is proportional to the applied normal load, the sliding distance and the tangent of the slope of the asperity and inversely proportional to the hardness of the softer material. This model holds for metal, but it is unsatisfactory for what regards polymers. The wear behavior of polymers is more complex, and one of the reason is the number of different deformation modes that a polymer can undergo. Ad example, smooth surfaces may deform elastically, while rough surface are more likely to deform plastically. Because of that, attempts to correlate wear of polymer to parameters predominantly plastic, like indentation hardness, were vane. *Ratner et al.* [25, 29, 33] have highlighted the importance of the elongation to break in the abrasive

wear process, and they have delineated the debris production as a sequence of three stages. Initially, *(1)* the surface deforms to bear the load, to an area of contact determined by the hardness, *(2)* then relative motion is contrasted by a frictional force, and *(3)* finally the material at contacting points is disrupted. The last step involves an amount of work equal to the integral of the stress-strain relationship, which can be approximated to product of the ultimate tensile stress S and the strain at failure ϵ. Thus, the removed material per unit sliding distance W is considered proportional to the probability of completion of the three stages:

$$W \propto \frac{1}{H} \times \mu L \times \frac{1}{S\epsilon} \tag{3.8.1}$$

Moreover, *Ratner et al.* [25, 29, 33] has included an additional term called damage efficiency, which account for the fact that not all the strain at rupture is involved in particle detachment, but significant part can be recovered elastically. Additionally, this takes into account the possibility of debris to reduce effective load, so wear rate. Good agreement has been found between this model and the experimental values, thus the product $S\epsilon$ plays a fundamental role in abrasive wear. Therefore, the worn volume is related to a quantity, which is representative of the toughness or strength of the bulk of the material.

Fatigue wear consists of material removal as a result of cyclic stress variations. Fatigue can be thought as a thermally activated process, in which the applied stress reduces the activation energy barrier for material chemical bonds rupture. In the widely accepted theory, the fatigue wear rate is inversely proportional to the number of cycles to failure n, and the fatigue properties of plastics are characterized by a relationship of the form:

$$n = \frac{\sigma_0}{\sigma}^{b_f} \tag{3.8.2}$$

Where n is the number of cycles to fail at an applied stress σ_0, σ is the ultimate strength of the material in a single application of stress and b_f represents the fatigue properties of the material. However, it is not always clear the point at which conventional abrasive wear turns into fatigue wear, but fatigue has appeared to be the dominant wear process in sliding of polymers (especially rubbers) against rounded asperities. Usually a combination of these is present in sliding of polymers, and wholly abrasive wear can only occur for the most rigid plastics sliding against very rough counterface. Fatigue wear is more sensitive to tempera-

ture changes than abrasive wear. Indeed, a temperature increase reduces the stress required to exceed the activation energy barrier, leading to a reducing of the fatigue life and to an increase of the wear rate. On the opposite, in abrasive wear the stress is already sufficient to exceed the activation energy barrier, and the effect of a temperature rise is much less important, until thermal softening has been reached [25, 33].

Adhesive wear involves the action of adhesive forces between the two sliding elements, that cause transfer of material from one surface to another; the transferred material can detach from the opposite surface later on, causing wear [33]. This is the most complex wear types among those possible for polymers. It is almost impossible to insulate and characterize it as an independent process because it enters in all the wear types. Adhesive wear could be considered as the permanent minimum occurring when all other wear factors are eliminated. Considering the evolution of the wear rate as the sliding distance increases, this initially experiences a rapid increase, then it gradually decreases until a stationary value is reached; then the wear rate keeps constant and the worn volume is proportional to the applied load. This evolution of the wear rate is attributed to the gradual reduction in roughness of the counterface, caused either by the formation of a polymer transfer film on the counterface, or by rounding of metal asperities by wear. The formation of this film changes the type of contact and the surface topography. The type of transfer layer, shown in figure 3.34, changes depending on the type of polymer: irregular lumps for rigid and brittle material, coherent film that decreases the roughness of the metal for more ductile polymers. Generally, wear rate seems to decrease with time as the transfer layer develops. Indeed, once the layer has formed, if the adhesive forces between it and the counterface are strong enough to retard the detachment of it, the wear is reduced. Hence, the stronger the adhesive forces, the lower the wear rate. When adhesive forces are involved in polymer sliding, the Archards law [63], which states a proportionality between the load and the worn volume, does not hold anymore. Indeed, this law holds if and only if changes in load do not cause changes in any other properties. Since with polymers, changes in load lead to frictional heating and changes in the apparent area of contact, it seems that the above rule is not valid, and the relationship may be merely empirical and valid for specific combination of materials, speed and load range and geometry of contact. Speed variations have effect on the wear rate too;

speed changes lead to frictional heating, which is somehow more sensitive to speed than to load. It was found that wear rate against speed shows a maximum, then a minimum and again a rapid growth. These can be explained considering that the main effect of speed increase at low speed is to raise the strain rate leading to a reduction in the elongation to fail, so wear rate increases. Above a certain speed level, the surface has reached a temperature sufficient to soften the polymers giving further ductility to the material; this reduces the wear rate. Finally, the surface temperature is so high that it melts the polymer, material is extruded out of the contact zone and wear rate sharply increases [29, 33].

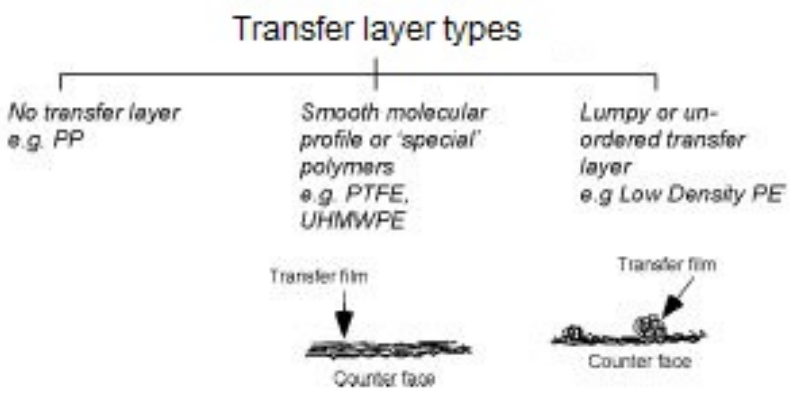

Figure 3.34: Types of transfer layers for certain semi-crystalline polymers when slid against a hard smooth surface [51]

The widely accepted wear classification of polymer is due to *Briscoe et al.* [51, 52], which discerns between interfacial and bulk deformation wear. In their study, authors have suggested that since the frictional energy, released at the contact spots, can be dissipated according two different mechanisms (interfacial or bulk/cohesive), two different wear mechanism can be deducted from them. This model has the merit of making the distinction between mild deformation, as the cohesive wear, and the more energy intense interfacial wear. The distinction comes from the extent of the deformation in the polymer material caused by the rigid asperity of the counterface (figure 3.30). In interfacial wear, the frictional energy is dissipated mainly by adhesive interactions, which lead to a more confined deformation, while in the cohesive wear by both adhesion and abrasive (subsurface) inter-

actions, so a deeper deformation [51, 52].

Fillers influence a lot the surface topography, and since its importance in the wear process, they influence the wear rate too. The transfer layer is affected by the presence of fillers, which may be included to improve the transfer layer adhesion, retarding its detachment from the counterface [26]. On the other hand, some of the fillers introduced may be abrasive towards the counterface. Moreover, water and organic fluids may inhibit the transfer, or plasticizing the polymer modifying the transfer properties. Therefore, these are part of the reasons of the irregular behavior of polymers in dry sliding.

The last two wear processes are erosive and corrosive wear [33]. Their importance is negligible compared to the above ones. Erosive wear is due to the relative motion between a solid and particles embedded in a fluid. Further division can be done between abrasive type erosion (fluid flow parallel to the surface) and impingement type erosion (fluid flow perpendicular to the surface). In corrosive wear the wear rate determining factor is chemical reaction with the environment, and it is a minor concern for polymers.

Chapter 4

Materials and Experimental Procedures

In this chapter, the detailed description of the utilized materials is provided, and the procedures followed during the experimental work are explained. Then, the ways the results of interest have been collected and organized are described.

4.1 Materials

Two materials have been provided by FCA for testing. Those are labelled as *CPN 4718* and *CPN 4919*, but from now on, they will be called as *Material A* and *Material B*, respectively; they are similar thermoplastic polyolefins, with few differences. In table 4.2 the main properties of these two are highlighted. They are copolymers, with a polyolefin base (polypropylene) and a rubber (EPDM or EPM), with several types of fillers and additive. Material A is a ductile $-20\ ^{\circ}C$ PP copolymer, which already contains scratch additive in its base. It is a talc filled polymer, very common in European automotive interiors applications. Material B is unfilled, $-30\ ^{\circ}C$ ductile PP copolymer, which is very widespread in North America car interiors applications. The material was provided in form of plaque on which six different textures are present. Texture types are listed in table 4.1, where MGD stands for Modified Gloss Diffusion, and it is an additional modification of the base texture, utilized to obtain low gloss surfaces. It consists of a micro-laser generated overlay technol-

Table 4.1: Texture types. Information coming from the technical data sheet provided by suppliers to FCA

Texture	Appearance	Characteristics	Label
Dayton	Animal	Random peak height, Random/irregular spacing, deep depth	A
Austin ML	Animal	Round peaks, Non-random spacing, deep depth	B
Shadow	Stipple	High peak count, Shallow depth, Sharp peaks	C
FF500 Initial	Animal	Small/round/smooth plateaus, Random irregular spacing, Deep depth	D
Dayton + MGD	Animal	Random peak height, Random/irregular spacing, deep depth	E
Austin ML + MGD	Animal	Rounder peaks, Non-random spacing, deep depth	F

ogy developed and translated to in-mold texturing applications. It diffuses the reflective light on the molded part resulting in low gloss, rich realistic texture finishes on all types of plastics.

Material A was provided only in one type, while Material B was provided in a variety of grades:

- With and without scratch additives;
- Resulting from 3 different injection molding processes (LDR 25:1, LDR 50:1 and precolor);
- In two colors (black and white).

When suppliers injection molds plastic components, they do that by using pellets of the resin and can either add colorant at the press or run pre-colored resin. In the case of coloring at the press, natural PP resin (white-ish colored pellets) is blended with a color concentrate that contains not only the pigments for color but also additives for stabilization, such as UV or heat, and it can also contain scratch packages. In this case, “50 : 1” or “25 : 1”

Table 4.2: Main properties of two materials. Information coming from the technical data sheet provided by suppliers to FCA

	Material A	Material B
Melt flow index $[g/10min]$	20	25
Density $[g/cm^3]$	1.03	0.9
Tensile yield stress $[MPa]$	19.5	21
Flexural modulus $[MPa]$	1900	1070
Notched Izod impact $[kJ/m^2]$		
@ 23 $°C$	48	30
@ -40 $°C$	8	8
Heat deflection temperature @ 0.45 MPa $[°C]$	107	86

refers to the letdown ration (LDR) of the color concentrate so would be incorporating 2% or 4% colorant pellets with natural pellets at the press for molding the part, respectively. In the case of "precolor", the resin supplier provides the pellets already compounded with color, additives, etc. for subsequent molding so will not be as sensitive to blending/mixing capability as when using color concentrate.

4.2 Wear tests

The samples are square plaques, of 1×1 $inch$, cut from the plaques supplied by FCA. Before testing, the surfaces of the sample that are not going to be tested have been rubbed on sandpaper sheet to get rid of all the residual debris formed during the cutting procedure. Then, the samples have been washed with acetone and dried with air. The utilized counterface are hardened stainless steel balls with a radius of 5 mm. Before and after testing, each sample and counterface has been weighted to evaluate the worn mass, hence the worn volume through the utilization of the density of the material; the values obtained are the average of three weighings. With reference to figure 4.1 *(b)*, the samples were positioned and clamped in the rotating platform, and the ball is located in the ball holder.

The performed tests were ball-on-disc wear tests, carried out on the universal micro-tribometer shown in figure 4.1 *(a)*, utilized in the rotative configuration. This machine is able to provide a rotating speed from 0.001 to 5000 rpm, and the utilized load module is able to exert a normal force from 0.2 up to 20 N. The tribometer is positioned on an air table, which is able to insulate the workplace from disturbing vibrations coming from the environment. The machine is able to perform both linear and rotating wear tests, depending on the mounted module, and the indenter or counterface shape can be of several type, depending on the selected holder.

Material A has been selected to be tested with the purpose of evaluating the texture and

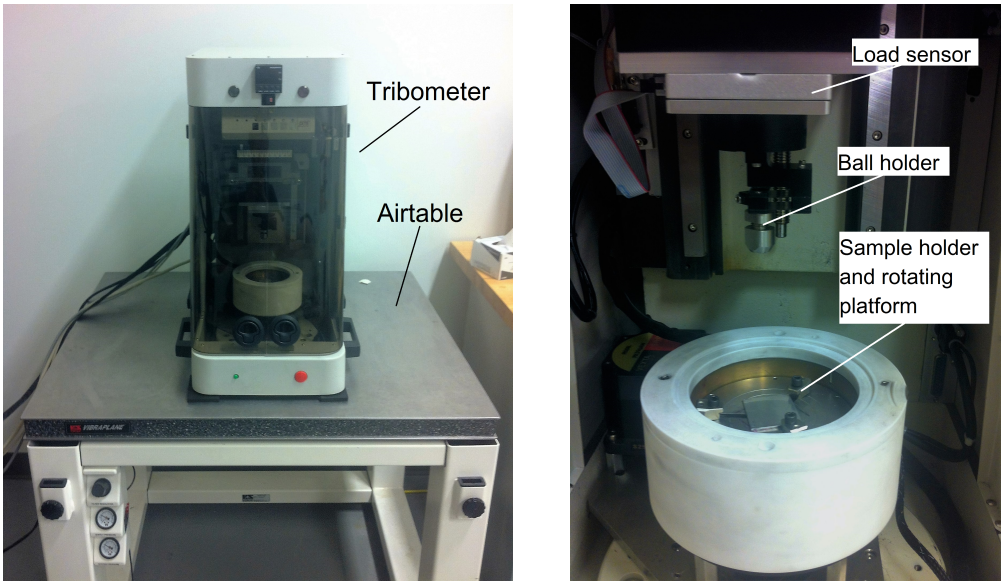

(a) Tribometer **(b)** Tribometer details

Figure 4.1: Machine apparatus utilized in testing: (a) universal tribometer, and (b) detailed view of the rotating platform and sample and counterface holders

load effect. For each texture, three samples have been obtained and tested under different load. The normal loads selected are 5, 7.5 and 10 N. Those are normal loads typical of the most commonly utilized polymer scratch and wear tests.

Material B has been tested to evaluate the influences of the presence of scratch additives, of the injection molding characteristics and of the color. To evaluate the influence of them, it has been chosen to test the Material B in the most critical condition, hence at 10 N of

Table 4.3: Test plan for Material A

Test number	*Texture*						*Load[N]*		
	A	B	C	D	E	F	5	7.5	10
1	■						■		
2	■							■	
3	■								■
4		■					■		
5		■						■	
6		■							■
7			■				■		
8			■					■	
9			■						■
10				■			■		
11				■				■	
12				■					■
13					■		■		
14					■			■	
15					■				■
16						■	■		
17						■		■	
18						■			■

normal load. Not all the textures have been tested, because the effect of them has been already evaluated with Material A; hence, the selected texture for testing of Material B was the Austin ML (texture B), because it has proven to be the one with the lowest worn volume and wear rate under this testing load. The test plan utilized in this study is summarized in table 4.3 and 4.4. The tests have been performed for one hour each. The ball holder have been positioned in a way to obtain a circumference of 8 mm radius, and the rotating speed has been set to 120 rpm. That has been designed to resemble the 100 mm/s linear speed, which is a typical scratching speed utilized in the most common scratch and mar tests.
The samples have been weighted before and after the ball-on-disk wear test, so the weight loss could have been computed. From the data about the weight loss M, expressed in grams, considering the specific weight of the material ρ, the volume loss V values have been

Table 4.4: Test plan for Material B

Test number	*Injection molding characteristics*			*Additive*		*Color*	
	LDR 25:1	LDR 50:1	Precolor	NO	YES	Black	White
1							
2							
3							
4							
5							
6							
7							
8							

calculated:

$$V = \frac{M}{\rho_s} \tag{4.2.1}$$

The wear rate is computed by dividing the worn volume by the sliding distance.

During the test, the machine have monitored the normal load, the friction force, and the friction coefficient (COF), defined as the ratio between the two:

$$COF = \frac{F_f}{L} \tag{4.2.2}$$

Also the vertical displacement of the indenter, needed to maintain the set normal load, has been measured during the test. This can be considered as the instantaneous depth of penetration, necessary to maintain the normal load prescribed by the test.

4.3 Microstructural analysis of worn surfaces

Once the tests are performed, the samples are dried. Then, they are analyzed through the high quality optical microscope shown in figure 4.2 *(a)*, to understand the deformation/damage mechanism and its features.

4.4 Surface profilometry

The worn surfaces are analyzed through the surface profilometer reported in figure 4.2 *(b)*, to evaluate the geometry of the damage, the pile-up on the wear track side, the depth of the damage and the difference in roughness between the obtained damage and the background, which are known to be indicative of the surface damage resistance of polymers and important for the damage visibility.

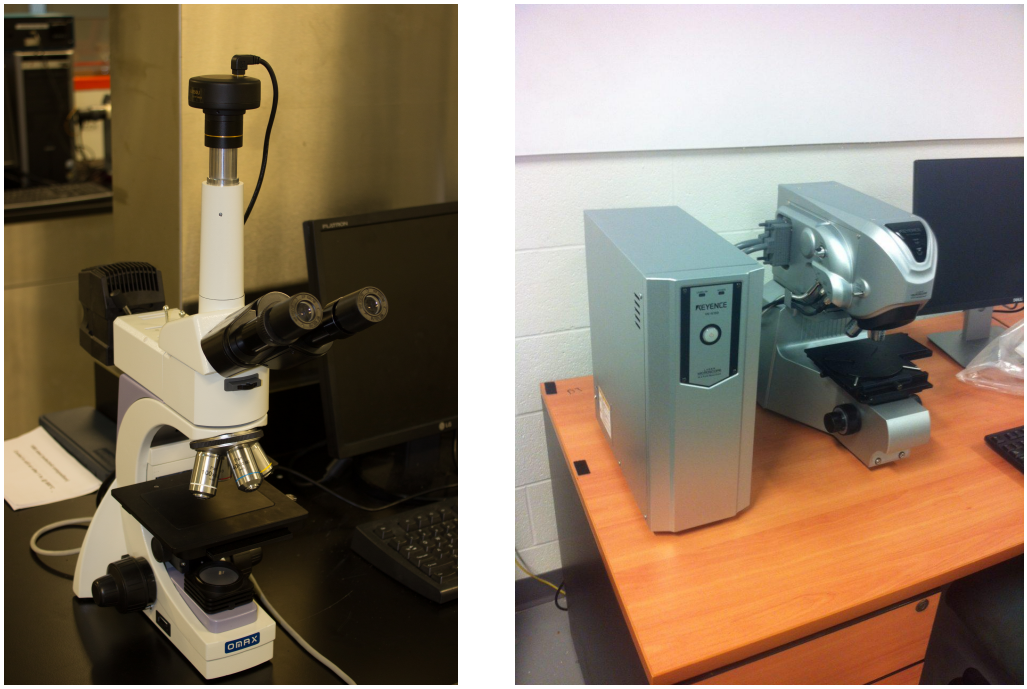

(a) Optical microscope **(b)** Surface profilometer

Figure 4.2: Equipment utilized in samples analysis

4.5 Spectrophotometry analysis

The worn samples are analyzed through the use of the portable spectrophotometer shown in figure 4.3. This machine is able to measure the CIELAB Color Space coordinates (L^*, a^*, b^*) of surfaces (figure 4.4 *(a)*), so it captures the way the surfaces, and the damage, interact with light. In particular, it is known from the literature that the important parameter for surface damage visibility is the L^*, which is measure of the surface lightness. As shown

in figure 4.4 *(b)*, the instrument is able to perform multi-angle color measurements. In this study, the measurements at angle of $-15°$, have been chosen, because this angle has proven to capture the variation due to the damage, consistently with what actually is seen by human eye.

Figure 4.3: Utilized portable spectrophotometer

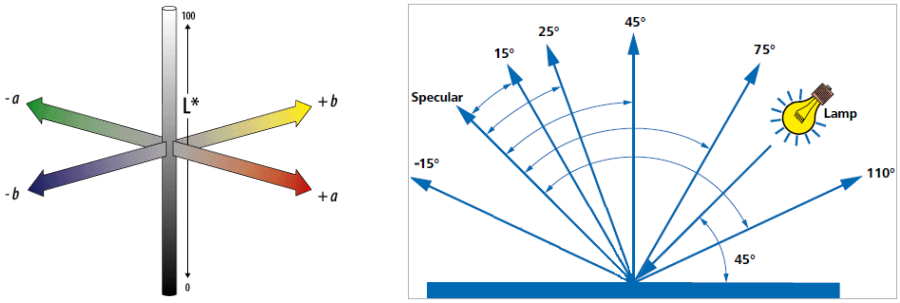

(a) CIELAB space **(b)** Multi-angle measurements possibility

Figure 4.4: Spectrophotometer working principle

4.6 ANOVA

ANOVA is a statistical tool which allows to understand if one or more factors (and their interaction) are *significant* regarding the investigated phenomenon. Furthermore, by the calculation of the percentages of contribution, it is possible to quantify the effect of the significant factors on the phenomenon [61, 62]. It presumes the possibility to split the variance in two components: a variance internal to the groups (WITHIN) and a variance among the groups (BETWEEN). Through the comparison of these two, it is possible to determine which factors are significant, and which are not. Since this tool needs a full factorial plan, and since the texture is known to be the most important factor among those considered, the ANOVA analysis has been performed in the case of Material A only. The analysis is so-called *two-ways ANOVA*, because the factors considered were two: applied normal load and texture. The phenomena, on which the significances of these two factors have been evaluated, were wear rate, penetration depth, raised shoulder (pile-up on the sides), roughness variation and damage visibility.

In this thesis, experiments have been performed only once, because of the high repeatability of the utilized equipment. When no repetitions are available, in the ANOVA, the interaction between factors is embedded into the residual, that means to consider it as non-significant. This is what is done in this thesis too. Hence, the interaction between applied normal load and texture has been considered non-significant and included into the residuals. The software utilized for the completion of this task is MINITAB®.

Chapter 5

Results

In this chapter results and images gathered during the experimental work are shown. The obtained graphs of the worn volume, wear rate and coefficient of friction (COF) are shown. The images showing the microstructure of the damage and the $3D$ representations are included, and the geometry measurements (damage depth, raised shoulder and roughness variations) are reported. Finally, the pictures of the tested samples and the damage visibility measurements are presented, and at the very end, the ANOVA analysis results are illustrated.

5.1 Wear rate

5.1.1 Texture effect

Considering the Material A, the volume losses at different normal loads, for different textures are compared in table 5.1, while the wear rate, defined as the worn volume divided by the slid distance, are plotted, against the normal load utilized during the tests, in figure 5.1. Since the sliding distance utilized for all tests is the same, there is a direct relationship between the worn volume and wear rate; this means that the sample showing the largest worn volume, presents the highest wear rate.

The counterfaces have shown no wear, as it was possible to forecast. Moreover, no transfer layer has been detected. Loose debris have formed, but these are easily detachable from the counterface by air. From the collected data, it has been possible to note a variation of the

Table 5.1: Worn volume [mm^3] of different textured sample of Material A

Textures		*Load [N]*		
		5	7.5	10
Texture A	Dayton	0.39	1.88	2.98
Texture B	Austin ML	1.00	2.04	2.91
Texture C	Shadow	1.20	2.30	3.66
Texture D	FF500	1.46	1.39	3.01
Texture E	Dayton +MGD	0.42	1.55	3.40
Texture F	Austin ML+MGD	0.19	1.26	3.50

best and worst in class with load change. Indeed, the texture showing the lowest wear at 5 and 7.5 N (texture F), does not show the lowest wear at 10 N; there, the best is texture B. Similarly, the worst texture at 5 N (texture D), is different from the worst at 7.5 and 10 N (texture C). Therefore, there is an interaction between surface texture and normal applied load. The load effect is visible on the wear rate curves. Two groups of curves can be made:

- In one group the wear rate against normal load is almost a straight line, without slope change. The textures in this group are the textures named Shadow, Austin ML and Dayton (texture A, B, C);
- In the second group, the slope of the curve changes. Above 7.5 N the slope is higher, thus the wear rate sensibility to normal load is higher. Textures in this group are the textures named FF500, Austin ML+MGD and Dayton+MGD (texture D, E, F);.

5.1.2 Scratch additive and injection molding process effect

As stated above, tests on the material labelled as Material B have been performed to analyze the influence of the injection molding process characteristics, scratch additives content and

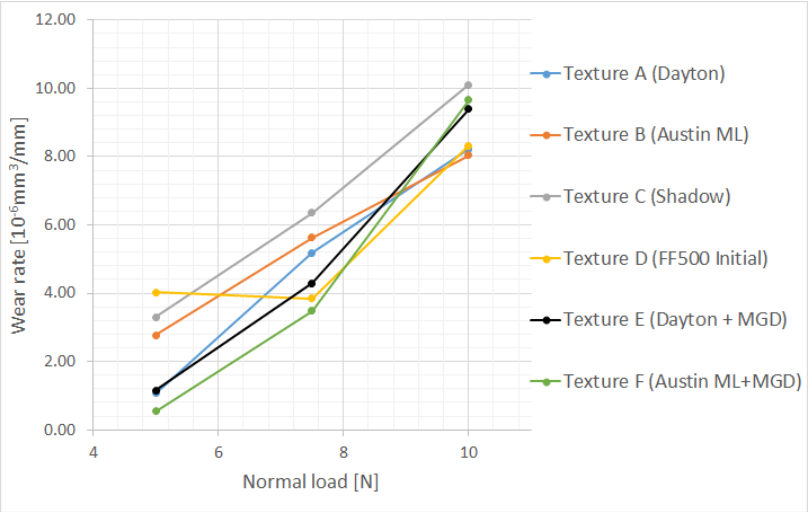

Figure 5.1: Wear rate against normal load for tested textures of Material A. A sharp change in the curve slope is visible in three curves (texture D, E and F), indicating a change in the deformation mechanism

plaque color. In figure 5.2, the volume loss of each sample is shown. In figure 5.3, the value of the wear rates are presented. The worst sample is the one with LDR 25:1, thus with the highest amount of color concentrate; if no scratch additive are considered, the best one is the precolored sample. Considering the sample with LDR 50:1, if scratch additives are included, the wear rate drops from 7.06 $\times 10^{-6}$ mm^3/mm to 2.15 $\times 10^{-6}$ mm^3/mm for black sample, and from 5.94 $\times 10^{-6}$ mm^3/mm to 1.23 $\times 10^{-6}$ mm^3/mm for white sample. On the opposite, scratch additives have a negative effect on the precolored samples: scratch additives lead to higher worn volume and wear rate if included in this material type.

5.1.3 Color effect

From figure 5.2 and 5.3 it could be pointed out that white plaques wear less that black one. However, color has influence on the perception of the surface damage, but it should not have any effects on the quantitative characterization of it: color is not a factor influencing the amount of worn volume and the value of wear rate. Therefore, these differences are attributed to random differences between the plaques from which the samples have been obtained, and not to the different color.

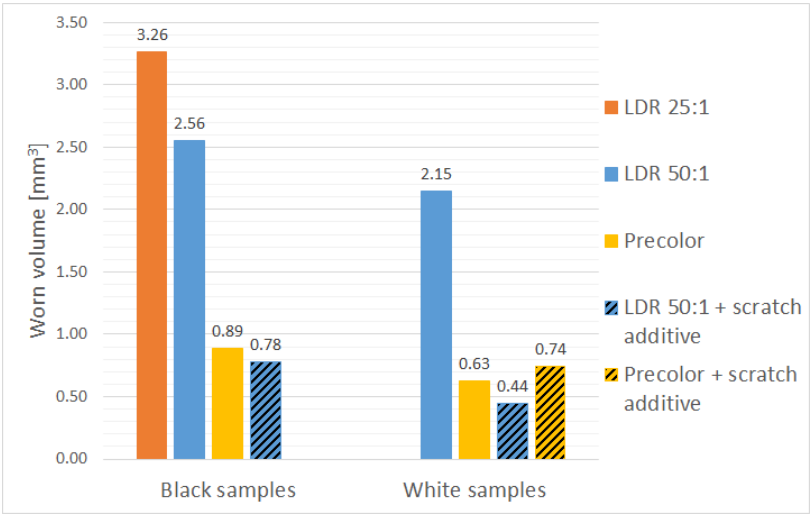

Figure 5.2: Worn volume of Material B samples. The opposite effect of the scratch additives on the LDR 50:1 and precolor sample is evident

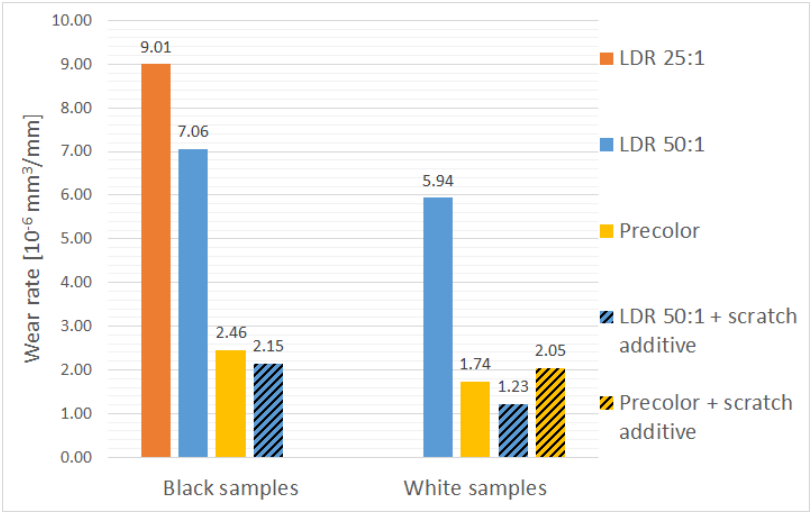

Figure 5.3: Wear rate of Material B samples. The opposite effect of the scratch additives on the LDR 50:1 and precolor sample is evident

5.2 Coefficient of Friction (COF)

As stated in previous section, the normal load, the friction force and the coefficient of friction (COF) have been monitored during the test. In figure 5.4 and 5.5, the evolution of the COF along the test is reported for the three utilized normal loads, for two textures of Material A. These figures report the evolution of the friction coefficient just in the first 20 seconds of the tests, to better highlight the oscillations amplitude affected by textures. In figure 5.6 and 5.7 the COF for different grades of Material B are shown. It is possible to note that the global evolution of the COF is the same in all the cases, with only differences in the initial peak, in the amplitude of the oscillations, and very small difference between the final steady-state values.

The friction coefficient increases sharply at the beginning of the test. It reaches its maximum in less than 10 seconds, then it starts to decrease. This rapid increase can be related to the static friction coefficient, which is known to be higher than the dynamic one. Indeed, to start sliding, the indenter has first to win the static friction force opposed by the polymeric surface. Once this force has been overtaken, the force required to maintain the motion is lower, so the COF diminishes. Once the maximum has been passed, COF diminishes, then it oscillates around a certain constant value (or the average trend can be considered slightly increasing). This means that the surface-counterface couple has reached a steady-state situation, in which the COF slightly increases with the carry on of the test, because the larger amount of material that is worn off and displaced aside.

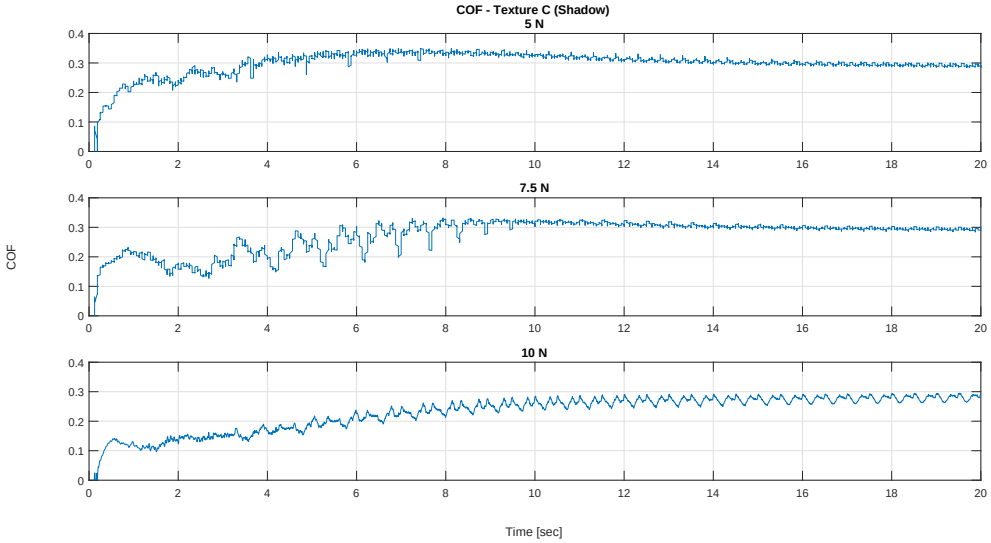

Figure 5.4: COF against testing time for Material A sample with texture C recorded during testing: 5 N case at the top, 7.5 N case in the middle, and 10 N case at the bottom. The graphs show the recorded COF in the first 20 seconds to display the oscillations due to the texture

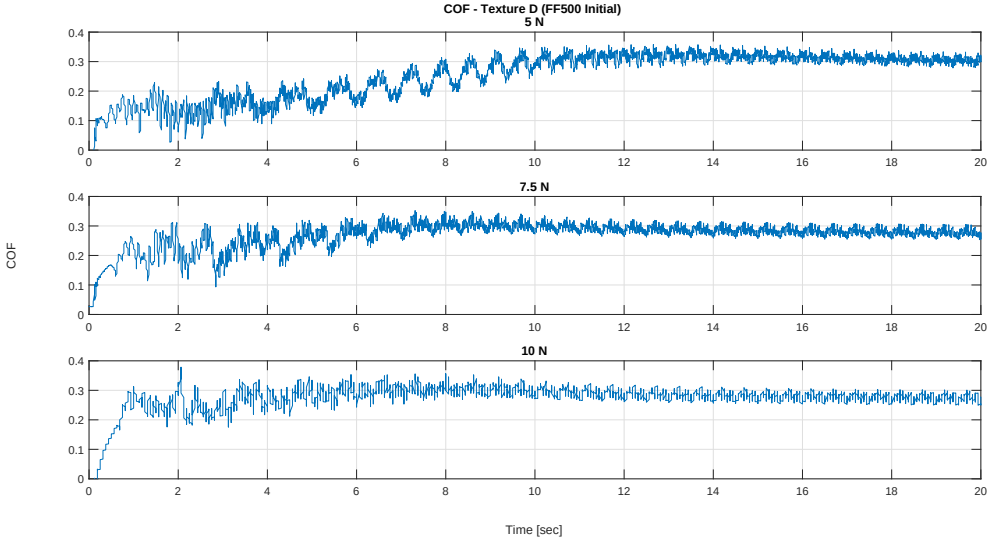

Figure 5.5: COF against testing time for Material A sample with texture D recorded during testing: 5 N case at the top, 7.5 N case in the middle, and 10 N case at the bottom. The graphs show the recorded COF in the first 20 seconds to display the oscillations due to the texture

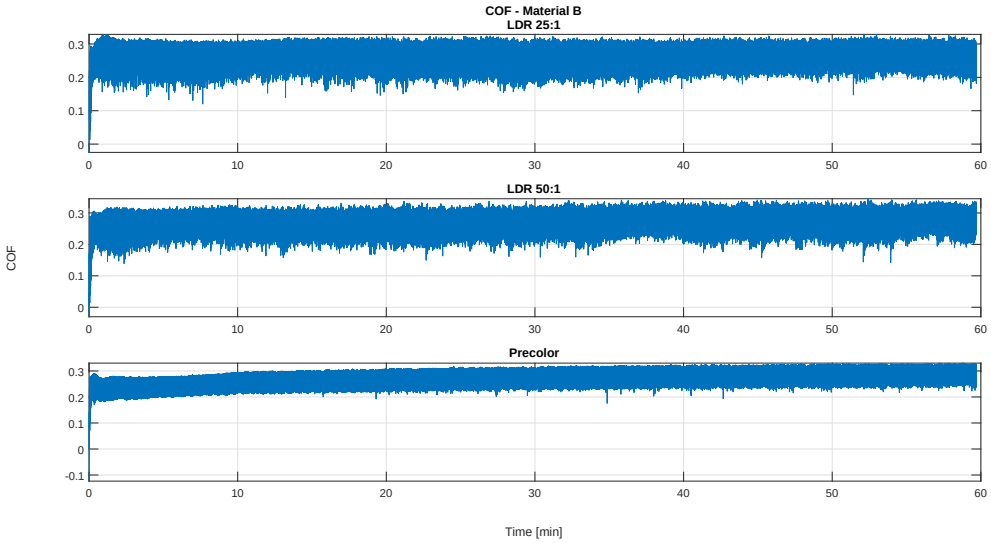

Figure 5.6: COF against testing time for Material B samples recorded during testing. This picture shows the results of the black samples with different injection molding processes

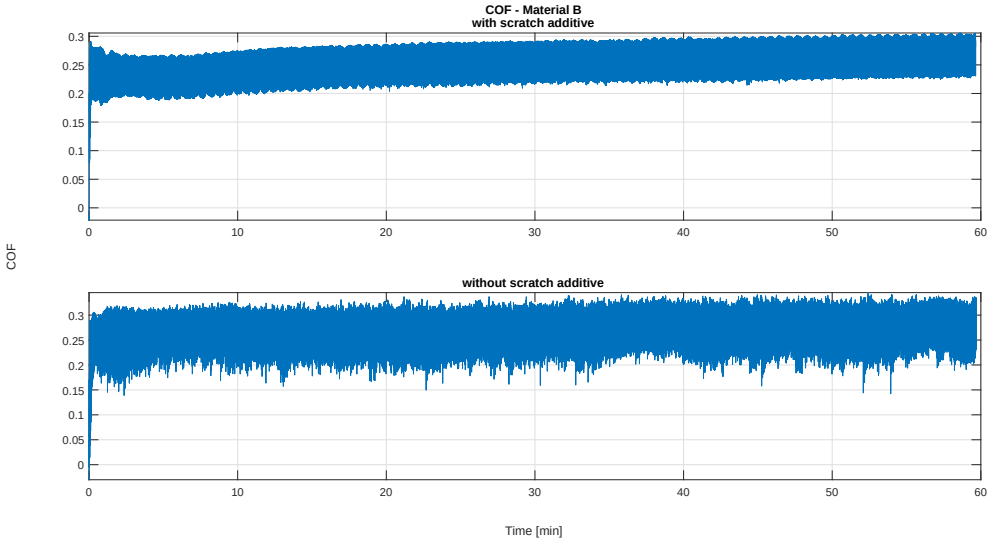

Figure 5.7: COF against testing time for Material B samples with (top) and without (bottom) scratch additives

5.2.1 Texture effect

The final steady-state COFs of the different textures at different normal loads for Material A are shown in figures 5.8. It is possible to note that the differences caused by the textures are not so significant; indeed the largest difference (the one at 7.5 N) between the highest (texture A) and the lowest (texture D) COF is 0.017. Normal load seems to have a slightly higher influence on the COF than the textures, but still the changes induced by the applied load are not so significant. Indeed, the maximum COF variation is for texture D, in the passage from 5 to 10 N, and it is 0.033. From the literature, the small influence of the normal load on the friction coefficient is confirmed; on the other hand, a variation of the testing speed would have lead to a significant change, because of the high sensibility of COF to this factor.

For sake of completion, the complete COF trends for all the textures are included in Appendix A.

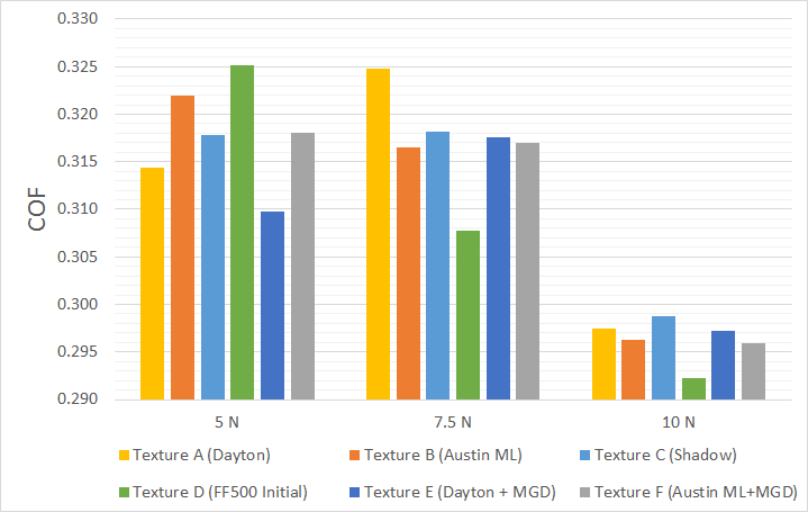

Figure 5.8: COF steady-state values of different textured samples of Material A. The differences are not significant, indicating the poor effect the textures have

5.2.2 Scratch additive and injection molding process effect

The final steady-state COFs of the different Material B grades are reported in figure 5.9. The presence of scratch additives has led to a reduction of 0.014 of the COF for the sample

with LDR 50:1. On the opposite, for the precolor case, the introduction of scratch additives has led to an increase of the COF (of 0.012). Therefore, the contrary effect of scratch additives, already present in the wear rate results, is again noticed. Still, the differences between the different material grades are not significant.

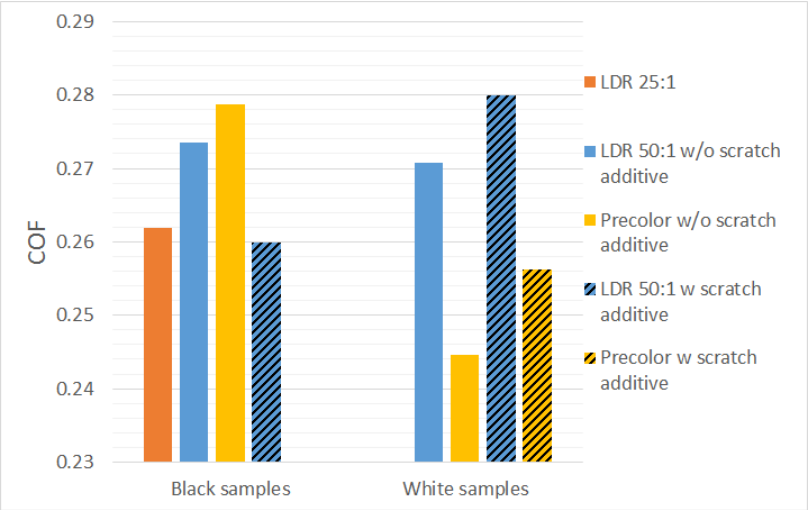

Figure 5.9: COF steady-state value of different Material B grades. The effect of scratch additives is visible

5.3 Optical microscopy analysis

Images of the damaged surface of Material A and Material B samples have been collected using an high quality optical microscope.

5.3.1 Material A

It is interesting to analyze the Material A sample, dividing them according to the two groups made before.

Group 1 (textures A, B, C)

The images of the worn surfaces of these textured samples are shown in figure 5.10, 5.11 and 5.12.

Considering texture C at 5 N displayed in figure 5.10, the damage looks like an ironing/flattening of the crests of the surface, with a relative change in the brightness. While in this case the wear track is well defined, on samples textured with texture B and texture A, the damage is not very neat and defined, and the boundaries are irregulars. The damage of these two textures is very similar; in some portion of the wear track, the centre seems to be characterized by flattening of the surface crest that changes the brightness. Some irregular spots are presents in the middle of the track; they could be consequences of the passage of the indenter form one grain of the texture to the following one.

At 7.5 N (figure 5.11), on the sample with texture C, two regions are detected in the damage. The central one is called broken region and in this region, stress whitening and damage due to poor friction conditions are included. Those are due to due to the ploughing of the tip on the surface. The damage feature is an irregular concave damage pointing toward the direction of sliding. It remembers somehow the fish-scale pattern, but it is more irregular; this is probably a consequence of the texture presence. Beside the broken region, there is the compressing deformation region, due to the compression of the material, which has been pushed sideways by the indenter motion. Again, the appearance of the damaged surface of texture B and texture A is similar. Also for these sample, the wear track is characterized by two regions, with the chaotic concave material drawing in the central one. However, while the boundaries between the compressing deformation region and the undamaged background are neat and well-defined for sample with texture C, in the other two cases, they are not.

For all the three textures, figure 5.12 shows that, at 10 N, the broken region is larger, and the entity of the deformation is larger. The damage is more extensive and the material drawing is higher. However, it is possible to note that the damage is similar to that occurring at 7.5 N, thus no change in the deformation/damage mode has occurred.

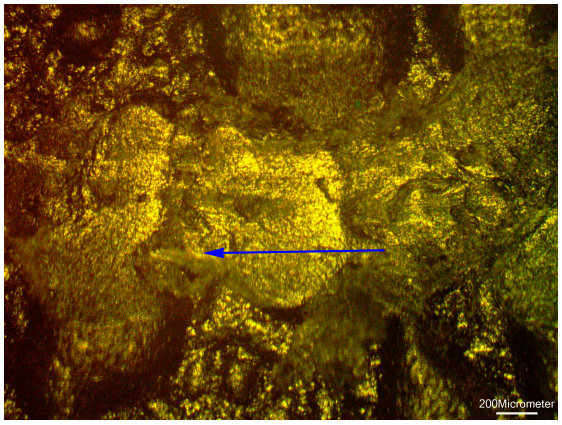

(a) Texture A

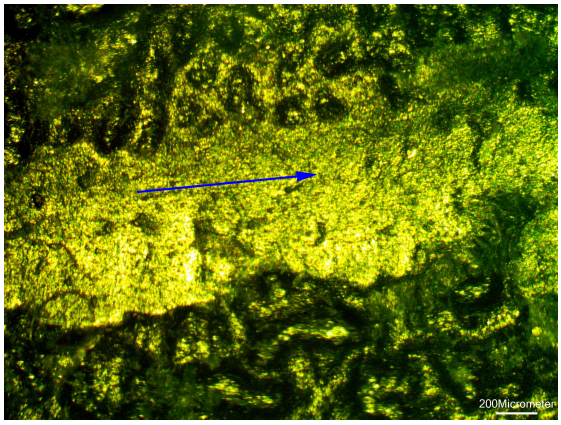

(b) Texture B

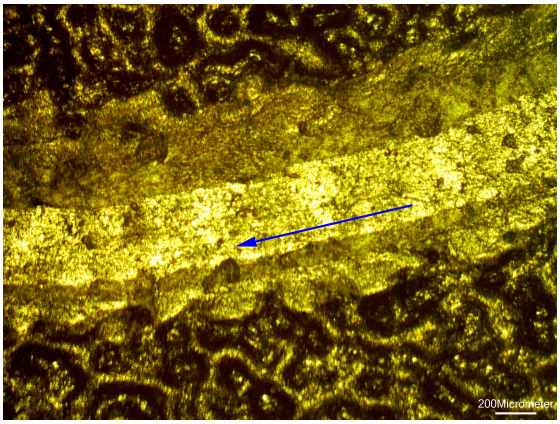

(c) Texture C

Figure 5.10: Optical microscope images of samples tested at 5 N (group 1). The dominant deformation mechanism is ironing or flattening of the surface crests. In (c), the broken and compressive regions are already visible

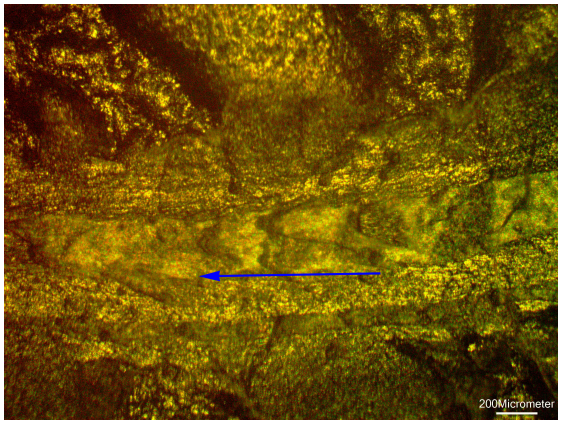

(a) Texture A

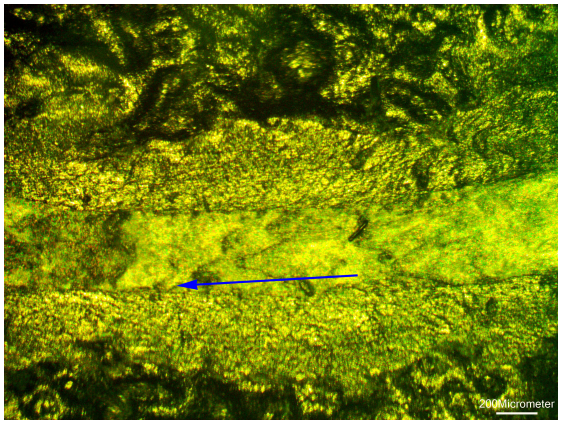

(b) Texture B

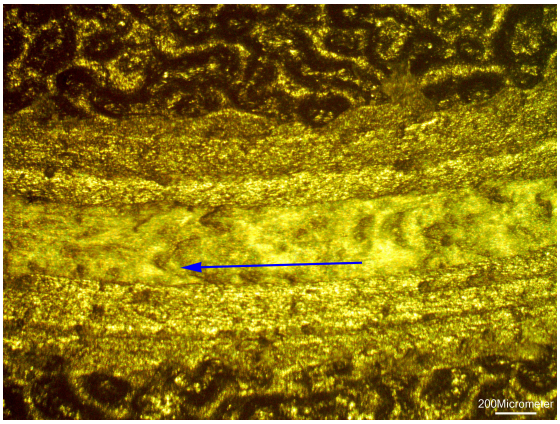

(c) Texture C

Figure 5.11: Optical microscope images of samples tested at 7.5 N (group 1). The wear track can be subdivided in two regions (broken and compressive). In the broken region, in the centre, ductile drawing is the main deformation mechanism, while the compressive regions result in material pile-up

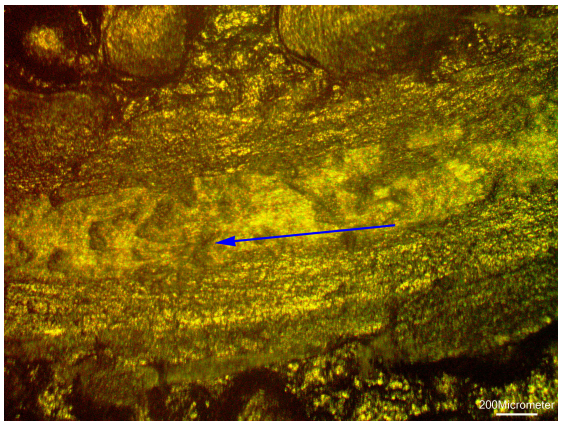

(a) Texture A

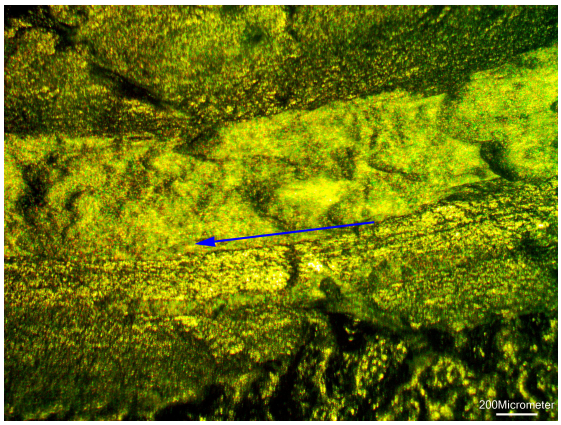

(b) Texture B

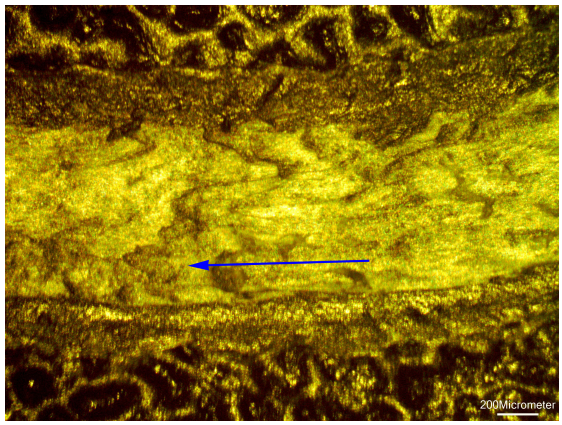

(c) Texture C

Figure 5.12: Optical microscope images of samples tested at 10 N (group 1). The damage is similar to that on samples tested at 7.5 N. The wear track is larger and ductile drawing more pronounced

Group 2 (textures D, E, F)

The images of the worn surfaces of these textured samples are shown in figure 5.13, 5.14 and 5.15.

Considering the sample with texture D, the damage is already extensive and highly visible at 5 N. Both the broken and the compressing deformation region have an irregular shape, with bright appearance. The particular pattern characterized by irregular concave shape pointing toward the motion direction, caused by material drawing, is already present. At 7.5 N, the damage increased proportionally. At 10 N, in several points of there is no more distinction between the two wear track regions visible before, but the wear tracks appears as a unique chaotic damage.

For the cases of textures E and texture F, at 5 and 7.5 N (figure 5.13 and 5.14), the damage is very similar to the cases of texture A and texture B, respectively. The main difference in the lightness of the damage itself, due to the presence of MGD, which lowers the gloss of the surface. Figure 5.15 reports the cases at 10 N; the present damage on texture E and texture F is different from the one of the original textures. Similarly to the case of texture D, the two tracks regions are no more visible. On their places, there is a unique wear tracks, with chaotic irregular features (this is more pronounced on texture F).

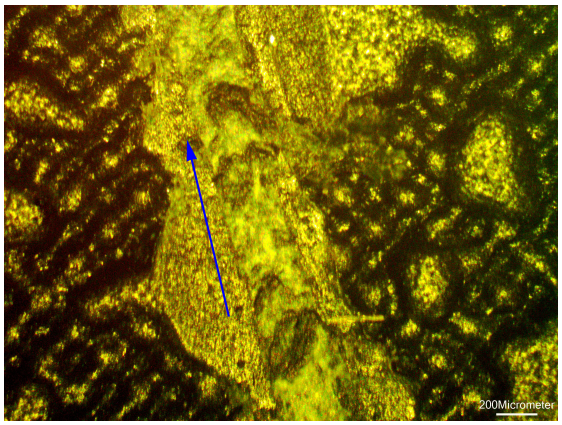

(a) Texture D

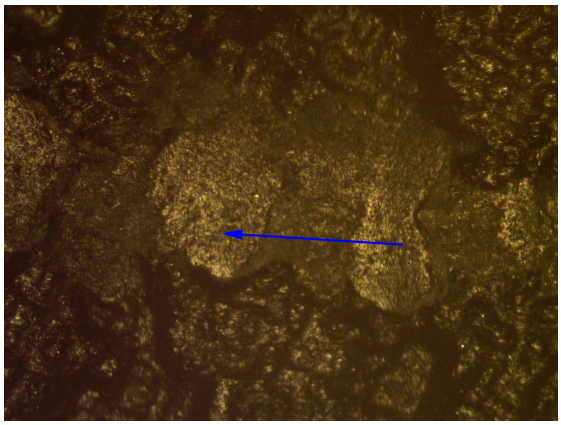

(b) Texture E

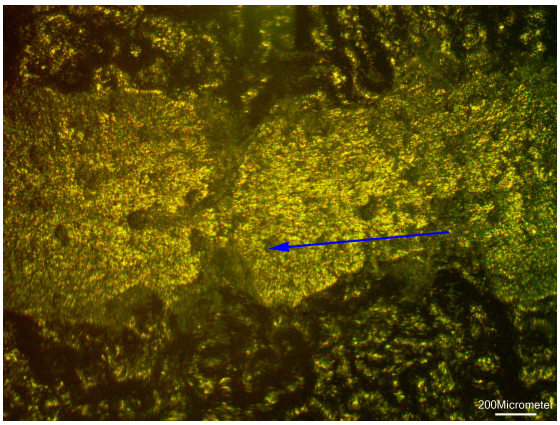

(c) Texture F

Figure 5.13: Optical microscope images of samples tested at 5 N (group 2). (a) The broken and compressive regions are visible, while in (b) and (c) the damage occurring is ironing

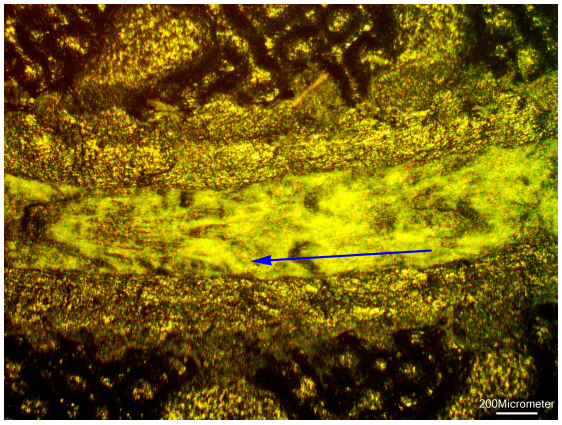

(a) Texture D

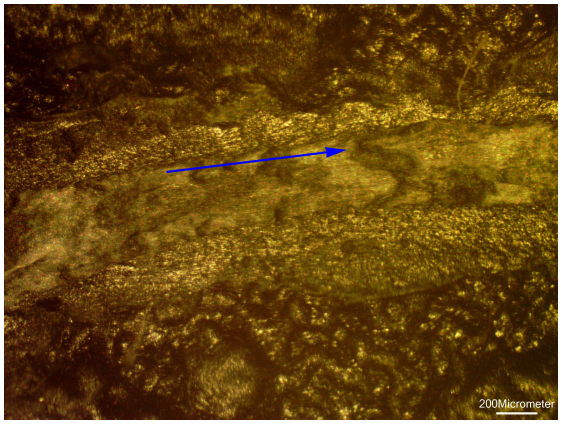

(b) Texture E

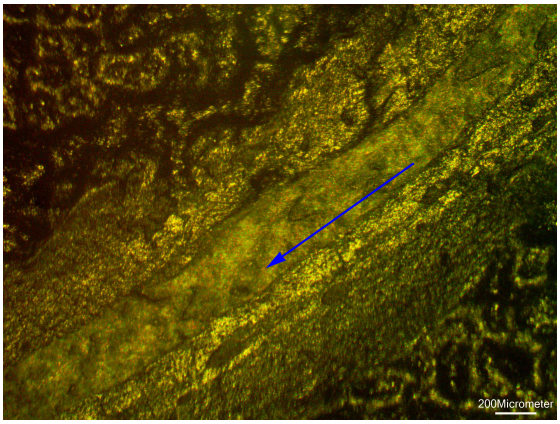

(c) Texture F

Figure 5.14: Optical microscope images of samples tested at 7.5 N (group 2).The wear track can be subdivided in two regions (broken and compressive). In the broken region, in the centre, ductile drawing is the main deformation mechanism, while the compressive regions result in material pile-up

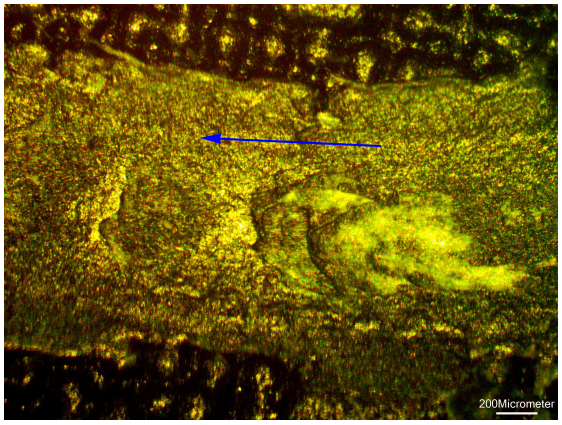

(a) Texture D

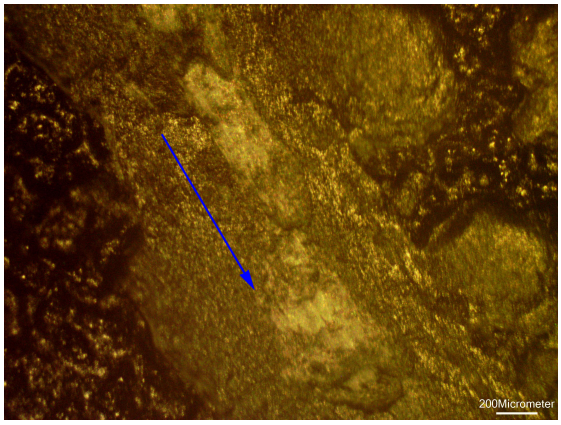

(b) Texture E

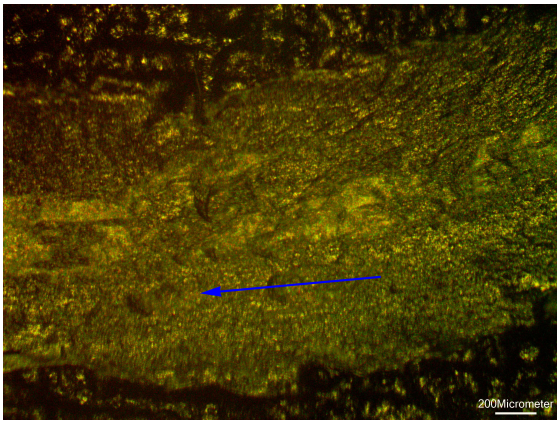

(c) Texture F

Figure 5.15: Optical microscope images of samples tested at 10 N (group 2). The wear track is not divided in the two regions of before, but it appears as unique characterized by irregular features, due to ploughing of the indenter

5.3.2 Material B

In figure 5.16 the damage occurring on the surface of Material B samples is shown.
Figure 5.16 *(a)* highlights the damage present on the sample with LDR 25:1. It is possible to note that there is not the distinction between the two regions of before (broken and compression deformation). The wear track has a bright appearance, with the centre characterized by dark concave damage features, pointing toward the sliding direction.
Considering the case of sample with LDR 50:1 shown in figure 5.16 *(b)*, the dark concave features at the center of the scratch track are still present, but they are smaller and less in number that the case of LDR 25:1. Moreover, the sides of the scratch tracks are not so defined.
The damage on the precolor sample, presented in figure 5.16 *(c)*, is quite difference from the other two cases. Indeed, there are concave dark damage features at the center of the track, but the shape of them is different. The track is characterized by small dark spots and small irregular damages. The dark spots are the residual valleys of the textures, which were not filled by the flattening and drawing of the crests. Overall, the contrast between the virgin background and the damaged area seems smaller than the other cases, also because the irregular boundaries between the virgin background and the damaged zone.
The introduction of scratch additive leads to a change in the appearance of the damaged area, as highlighted in figure 5.16 *(d)*. Indeed, the damage is no more characterized by big dark parabolic features pointing toward the sliding direction, but in the wear track, small irregular dark spots are present, similar to the precolor case. The limits between the damaged area and the virgin background are confused.
The visible damage on the surface of white samples is basically the same of black ones. What changes is its appearance and its contrast with the background.

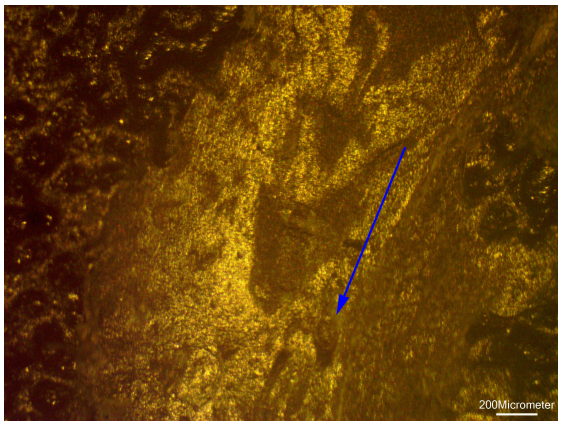

(a) LDR 25:1, black

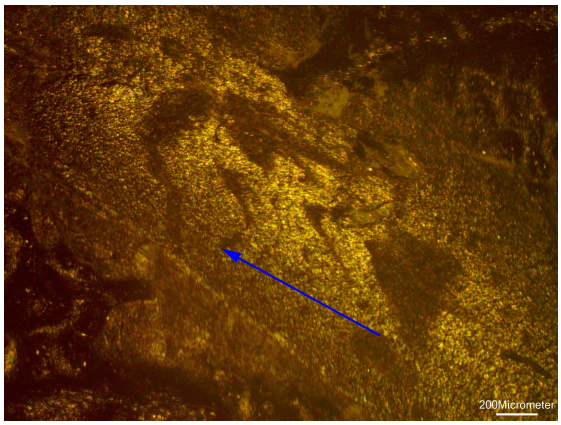

(b) LDR 50:1, black

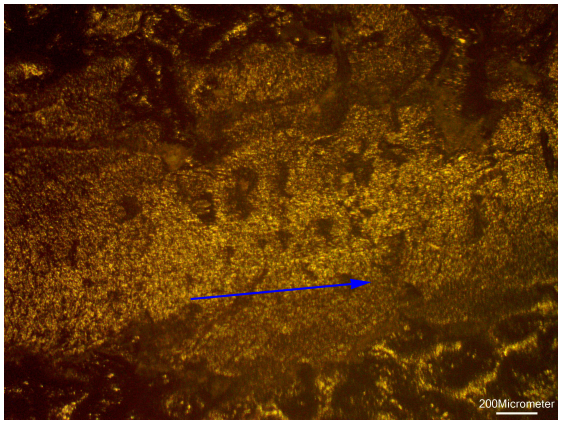

(c) Precolor, black

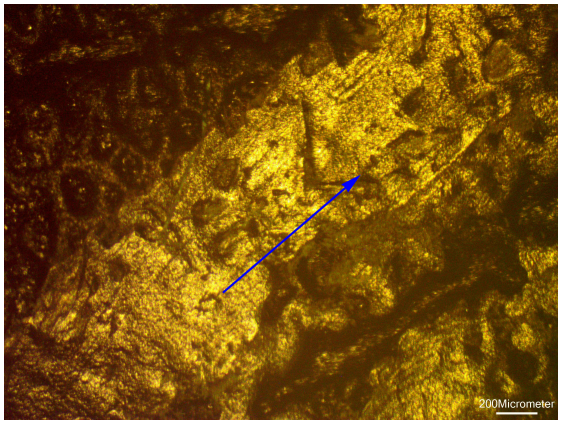

(d) LDR 50:1 + scratch additive, black

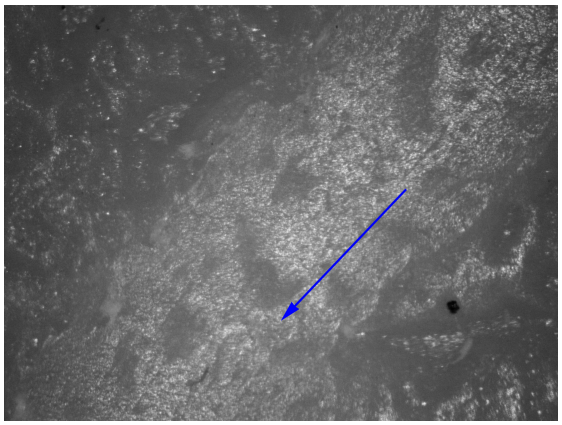

(e) LDR 50:1, white

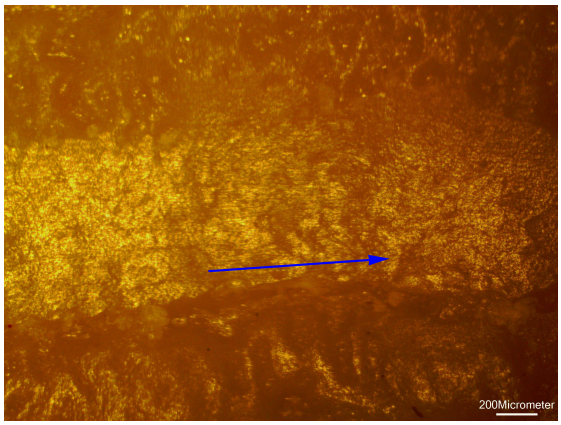

(f) Precolor, white

Figure 5.16: Optical microscope images of Material B samples

5.4 Surface profilometry

Through a surface profilometer, the geometry of the wear tracks has been obtained. Figure 5.17 and 5.21 shows the surfaces profiles gathered. In this graphs, colors help in representing the different heights of the surface elements (wear track, groove edges, texture, etc.), so the shape of the damage surfaces, and the differences between them, are easily understandable.

5.4.1 Material A

From figure 5.17, it is possible to see the extension of the wear track, so of the damage, which comes with load increasing; going from 5 to 10 N, the wear track becomes larger and deeper. Comparing the surface profile of different textures, it is possible to note how textures like texture A and B, characterized by round/rough peaks and large and deep grains, contribute to the resistance to deformation. Indeed, on samples with those textures, at 5 N the damage consists of only a flattening of the surface crests, and at 7.5 N also the damage is limited. On the opposite, textures with high peak counts and sharp or smooth peaks, like texture C and D, present well defined wear track at 5 N already. In figure 5.17, 3D surface profile of texture A and C only are shown, for sake of comparison and space. The surface profiles of the other textures are included in appendix B.

According to the literature, the quantities important for scratch visibility are the groove depth and the pile-up on the sides, and the roughness of the wear tracks, or better, the roughness change, between the virgin background and the damaged area. The residual depth of penetration, the raised groove shoulder and the change in roughness (i.e. the roughness difference between the wear track and the virgin background) are shown in figure 5.18, 5.19 and 5.20, respectively. While the behavior of the roughness change seems to be very chaotic and random, without a clear dependence from neither the texture, nor the load, both the pile-up on the sides and the wear track depth increases with the load (exception for the shoulder edge of texture A). It is interesting to note that, for what regards the depth of the damage, textures characterized by large, deep grains with round and random peaks heights, position at the bottom of the graph; they present the lowest wear track depth.

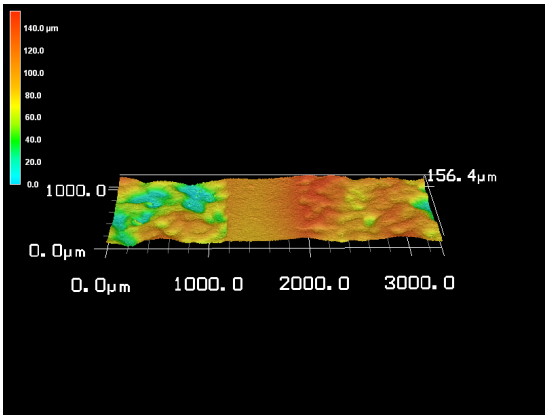

(a) Texture A - 5 N

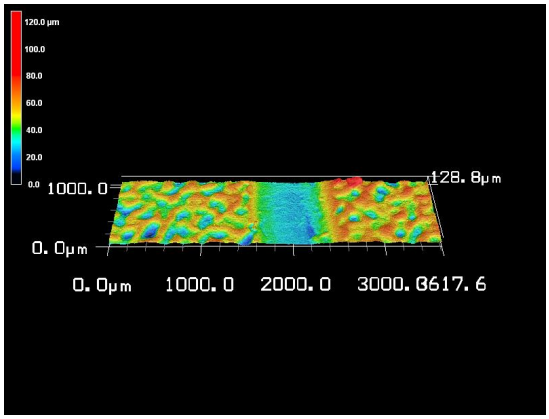

(b) Texture C - 5 N

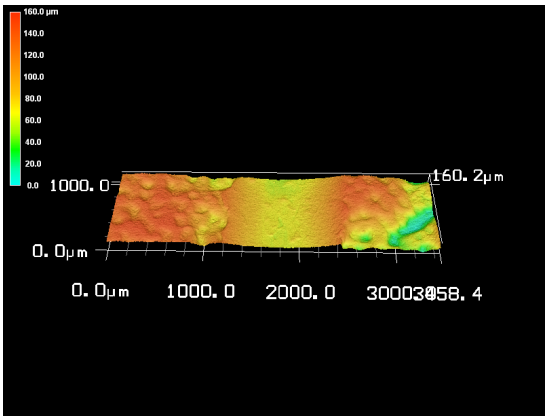

(c) Texture A - 7.5 N

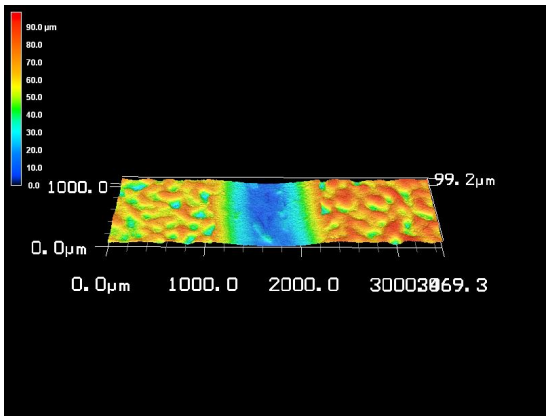

(d) Texture C - 7.5 N

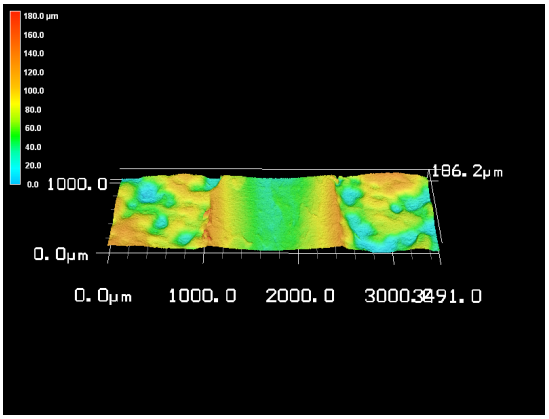

(e) Texture A - 10 N

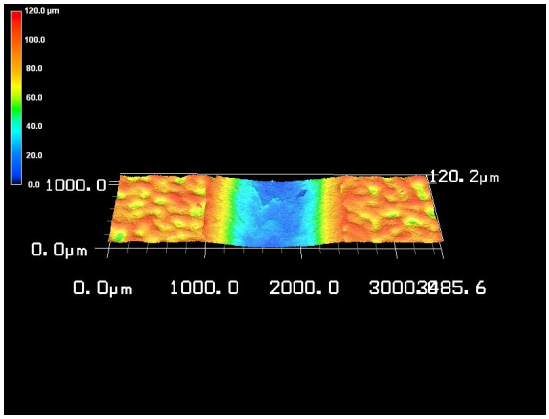

(f) Texture C - 10 N

Figure 5.17: Surface profiles of Material A samples. The wear tracks and the textures are easily distinguishable

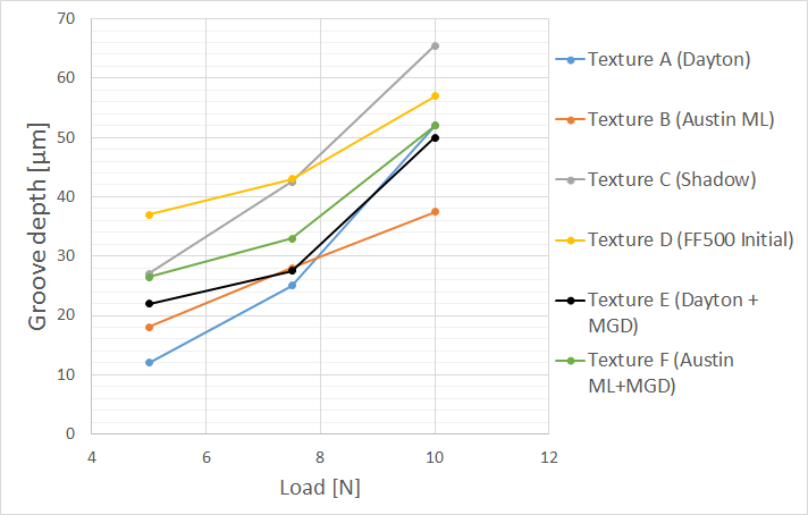

Figure 5.18: Residual penetration depth of Material A samples. The depth increases with the load, and lowest depth have been found for textures A and B

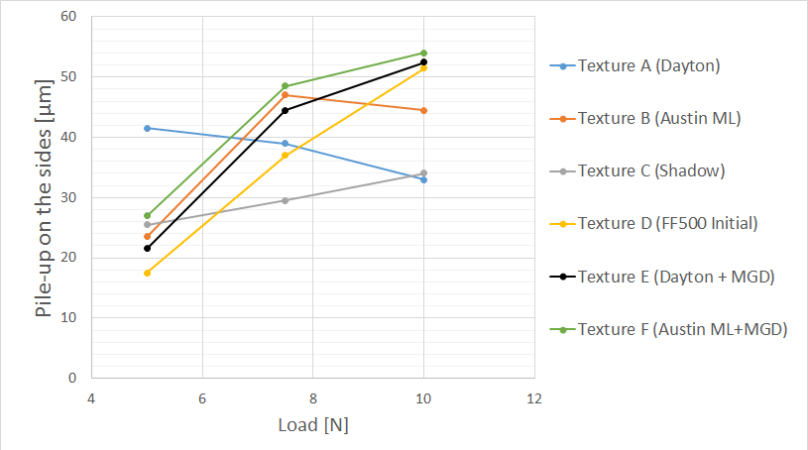

Figure 5.19: Groove raised shoulder of Material A samples. The pile-up on the edge increases with the load

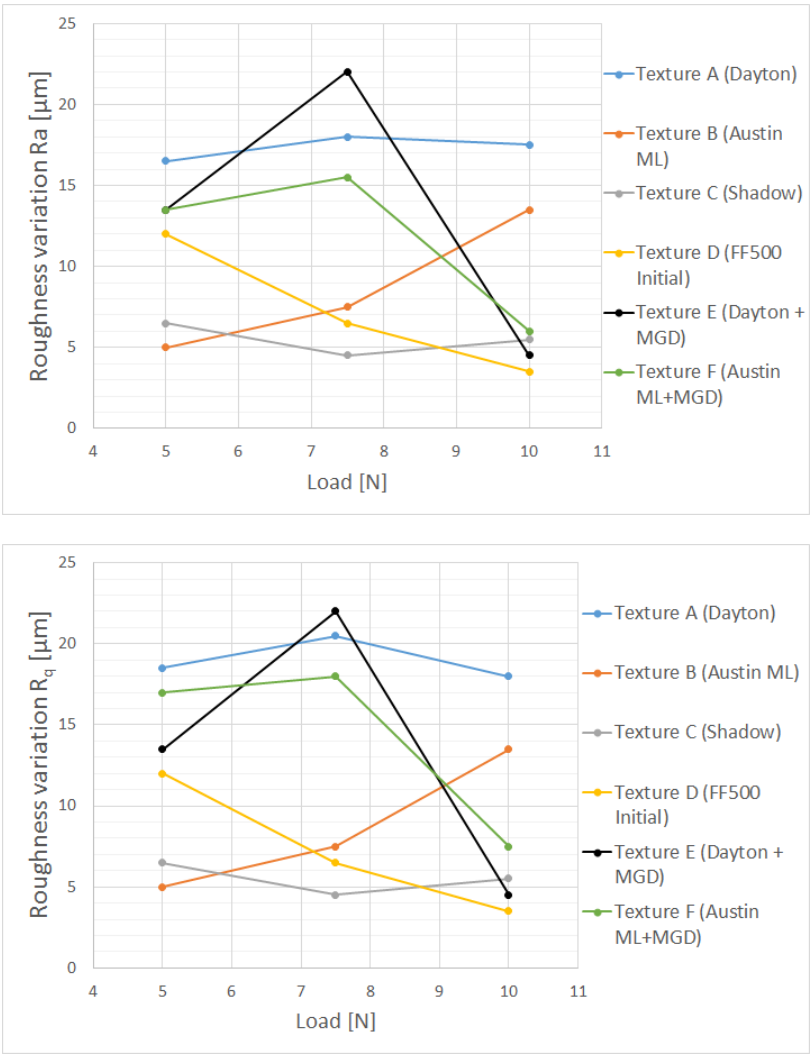

Figure 5.20: Roughness change of Material A samples. The trend is complex and seems random. The pictures do not show correlation with the damage visibility

5.4.2 Material B

In figure 5.21, the samples of Material B are shown. It is possible to note that the wear track is very deep and severe in the LDR 25:1 sample. In this sample, the counterface has actually penetrated the surface, causing massive damage, extensive deformation and material removal. On the opposite, the precolor sample shows a slightly milder and less pronounced wear track than the LDR 50:1 sample. In figure 5.21 *(f)-(g)-(h)*, it is possible to note the beneficial effect of the scratch additives on the surface damage. The wear tracks is no more a deep groove, but it just consists of a flattening of the surface texture. Indeed, the sliding of the counterface has caused plastic deformation of the texture crests; this deformed material has flowed in the valleys of the texture, filling them. Therefore, the residual track is flat, almost on the same height level of the original surface.

Obviously, the shape of the damaged surface for the black and the white samples are completely analogous. In fact, as stated above, the different color should not influence the geometry of the damaged surface.

The residual depth of penetration, the raised groove shoulder and the change in roughness are shown in figure 5.22, 5.23 and 5.24, respectively. In these figures, the data relative to samples made of Material B are reported. For sake of completion, these are divided in black and white samples, even though the color does not have any influence on the quantitative aspect and on the geometry of the damage.

Among the samples not containing scratch additive, the one with LDR 25:1 have shown the largest groove depth (43 μm) and the largest pile-up on the sides (62.5 μm). On the contrary, the precolor sample presents the lowest residual penetration depth (11.5 μm) and groove side ()30.5 μm). It is possible to note that both the groove depth and the pile-up on the sides reduces, if scratch additives are included into the material.

As stated before, roughness variation is an important quantity for scratch visibility: the highest the roughness change, the larger the amount of light diffractional scattering which triggers the human eye perception. Therefore, the larger the light scattering, the more visible is the surface damage. In figure 5.24, data relative to two roughness measuring methods have been reported (R_a and R_q). The trend among the samples is again the usual one: precolor sample is the one with the lowest roughness variation, which could mean lowest

damage visibility, and the effect of scratch additives is beneficial. It is easy to understand that, since scratch additives reduce the surface damage vulnerability of the material (so less damage occurs on the surface), the variation of roughness respect the undamaged surface portion is low. However, an exception has occurred: the sample with LDR 25:1 has shown lower roughness variation than the one with LDR 50:1.

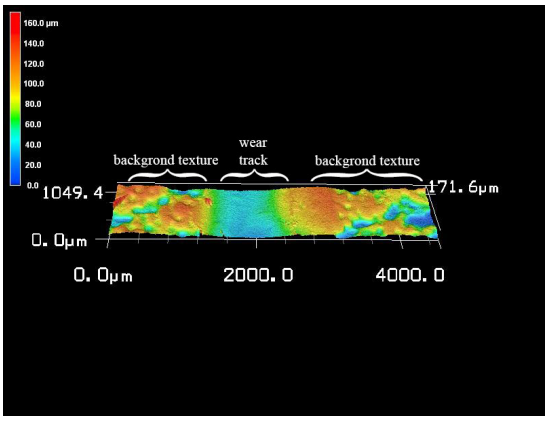

(a) LDR 25:1 - black

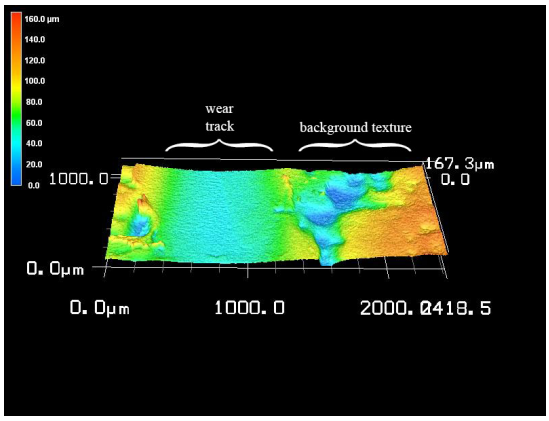

(b) LDR 50:1 - black

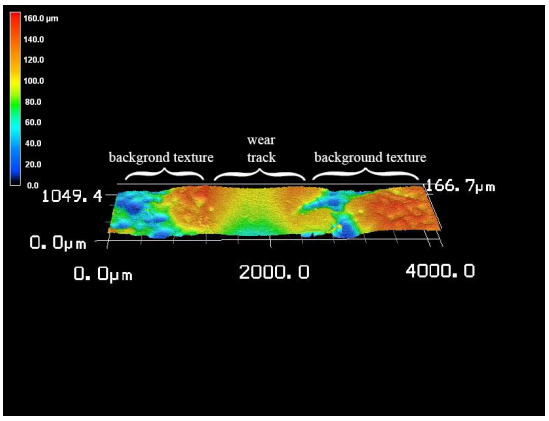

(c) Precolor - black

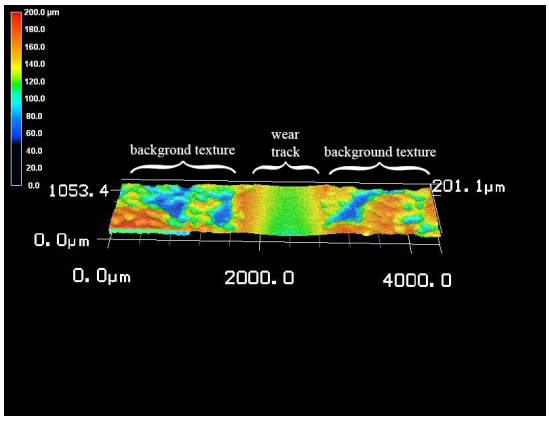

(d) LDR 50:1 - white

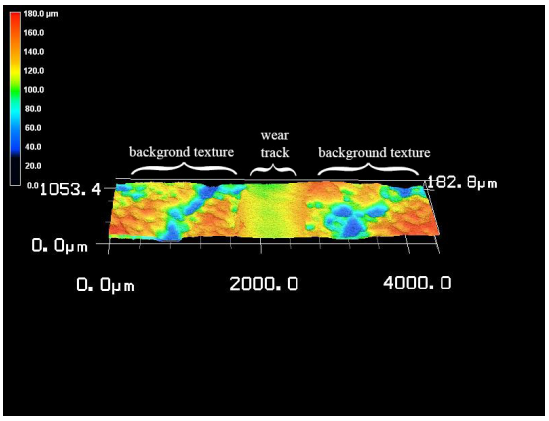

(e) Precolor - white

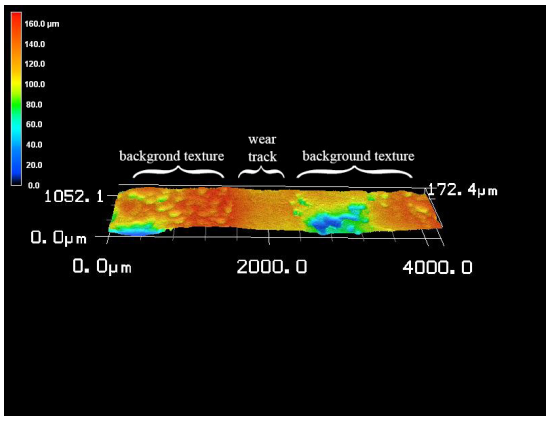

(f) LDR 50:1 - scratch additive - black

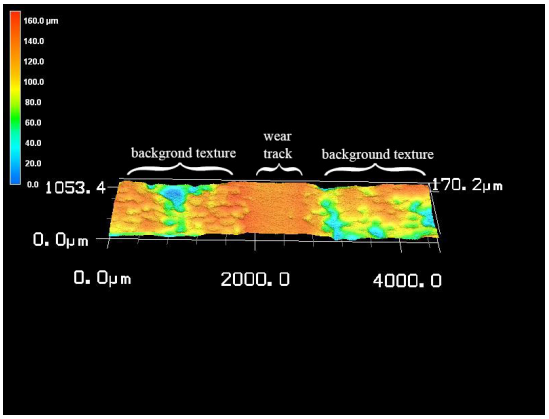

(g) LDR 50:1 - scratch additive - white

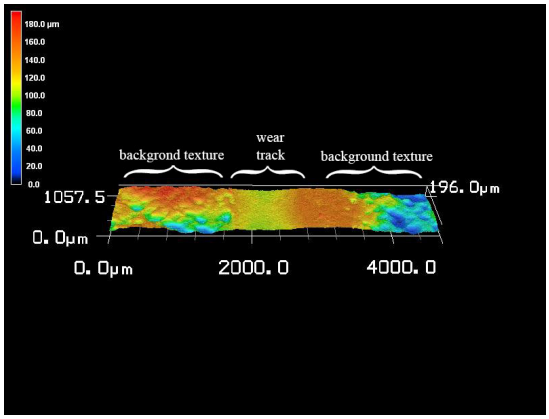

(h) Precolor - scratch additive - white

Figure 5.21: Surface profiles of Material B samples. The wear tracks are highlighted in some images, because they are scarcely visible, due to the resistance of the material. The pattern with peaks and valleys on the side is the texture

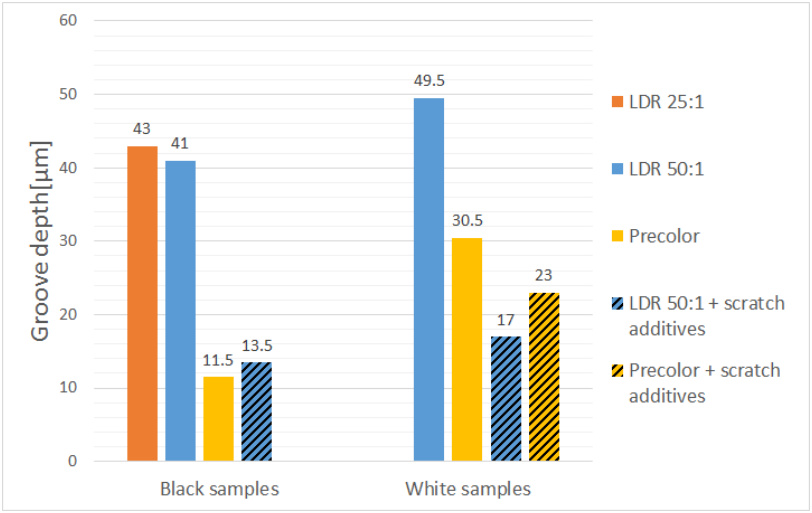

Figure 5.22: Residual penetration depth of Material B samples. The precolor samples shows the lowest wear track depth; the beneficial effect of scratch additives is visible

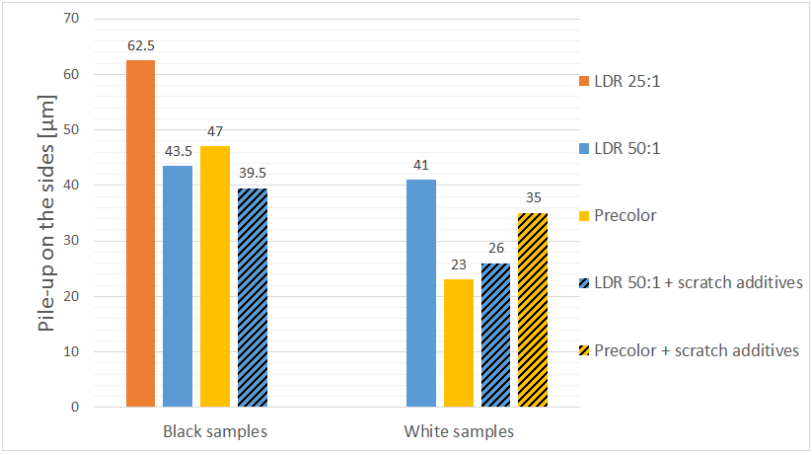

Figure 5.23: Groove raised shoulder of Material B samples. The precolor samples shows the lowest pile-up; the effect of scratch additives is visible

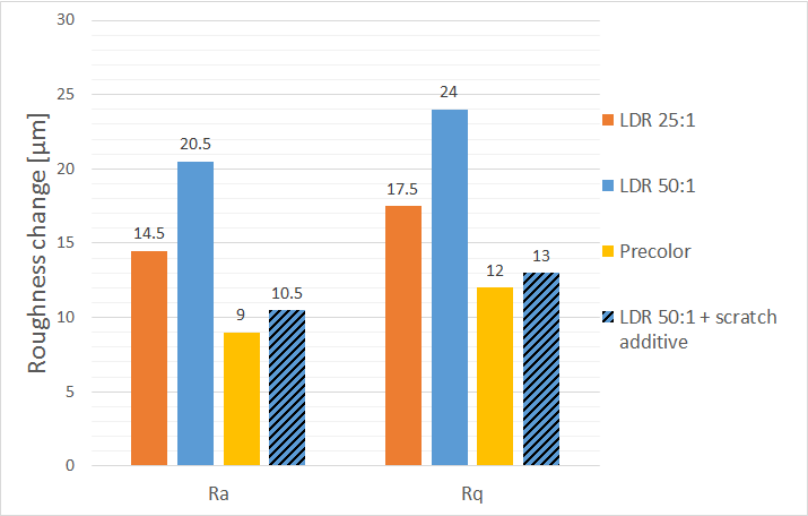

Figure 5.24: Roughness change of Material B samples. The precolor samples shows the lowest roughness variation; the effect of scratch additives is visible

5.5 Visual analysis

Pictures of the tested samples have been taken through the use of a DSLR (Digital Single-Lens Reflex) Camera Canon EOS 600D, and they are reported in this section.

In figure 5.25, the samples of Material A with different textures and tested at different normal load are compared. Just looking at them, it is possible to note how the damage is less visible with large and deep texture grains and, obviously, with low load. This confirms what has been found in the literature: the capability of texture, characterized by large and deep grains, to hide/mask the surface damage. The black and white samples made of Material B are shown in figure 5.26 *(a)* and *(b)*, respectively. With these samples, it is much more difficult to notice difference in the surface damage just by looking at them, especially for the white samples. From figure 5.28 to 5.31, the results obtained through the spectrophotometer are shown. It is important to remind that the interesting value L^* is the coordinate of the Lab Color Space (CIELAB), which represents the lightness of the surface. The change in lightness ΔL^*, between the undamaged background and the damaged area, is the important parameter for surface damage visibility. In figures 5.28 and 5.29, the absolute difference in L^* is reported, but this could be an issue for the comparison

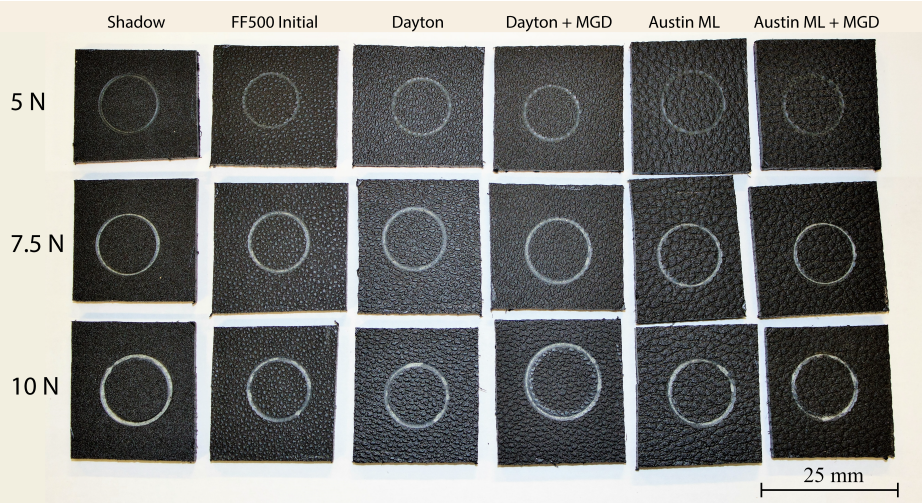

Figure 5.25: Material A samples comparison. The lowest damage visibility is for textures Dayton and Austin ML; the damage visibility increases with the increasing of the load from 5 to 10 N

of samples, whose virgin surfaces have different L^* values. To correct this disparity, the ΔL^* value has been normalized against the luminance of the virgin surface L^*_{virgin}, thus $\Delta L^*\%$ has been obtained:

$$\Delta L^*\% = \frac{\Delta L^*}{L^*_{virgin}} \tag{5.5.1}$$

The normalization results in a measurement of the contrast with respect to luminance, and this has been found to be representative surface damage visibility, more than the absolute difference ΔL^* [14, 41]. The $\Delta L^*\%$ for the Material A and Material B samples are shown in figures 5.30 to 5.31, respectively.

The applied normal load tends to increase the luminance contrast. Texture A shows the lowest $\Delta L^*\%$, texture D the largest.

Regarding Material B, among black samples, the precolored is the one with the lowest surface damage visibility, while the samples with LDR 25:1 and LDR 50:1 present similar $\Delta L^*\%$. The presence of scratch additives is beneficial, since it has led to a reduction of the contrast. It is interesting to note how the $\Delta L^*\%$ values of pure white samples are lower than the ones of the black counterparts, meaning that brighter color promotes surface damage visibility resistance. This is consistent with what has been found on the literature.

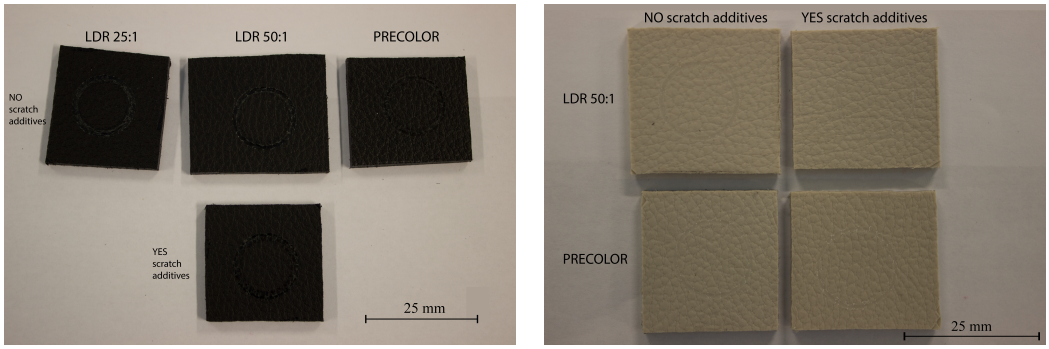

(a) Black **(b)** White

Figure 5.26: Material B samples. The lowest damage visibility is for precolor white sample

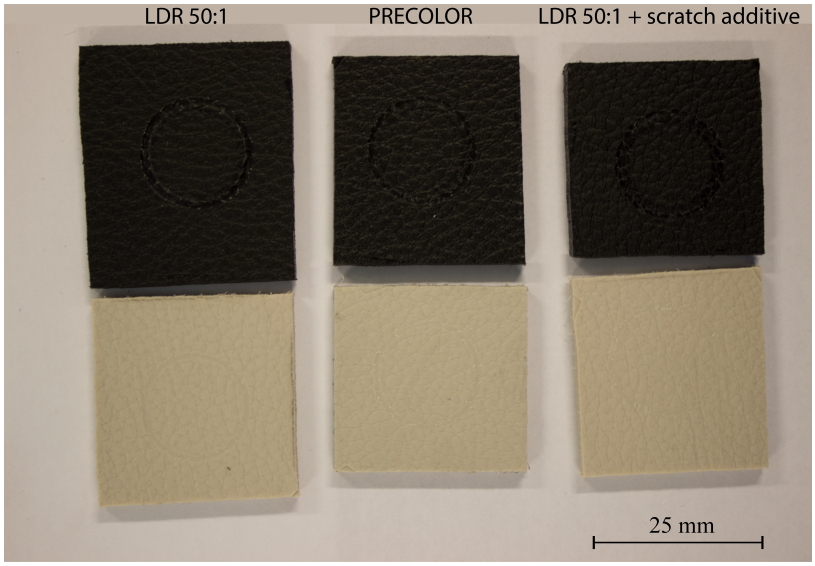

Figure 5.27: Material B samples - color comparison. This image shows the lower damage visibility of white samples respect black ones

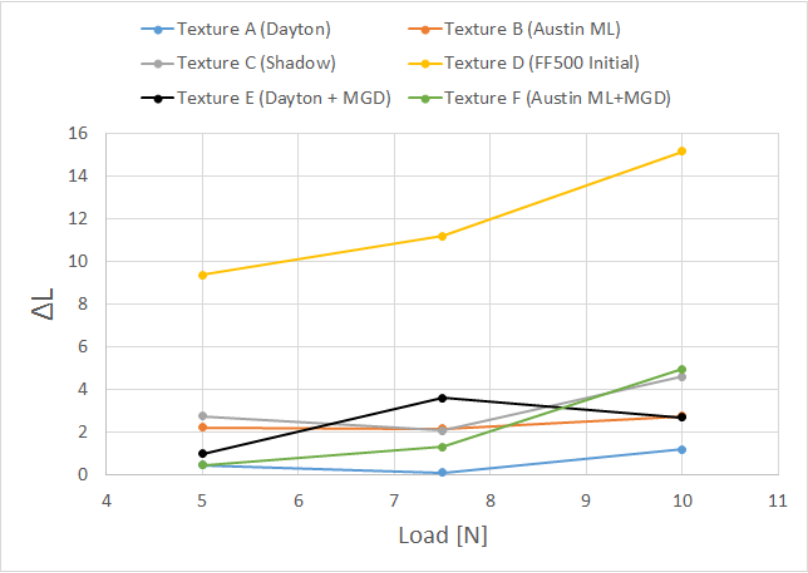

Figure 5.28: ΔL^* for Material A samples. ΔL^* increases with the load; the lowest ΔL^* is for texture A (Dayton)

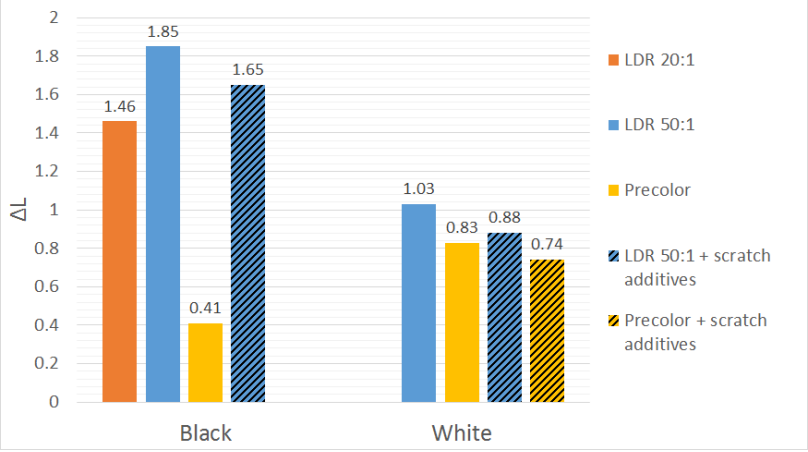

Figure 5.29: ΔL^* for Material B samples. The beneficial effect of scratch additives is visible; white colored samples have lower damage visibility than black ones

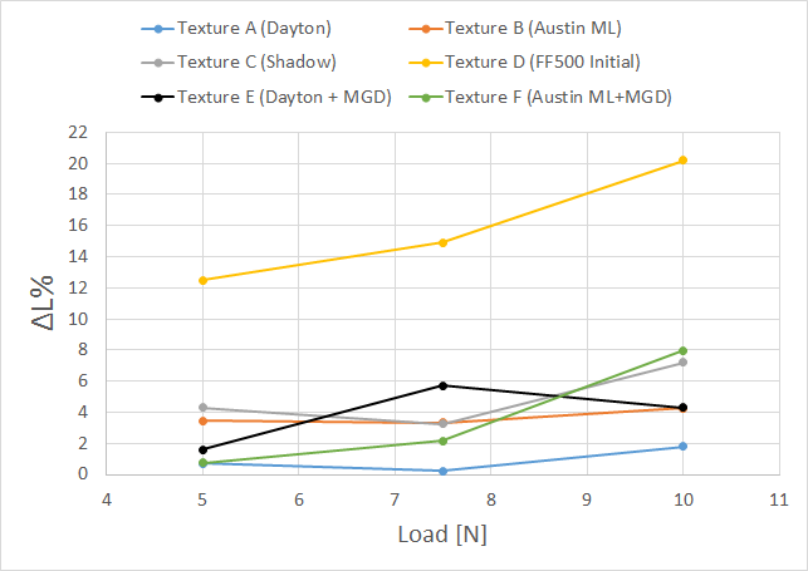

Figure 5.30: $\Delta L^*\%$ for Material A samples. ΔL^* increases with the load; the lowest ΔL^* is for texture A (Dayton)

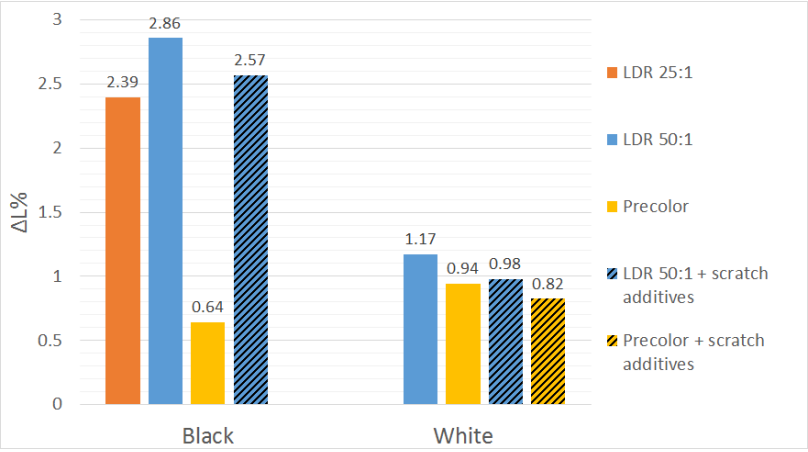

Figure 5.31: $\Delta L^*\%$ for Material B samples. The beneficial effect of scratch additives is visible; white colored samples have lower damage visibility than black ones

5.6 ANOVA

Tables from 5.2 to 5.6 show the results coming from the ANOVA.
In these table, the investigated phenomena are, in order, the wear rate, the contrast in luminance $\Delta L^*\%$, the raised wear track shoulder, the change in roughness and the wear track depth. The two factors, whose significances are analyzed, are texture, that has 6 levels, and applied normal load, which has 3 levels. The risk adopted in the analysis is 5%, as usual in statistical analysis. A factor, to be significant, need to be characterized by

Table 5.2: ANOVA table for wear rate vs. texture and normal load

Source	DF	Adj SS	Adj MS	F-Value	P-Value
Texture	5	7.780	1.556	1.29	0.343
Load	2	141.431	70.715	54.44	0.000
Error	10	12.100	1.210		
Total	17	161.310			

Table 5.3: ANOVA table for raised wear track shoulder vs. texture and normal load

Source	DF	Adj SS	Adj MS	F-Value	P-Value
Texture	5	308.2	61.65	0.84	0.550
Load	2	1181.4	590.72	8.05	0.008
Error	10	733.4	73.34		
Total	17	2223.1			

Table 5.4: ANOVA table for roughness change vs. texture and normal load

Source	DF	Adj SS	Adj MS	F-Value	P-Value
Texture	5	283.07	56.61	2.43	0.109
Load	2	48.53	24.26	1.04	0.389
Error	10	233.31	23.33		
Total	17	564.90			

a $P - Value$ lower than the assumed risk (lower than 0.05). For what concerns the wear rate and the wear track shoulder, it is possible to note that texture has a $P - Value$ higher than 0.05, while the one of the applied normal load is lower. So, it is possible to state that the texture is not-significant on the wear rate and on the pile-up on the sides, while the normal load is, with a risk (of failing) of 5%. On the other hand, considering the damage depth and the contrast in luminance $\Delta L^*\%$, the $P - Value$ of both factors is lower than 0.05. This means that, both texture and applied normal load are significant factors for the damage depth and for $\Delta L^*\%$(thus for surface damage visibility), with a risk (of failing) of 5%. In this case is it interesting to evaluate the percentage of contribution of each factor on the measured luminance contrast. To do that, the adjusted sums of squares ($Adj\ SS$) are utilized and the resulting percentages of contributions are reported in table 5.5 and 5.6. Finally, neither the applied normal load, nor the texture have been found to be significant for the difference in roughness, between the wear track and the undamaged background.
The residuals plots are illustrated in Appendix C, to verify the assumptions that the residuals are normally distributed, have constant variance, and are independent from one another.

Table 5.5: ANOVA table for penetration depth vs. texture and normal load

Source	DF	Adj SS	Adj MS	F-Value	P-Value	Contribution %
Texture	5	868.8	173.76	7.58	0.003	23.8
Load	2	2546.1	1273.04	55.53	0.000	69.9
Error	10	229.2	22.92			6.3
Total	17	3644.1				

Table 5.6: ANOVA table for $\Delta L^*\%$ vs. texture and normal load

Source	DF	Adj SS	Adj MS	F-Value	P-Value	Contribution %
Texture	5	432.61	86.523	21.87	0.000	83.38
Load	2	46.65	23.327	5.90	0.020	9.00
Error	10	39.56	3.956			7.62
Total	17	518.83				

Chapter 6

Discussion

In this chapter, a discussion and interpretation of the results highlighted in Chapter 5 are given.

From figure 5.1, the worn volume and the wear rate are higher for texture with very fine and small grains, like texture C (Shadow). Textures with larger and grosser grains, like texture B (Austin ML), behave better; the lost volume and wear rate is lower, meaning that it is more difficult to wear off large and deep grains than shallow and small ones.
A variation of the slope of the wear rate curve indicates a variation in the wear deformation mechanism. This means that, once a certain load level has been reached, the deformation mechanism changes, passing from a milder one to a more severe one, which leads to higher damage. Since slope variation occurs only in certain textures, different texture types can influence the type of deformation mechanism, triggering or not a change in that. It is interesting to note that both the texture with MGD are characterized by a slope change. This could be attributed to the particular micro-laser generated overlay technology utilized to obtain low gloss surface (like a texture on a texture), which could lead to high damage sooner than the case of no treated surfaces. Changes in the deformation mechanisms are confirmed by the images of the worn surfaces obtained through the optical microscope.

Comparing the images gathered on the surface of samples tested at 7.5 with those at 10 N, variations in the damage appearance, so in the deformation mechanism, are visible only on the three textures, whose slope of the wear rate curve varies. Samples, whose slope of wear rate against load curves does not change, have shown the same damage mechanism, whatever the applied load.

It has been found that the presence of scratch additive can have either a positive effect on the wear rate (that is the case of samples with LDR 50:1), either a negative effect (like the precolor sample). This opposite effect of scratch additives on LDR 50:1 and precolored samples can be seen also in the friction coefficient (COF) results. The purpose of scratch additives is to reduce the scratch vulnerability of the polymeric surface. In doing so, the friction coefficient of the surface can be reduced; lower COF leads to further lower deformation, thus to lower scratch visibility, also because the stick-slip phenomenon is reduced. This is what has happened for the sample LDR 50:1, while for the precolored sample, the COF has increased.

The evolution of the COF during the test is analogous to that found in other studies [34, 55]. The fluctuations have two main causes: stick-slip phenomenon and texture bumps influence. Therefore, the amplitude of the COF fluctuation depends both on the adhesion forces between the indenter and the counterface and on the texture grains dimensions.

Stick-slip phenomenon causes an oscillation of the actual velocity of the scratcher, even though the test is designed for taking place at constant speed, because of periodic formation (stick) and breakage (slip) of adhesion bonding between the tip and the substrate. In the "stick" phase the tip slows down (the accumulated material ahead of the indenter provides further motion resistance), it adheres to the surface of the polymer, no relative motion occurs between the two, and the stress on the surface induces deformation in the material under the indenter. The tangential stress increases until it exceeds the critical stress of the material, the "slip" phase starts, the scratcher moves faster and material piles up ahead of the indenter, until new adhesion bonds form, causing the repetition of the phenomenon. This involves not only tangential stick-slip motion, but also a periodical vertical impact of the tip on the PP surface, leading to forces higher than the prescribed one; pre-mature severe damage can result from that. Once the stress has become lower than the critical one,

the stick process happens again. Hence, the fluctuations result from the accumulation and release of the tangential force.

The presence of texture grains can further enhance the COF fluctuations. Indeed, when the tip of the indenter faces one bump, this represents an obstacle to the motion and a certain force must be exerted to overcome or flatten this bump. Hence, the friction force increases. Once the bump has been passed, the force required to continue the motion drops, so does the COF, until the next bump is approached. Due to the particular texture present on the polymer surface, this phenomenon is repeated as the sliding continues, and fluctuations occur in the COF occur.

It is interesting to note that, even though textures and roughness are different, the steady-state COFs are similar. This can be explained recalling what has been stated in the friction section. The friction coefficient consists of two components: one is the traditional surface sliding coefficient, the other represents additional scratch resistance forces due by various deformation mechanism. In the first part of the test, the traditional component of friction dominates. This is influenced by the surface finishing and texture, which have effect on the initial COF peaks, on the time employed to reach it and on the amplitude of the following oscillations. As the test proceeds, the damage tracks is continuously worn out because of the deeper penetration of the counterface into the polymer. Therefore, the COF component related to the material ploughing resistance becomes the major contribution, inhibiting the effect of texture and roughness. Because of that, all the tested samples having different texture, but which are made of the same material (Material A), show similar final COF.

From the microstructural images, it is possible to predict a lower damage visibility from those samples with texture characterized by large and deep grains. Indeed, these features promote confuse and irregular boundaries between the wear track and the undamaged background, that is a beneficial effect from a scratch visibility point of view (boundaries which are low defined trigger poorly the eye perception, compared to neat and defined boundaries). This has been confirmed by the results obtained through the spectrophotometer: it is possible to note that textures with large grains, deep depths and rough/round peaks (like texture A and B), are characterized by a lower surface damage visibility (low $\Delta L^*\%$). Hence, these textures are able to hide the damage, as it has been found in the literature. As

could be expected, higher load promotes higher damage visibility. On surface with texture with MGD, which modifies the gloss of the surface, the damage appears darker. However, this does not mean that the damage in this case is less visible that the one in the original texture cases, because it is known that it is the contrast with the background that is important for the damage visibility, and not the absolute brightness of the damage [14].

It is interesting to compare figure 5.22, 5.23, 5.24, 5.30 and 5.31 to the wear rate and worn volume data shown in figure 5.2 and 5.3. Those graphs refer to Material B samples. Good agreement have been found between the amount of lost material (and wear rate), the depth, the groove shoulder, the roughness variations and the luminance contrast; the material with the highest amount of removed material is also the one with the biggest characteristic features of the damaged area, the largest change in the surface roughness and the largest surface damage visibility. Scratch additives have been found to be effective in the reduction of penetration depth, wear track shoulder, roughness variation and luminance contrast. Indeed, scratch additive are able to boost the mechanical properties (especially the elastic modulus) of the material because of their chemical structure and their effective bounds to the polymer matrix; according to the literature, improved mechanical properties induce higher scratch resistance to the material, thus lower damage. From the scratch visibility point of view, it has been found that the obtained wear track shape (figure **??** $(f)-(g)-(h)$) involves low damage visibility. So, the strict relationship found in the literature between penetration depth, wear track shoulder, roughness variation and luminance contrast seems to be confirmed in this study. However, considering Material A samples, different fundings have been obtained. From the comparison between figures 5.18, 5.19 and 5.20 to figure 5.30, it is possible to understand which parameter correlates better with surface damage visibility. While both the roughness variation and the pile-up on the sides show poor (or no) correlation with the luminance contrast, the wear track depth presents the same behavior of $\Delta L\%$. This means that, among the considered parameters, thought significant for surface damage visibility, the wear scar depth is the most important. The obtained low (or no) influences of roughness variation and wear track raised shoulder seem to be in contrast with the literature [16]. However, it is important to point out that the studies found in the literature refers to flat samples without texture. On the opposite, in

this study, the samples are textured. This has introduced a further level of complexity, hiding/eliminating the strict relationship between damage visibility and wear track shoulder and roughness change. For Material B samples, this relationship still holds, but this is due to the fact that all samples present the same texture. It is possible to state that, the pile-up on the sides and the roughness difference between the damaged and undamaged area are not able to account for the difference surface damage visibility induced by different texture.

Chapter 7

Conclusions

In this thesis, effect of normal applied load, surface texture, gloss and color, scratch additive content and injection molding process characteristics were studied for two thermoplastic polyolefins (Material A and B).

Firstly, the influence on the damage from a quantitative point of view has been evaluated, by measuring COF, wear rate and the characteristic dimensions of the damage, such as material pile-up on wear track sides, wear track depth and roughness variation. Then, correlations between the above mentioned findings and surface damage visibility have been developed.

The conclusions of this study are summarized below:

- An increase in the normal load from 5 N to 10 N led to higher wear rates and more extensive damage. Transition in the wear mechanism from ductile drawing to more severe ploughing has been detected for texture D, E and F, in material A.
- Textures characterized by large and deep grains and round peaks, like Dayton and Austin ML, have promoted surface damage resistance. These types of texture showed low wear rate and no transition from mild to severe wear. Moreover, the lowest penetration depth and damage visibility were observed in these cases.
- The fluctuations in COF at the initial stages of wear tests were due to the surface

texture presence. At steady-state condition, when the texture has been worn out, all the materials showed the same value of COF.

- More surface damage was observed for samples with low gloss surfaces. This technique utilized to obtain low gloss (MGD) has weakened the surfaces promoting the transition from mild to severe wear mechanism described earlier.
- Scratch additives, studied in Material B, are not always beneficial for lowering wear rate, while they showed positive effects on the surface damage visibility. Indeed, they have an opposite behavior, on wear rates, depending on the type of injection molding process utilized for the plaques (for LDR 50:1 sample, the wear rate was reduced while for precolor sample, the wear rate was increased). However, scratch additives were effective in the reduction of the damage characteristic dimensions (i.e. penetration depth, pile-up on wear track sides and roughness variation) as well as on the luminance contrast, thus damage visibility.
- Lighter color has proven to be more resistance to surface damage visibility than darker color (lower luminance contrast $\Delta L^*\%$)
- According to ANOVA:
  - Normal load has been found to be significant for wear rate and wear track pile-ups, while the effect of texture was not significant.
  - Normal load and texture were found to be significant for wear track depth and luminance contrast.
- For Material B, good agreement was found between wear rates, dimensions of the groove depth, pile-ups, roughness variations and luminance contrast. The precolor sample showed the smallest wear track depth, pile-up and roughness variation, as well as the lowest damage visibility and wear rates.
- Correlations between wear track pile-ups, roughness variation and surface damage visibility were not observed for textured samples (Material A). Among those considered, the most important wear track geometric characteristic for damage visibility of textured samples is the wear track depth.

Chapter 8

Recommendations

For future studies on this topic, some modifications and improvements can be performed to improve the reliability of results. Some recommendations can be done:

- Replications of the tests could be performed to improve the reliability of the results. Moreover, the replications would allow the ANOVA analysis to take into account possible interactions between the analyzed factors.
- A full factorial plan, considering at the same time either the load, either the textures and either the different material grades could be done. This would give the possibility to use the ANOVA analysis (since it requires a full factorial plan), and the significance of the factors analyzed in this study, and their interactions, could be performed.
- A way to improve the damage visibility measurement, could be the measure of gloss variation through a glossmeter, in addition to the luminance contrast. By the combination of these two quantities, e.g. with a weighted sum, a more precise indication of how much the damage is effectively visible could be obtained.
- It could be interesting to carry out tests at different temperature, to account for its effect. Indeed, it is known that the temperature in the vehicle could reach up to

$70° - 80°C$, in a sunny day. At this temperature, the material could soften; and this would have an effect on the surface damage dimension and visibility.

- A polymeric counterface could be considered, to reproduce a situation closer to the reality. Ad example, the rubbing that occurs when customers open or close the doors is between the door panel (made of TPO) and the shoes, or the shoe sole; these are usually made of polymeric material (like polyurethane, PVC, etc.).

- A study of the viscoelasticity, and its effect, of the considered material (TPOs) could be included in future works. In fact, polymeric materials are able to heal with time (viscoelastic recovery), once a damage has been performed on their surface, reducing it. The size and visibility of the damage change if they are measured right after the test, or after some hours. The comparison between measurements collected at different times after the test end could be interesting and could give an evaluation of the viscoelasticity, and of the healing capability of the analyzed material.

Bibliography

[1] B. J. Briscoe, P. D. Evans, E. Pelillo, S. K. Sinha, *Scratching Maps for Polymers*, Wear, 200, 137-147, 1996

[2] M. Hamdi, H. J. Sue, *Effect of Color, Gloss and surface Texture perception on Scratch and Mar Visibility in Polymers*, Materials & design, 83, 528-535, 2015

[3] W. Brostow, J. Deborde, M. Jaklewicz, P. Olszynski, *Tribology with Emphasis on Polymers: Friction, Scratch Resistance and Wear*, Journal of Materials Education, vol.24, 2003, p. 119-132

[4] W. Brostow, V. Kovaevi, D. Vrsaljko, and J. Whitworth, *Tribology of Polymers and Polymer-based Composites*, Journal of Materials Education, vol.32, 2010, p. 273-290

[5] C. Xiang, H. J. Sue, J. Chu, B. Coleman, *Scratch Behavior and Material Property Relationship in Polymers*, Journal of Polymer Science: Part B: Polymer Physics, vol. 39, 47-59, 2001

[6] W. J. Noh, J. G. Noh, *A study on scratch resistance improvement of polypropylene compounds*, SAE International, 2011-01-0461, 2011

[7] R. Hotton, *Optimization of Scratch Resistance of Molded in Color Interior Thermoplastics Olefins Injection Molded Plastics*, SAE International, doi: 10.4271/2011-01-0464, 2011

[8] R. Browning, G. Lim, H. Jiang, H. J. Sue, *Scratch behavior of Anisotropic Polypropylene surfaces*, Society of Plastics Engineers, Automotive Thermoplastic Polyolefins (TPO) Global Conference, 422-430, 2006

[9] Y. Li, B. Yang, Z. Lou, S. Jin, *Study of Scratch Resistance of Polypropylene Compound for Automobile*, Society of Plastics Engineers - 11th-Annual SPE TPO Conference - The World's Leading Automotive Olefins Forum, 2009

[10] R. S. Hadal, R. D. K. Misra, *Scratch deformation behavior of thermoplastic materials with significance differences in ductility*, Materials science and engineering, 398, 252-261, 2005

[11] B. J. Briscoe, E. Pelillo, S. K. Sinha, *Scratch Hardness and Deformation Maps for Polycarbonate and Polyethylene*, Polymer engineering and science, 36, 2996-3005, 1996

[12] R. S. Kody, D. C. Martin, *Quantitative Characterization of Surface Deformation in Polymer composites using Digital Image Analysis*, Polymer Engineering and Science, Vol. 36, No. 2, 1996

[13] J. Chu, C. Xiang, H.J. Sue, R. Damon Hollis, *Scratch Resistance of Mineral filled Polypropylene materials*, Polymer Engineering and Science, 40, 944-955, 2000

[14] P. Liu, R. L. Browning, H. J. Sue, J. Li, S. Jones, T. Traugott, *Critical Assessment of Scratch Visibility Determination Methodologies*, ANTEC, 940-944, 2011

[15] P. Rangarajan, M. Sinha, V. Watkins, K. Harding, J. Sparks, *Scratch Visibility of Polymers Measured Using Optical Imaging*, Polymer Engineering and Science, vol. 43, No. 3, 749-758, 2003

[16] H. Jiang, R. Browning, M. Hossain, H. J. Sue, M. Fujiwara, *Quantitative Evaluation of Scratch Visibility Resistance of Polymers*, Applied surface science, 256, 6324-6329, 2010

[17] H. Jiang, Q. Cheng, C. Jiang, J. Zhang, Y. Li, *Effect of stick-slip on the scratch performance of polypropylene*, Tribology International, 91, 15, 2015

[18] P. Kurkcu, L. Andena, A. Pavan, *An experimental investigation of the scratch behavior of polymers: 1. Influence of the rate-dependent bulk mechanical properties*, Wear, 290-291, 86-93, 2012

[19] P. Kurkcu, L. Andena, A. Pavan, *An experimental investigation of the scratch behavior of polymers: 2. Influence ofhardorsoft fillers*, Wear, 317, 277290, 2014

[20] V. Chivanasoontorn, N. Aoki, M. Kotaki, *Effect of Scratch Velocity on Scratch Behavior of Injection-Molded Polypropylene*, Journal of Applied Polymer Science, Vol. 125, 28612866, 2012

[21] V. Chivanasoontorn, S. Tsukise, M. Kotaki, *Surface Texture effect on Scratch behavior of Injection Molded Plastics*, Polymer engineering and science, 1862-1867, 2012

[22] H. Jiang, R. Browning, H. J. Sue, *Understanding of Scratch-induced Damage Mechanisms in Polymers*, Polymer, 50, 4056-4065, 2009

[23] H. Unal, A. Mimaroglu, *Friction and wear behaviour of unfilled engineering thermoplastics*, Materials and Design, 24, 183187, 2003

[24] T. Korpela,M. Suvanto, T. T. Pakkanen, *Friction and wear of periodically micropatterned polypropylene in dry sliding*, Wear, 289, 18, 2012

[25] J. K. Lancaster, *Basic mechanisms of friction and wear of polymer* Plastics & polymers, 297-306, 1973

[26] B. J. Briscoe, D. Tabor, *Friction and Wear of polymers: the role of Mechanical Properties*, The British polymer journal, vol. 10, 1978

[27] G. Erhard, *Sliding Friction behavior of Polymer-Polymer material combinations*, Wear, 84, 167-181, 1983

[28] E. Santner, H. Czichos, *Tribology of Polymers*, Tribology International, vol. 22, No. 2, 103-109, 1989

[29] J. K. Lancaster, *Material-specific wear mechanisms: relevance to wear modelling*, Wear 141, 159-183, 1990

[30] G. Liu, M. Xiang, H. Li, *A Study on Sliding Wear of Ultrahigh Molecular Weight Polyethylene/Polypropylene Blends*, Polymer engineering and science, Vol. 44, No. 1, 2004

[31] A. Dasari, J. Rohrmann, R.D. Misra, *Micro-and nanoscale evaluation of Scratch Damage in Poly(propylene)s* Macromolecular materials and engineering, 287, 889-903, 2002

[32] M. Wong, A. Moyse, F. Lee, H. J. Sue, *Study of surface damage of polypropylene under progressive loading*, Journal od material science, 39, 3239-3308, 2004

[33] J. K. Lancaster, *Friction and wear*, Polymer science, 959-1046, 1972

[34] H. Jiang, R. Browning, J. Fincher, A. Gasbarro, S. Jones, H. J. Sue, *Influence of surface roughness and contact load on friction coefficient and scratch behavior of thermoplastic olefins*, Applied Surface Science, 254, 4494-4499, 2008

[35] R. Browning, H. Jiang, P. Liu, A. Moyse, H. J. Sue, *Recent progress in scratch & mar testing and evaluation of thermoplastic olefines*, International Polyolefins Conference 2010

[36] R. Browning, G. T. Lim, A. Moyse, L. Sun, H. J. Sue, *Effects of Slip Agent and Talc Surface-Treatment on the Scratch Behavior of Thermoplastic Olefins*, Polymer engineering and science, 601-608, 2006

[37] R. D. K. Misra, R. Hadal, S. J. Duncan, *Surface damage behavior during scratch deformation of mineral reinforced polymer composites*, Acta Materialia, 52, 4363-4376, 2004

[38] R. Browning, H. Jiang, A. Moyse, H. J. Sue, Y. Iseki, K. Ohtani, Y. Ijichi, *Scratch behavior of soft thermoplastic olefins: Effects of ethylene content and testing rate*, Journal of Materials Science, 43, 1357-1365, 2008

[39] J. Chu, C. Xiang, H.J. Sue, R. Damon Hollis, *Scratch resistance of mineral filled polypropylene materials*, Polymer engineering and science, 40, 944-955, 2000

[40] J. Anderson , M. Brown, C. Kan, K. Nanjundiah, V. Kalihari, *Quantitative method for evaluating fingernail induced mar damage of coatings*, Journal of Coatings Technology and Research, vol. 10, 579-588, 2013

[41] P. Liu, R. L. Browning, H. J. Sue, J. Li, S. Jones, *Quantitative scratch visibility assessment of polymers based on Erichsen and ASTM/ISO scratch testing methodologies*, Polymer testing, 30, 633-640, 2011

[42] E. Lebert, L. M. Romano, *Scratch and mar resistance of automotive plastics using Erichsen scratch hardness tester*, Doc.No. LP-463DD-18-02, 2015

[43] ASTM Standard D 7027-05, *Standard Test Method for Evaluation of Scratch Resistance of Polymeric Coatings and Plastics Using an Instrumented Scratch Machine1*, ASTM International, 2005, West Conshohocken, PA 19428-2959

[44] H. Pelletier, C. Mendibide, A. Riche, *Mechanical characterization of polymeric films using depth-sensing instrument: Correlation between viscoelastic-plastic properties and scratch resistance*, Progress in Organic Coatings, 62, 162178, 2008

[45] Erichsen. 2015. *SCRATCH HARDNESS TESTER 430 P-I (REFERENCE CLASS) [ONLINE]*, Available at: https://www.erichsen.de/surfacetesting/hardness-1/scratch-hardness-tester-430-p-i-reference-class. [Accessed 6 May 2016]

[46] Hunterlab. 2013. *Brief Explanation of delta E or delta E* [ONLINE]*, Available at: https://support.hunterlab.com/hc/en-us/articles/203023559-Brief-Explanation-of-delta-E-or-delta-E-. [Accessed 6 May 2016]

[47] P. N. Gardner. 2013. *Professional Gloss Meters [ONLINE]*, Available at: https://www.gardco.com/pages/gloss/tqc-glossmeter.cfm. [Accessed 6 May 2016]

[48] Taber Industies. 2011. *Multi-Finger Scratch/Mar Tester [ONLINE]*, Available at: http://www.taberindustries.com/multi-finger-scratch-mar-tester. [Accessed 6 May 2016]

[49] N.K. Myshkin, M.I. Petrokovets, A.V. Kovalev, *Tribology of polymers: Adhesion, friction, wear, and mass-transfer* Tribology International, 38, 910921, 2005

[50] R. Tuszynski, *Friction and Wear Testing* Engineered Materials Handbook Desk Edition, ASM International, 459-466, 1995

[51] B. J. Briscoe, S. K. Sinha, *Wear of Polymers* Proc. Inst. Mech. Eng. J., J. Eng. Tribol., Vol 216, 2002

[52] B. J. Briscoe, *Wear of Polymers: an Essay on Fundamental Aspect* Tribology International, vol.14, 1981, 231-243

[53] J. G. Drobny, *Handbook of thermoplastic elastomers* Plastic Design Library, 2007

[54] J. A. Brydson, *Plastic materials* Butterworth-Heinemann, 1999

[55] D. Cho, B. Bhushan, J. Dyess, *Mechanisms of static and kinetic friction of polypropylene, polyethylene terephthalate, and high-density polyethylene pairs during sliding* Tribology International, vol. 94, 2016, 165175

[56] I. Mathias. 2016. *Immiscible polymer blends [ONLINE]*, Available at: http://pslc.ws/macrog/iblend.htm. [Accessed 21 April 2016]

[57] Buy Car Cyprus. 2015. *Vehicle bumpers [ONLINE]*, Available at: http://buycarcyprus.com/tag/vehicle-bumpers. [Accessed 21 April 2016]

[58] World Motor Media. 2013. *Door panel photos [ONLINE]*, Available at: http://gtcarlot.com/data/Jeep/Renegade/2015/102411662/DoorPanel.html. [Accessed 21 April 2016]

[59] Tai Sin Electric. 2016. *Cables and wires. [ONLINE]*, Available at: http://www.taisin.com.my/. [Accessed 21 April 2016]

[60] The DOW Chemical Company. 2016. *Interior design. [ONLINE]*, Available at: http://www.dow.com/elastomers/markets/transport/internal/. [Accessed 25 June 2016]

[61] A. Germak, G. Genta, G. Barbato, *Misurare per decidere*, Società Editrice Esculapio, Bologna, 2014

[62] S. Zani, *Analisi dei dati statistici*, Giuffrè editore, vol. I, Milano, 1994

[63] J. F. Archard, W. Hirst, *The wear of metals under unlubricated conditions*, Proceedings of the Royal Society of London. Series A, Mathematical and Physical Science, Vol. 236, No. 1206, 1956, 397-410

Appendix A:
Evolution of COF for different textured samples

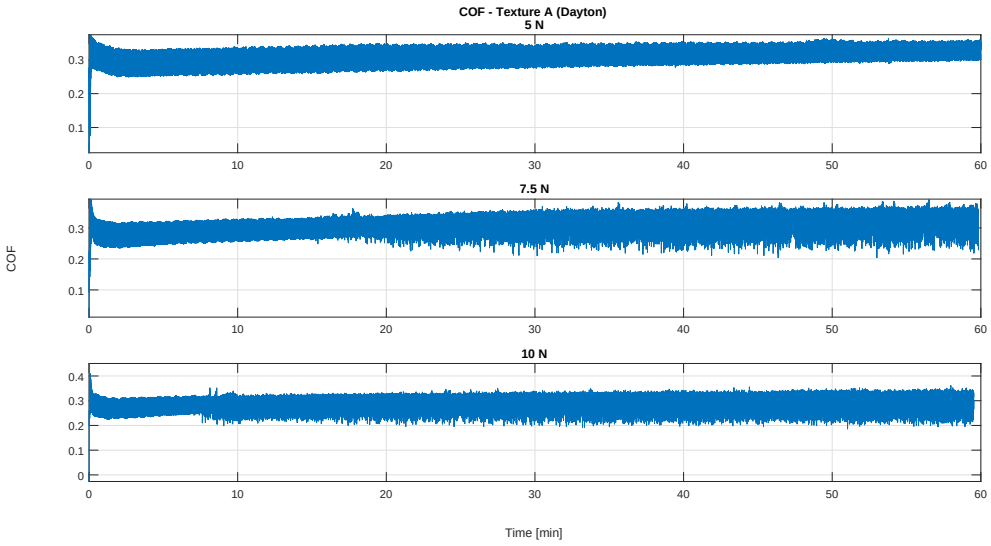

Figure 1: COF against testing time for Material A sample with texture A

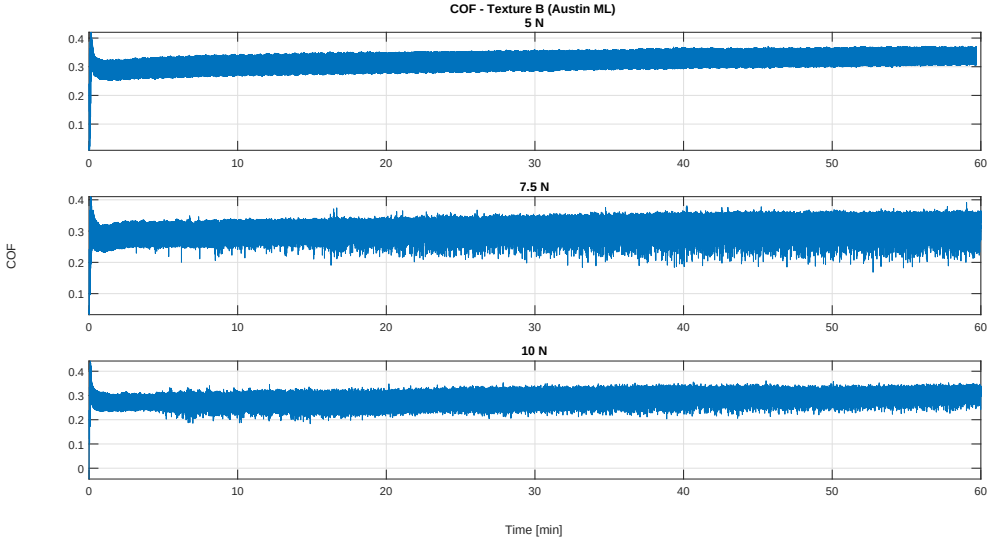

Figure 2: COF against testing time for Material A sample with texture B

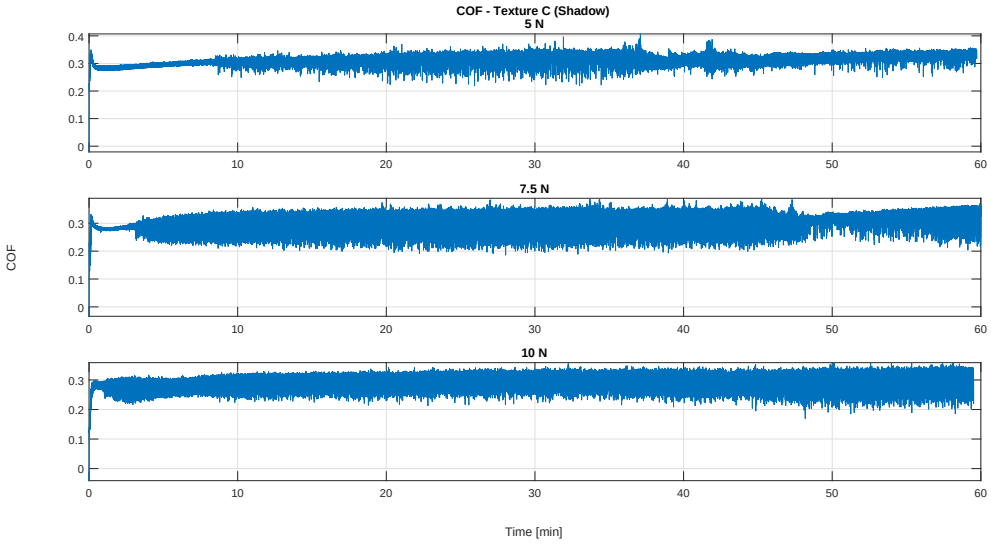

Figure 3: COF against testing time for Material A sample with texture C

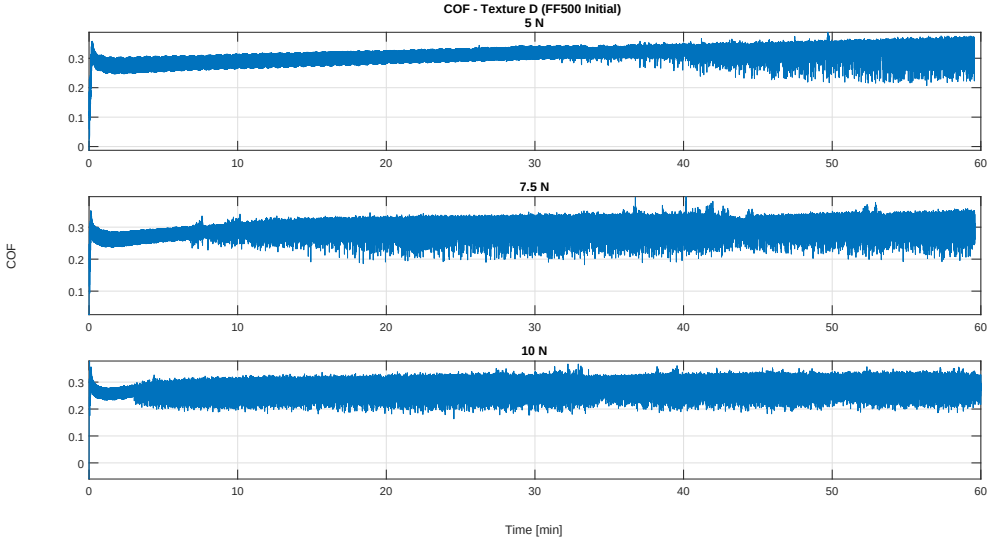

Figure 4: COF against testing time for Material A sample with texture D

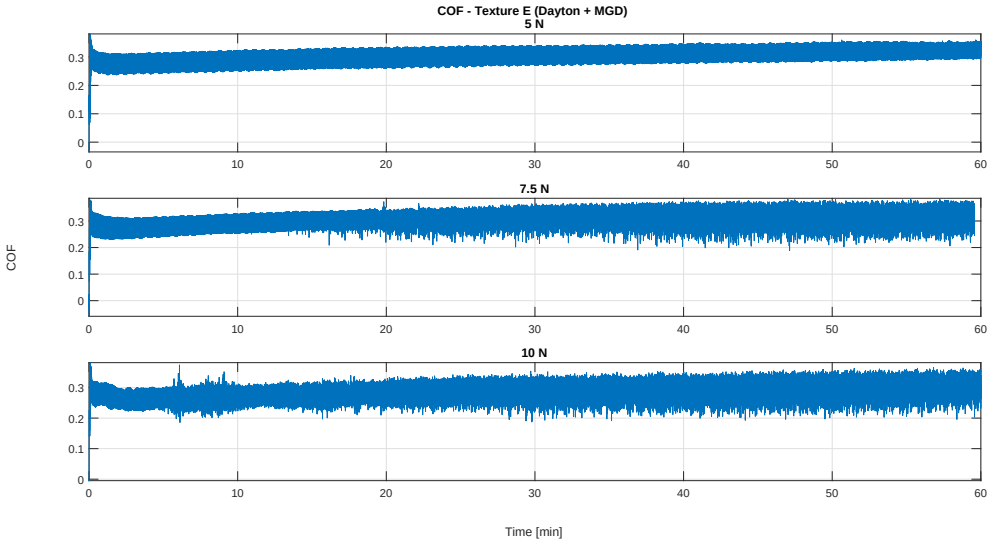

Figure 5: COF against testing time for Material A sample with texture E

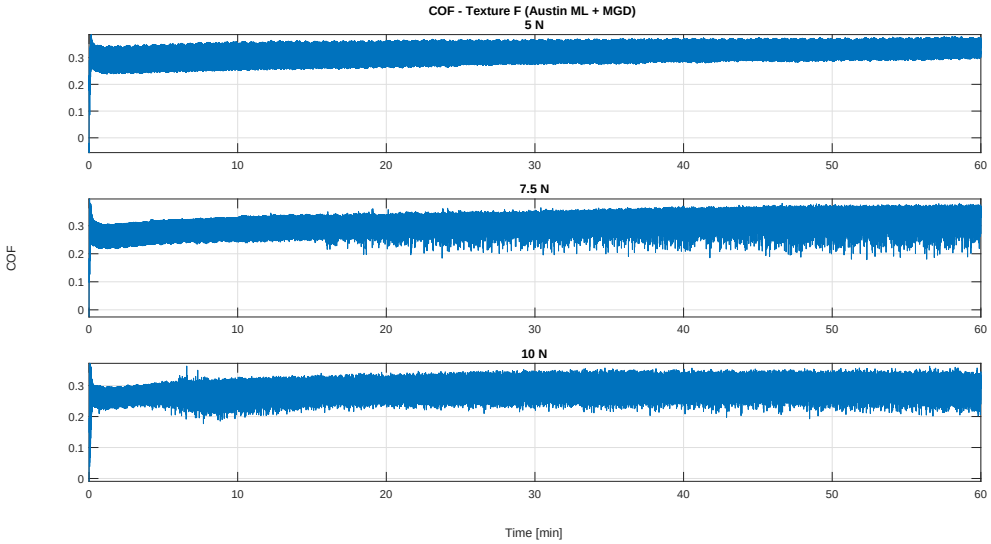

Figure 6: COF against testing time for Material A sample with texture F

Appendix B:
Surface profile of Material A samples

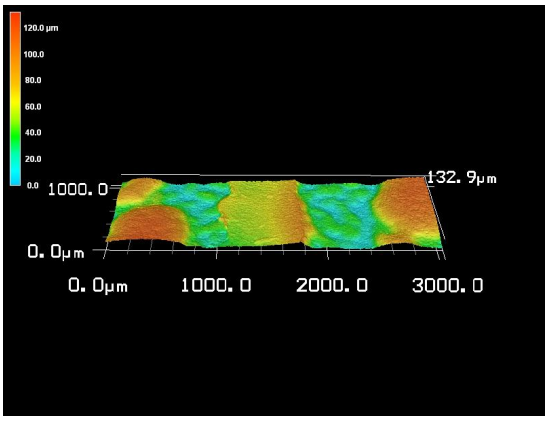

(a) Texture B - 5 N

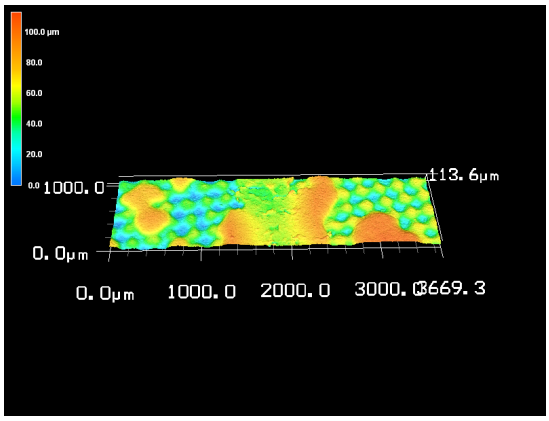

(b) Texture D - 5 N

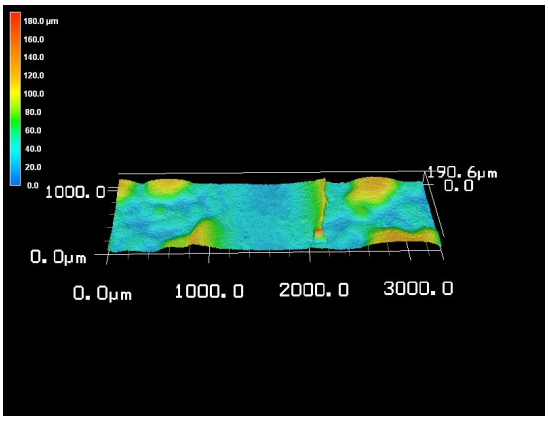

(c) Texture B - 7.5 N

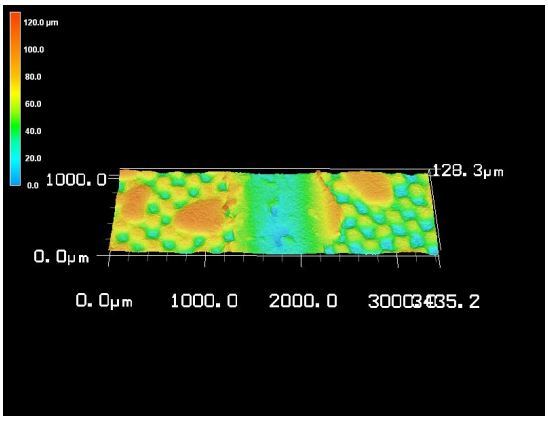

(d) Texture D - 7.5 N

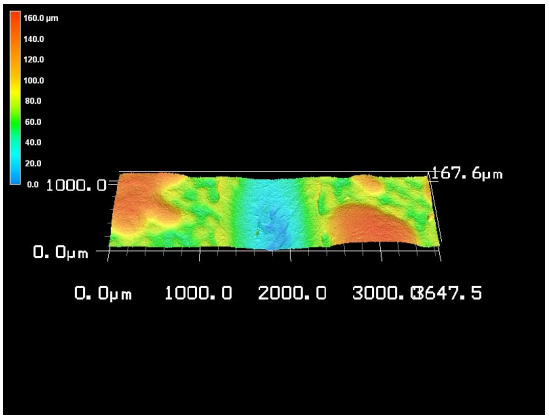

(e) Texture B - 10 N

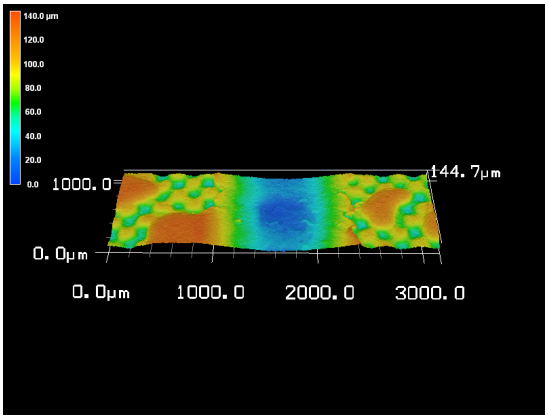

(f) Texture D - 10 N

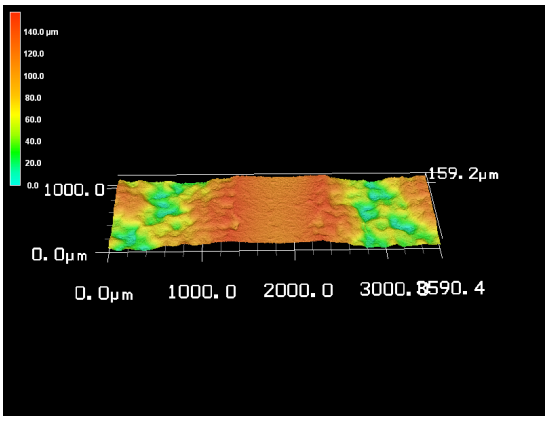

(g) Texture E - 5 N

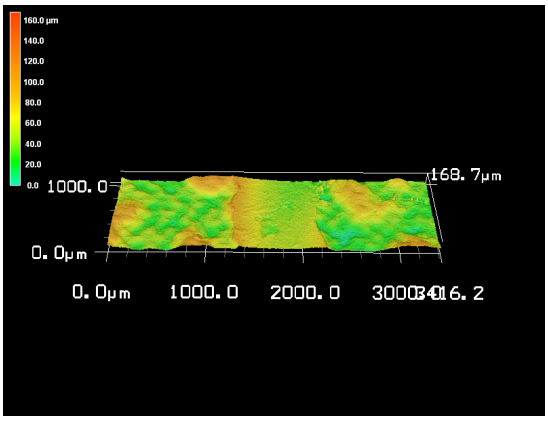

(h) Texture F - 5 N

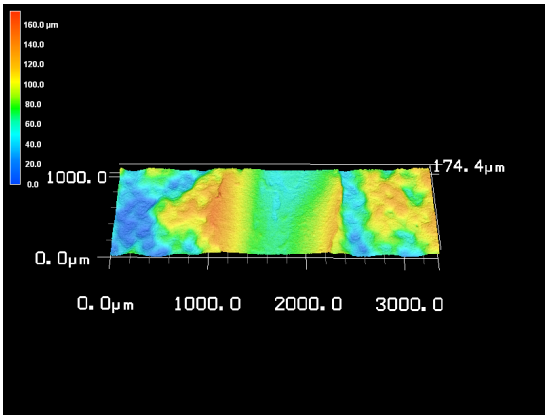

(i) Texture E - 7.5 N

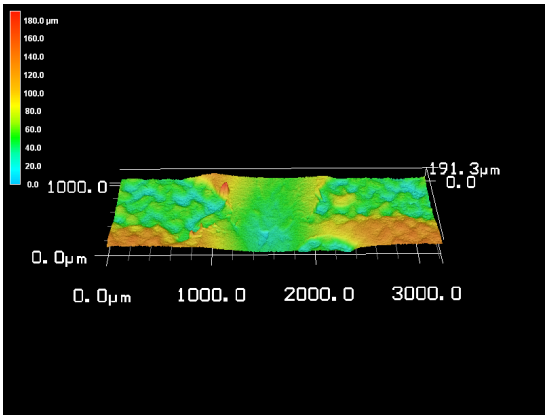

(j) Texture F - 7.5 N

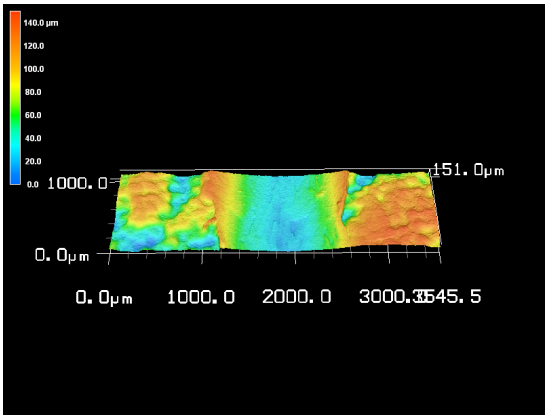

(k) Texture E - 10 N

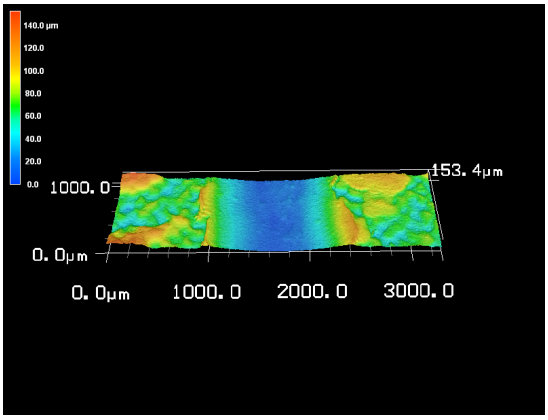

(l) Texture F - 10 N

Figure 1: Surface profiles of Material A samples

Appendix C:

ANOVA residuals plots

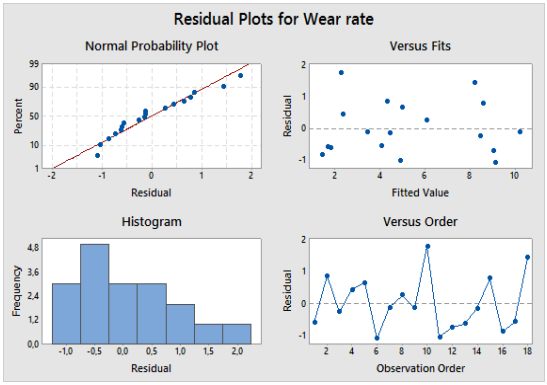

(a) Wear rate

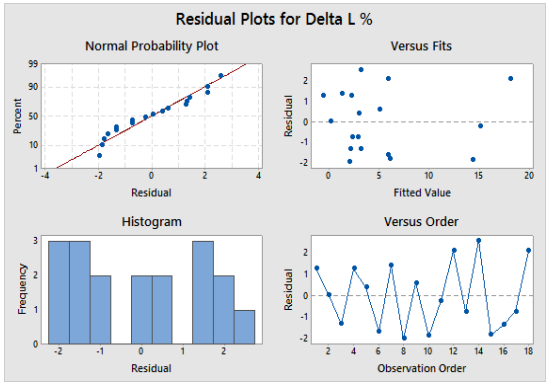

(b) $\Delta L\%$

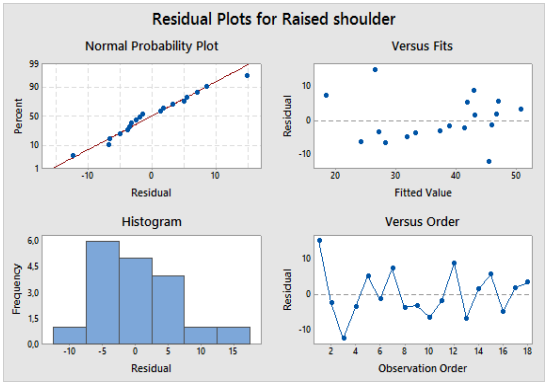

(c) Raised shoulder

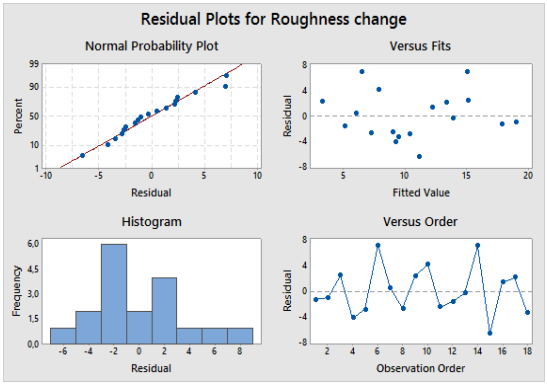

(d) Roughness change

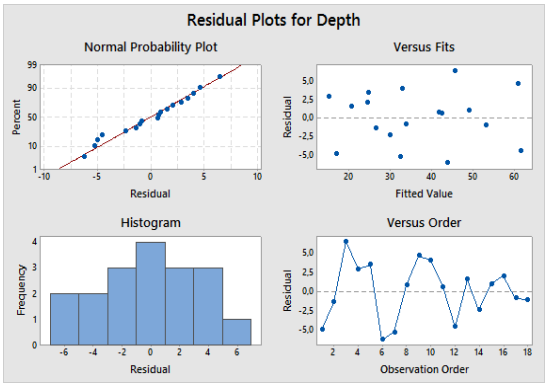

(e) Wear track depth

Figure 1: Residuals plots for wear rate and $\Delta L^*\%$ vs. texture and normal load

Vita Auctoris

NAME:	Davide Pezzetti-Tonion
PLACE OF BIRTH:	Cuorgné, TO, Italy
DATE OF BIRTH:	1992
EDUCATION:	Politecnico di Torino, B.Sc. in Automotive Engineering, Torino, Italy, 2014
	Politecnico di Torino, M.A.Sc. in Automotive Engineering, Torino, Italy, 2016
	University of Windsor, International M.A.Sc. in Mechanical Engineering, Windsor, Canada, 2016